NASA CR-169,651

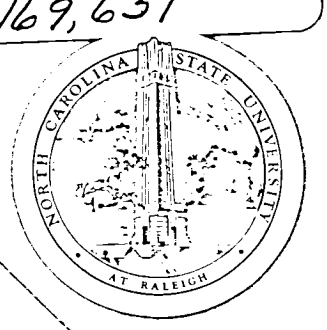

ABSTRACT

WOLF, KAYE WOODROOF. Effect of Ionizing Radiation on the Mechanical and Structural Properties of Graphite Fiber Reinforced Composites (under the direction of DR. R. E. FORNES).

It is widely known that graphite fiber composites have many properties which make them attractive candidates for aerospace applications. Therefore it is important to determine the effects of ionizing radiation on composite integrity, particularly ultimate stress and modulus. T300/5208 (graphite/epoxy) and C6000/PMR 15 (graphite/polyimide) composites were exposed to various levels of 0.5 MeV electron radiation with the maximum dose being 10,000 Mrad. A three-point bending test was used to evaluate the ultimate stress and modulus of the composites. In all composites except transverse samples of C6000/PMR 15 ultimate stress values remained approximately constant or increased slightly. The modulus values remained approximately constant for all composite types regardless of the radiation level.

In an effort to more fully understand these results, the emphasis of the investigation was focused on interfacial aspects of composites. Interlaminar shear tests were performed on T300/5208 and C6000/PMR 15 composites irradiated to 10,000 Mrad. There was an initial increase in interlaminar shear strength (up to 1,000 Mrad) followed by a sharp decrease with further radiation exposure. Using scanning electron microscopy no visual differences in the mode of fracture could be detected between ruptured control samples and those exposed to various levels of radiation. Electron spectroscopy for chemical analysis

(ESCA) revealed little change in the surface elements present in control and highly irradiated T300/5208 composite samples.

EFFECT OF IONIZING RADIATION ON THE MECHANICAL AND STRUCTURAL PROPERTIES OF GRAPHITE FIBER REINFORCED COMPOSITES

by

KAYE WOODROOF WOLF

A thesis submitted to the Graduate Faculty of
North Carolina State University at Raleigh
in partial fulfillment of the
requirements for the Degree of
Doctor of Philosophy

FIBER AND POLYMER SCIENCE

RALEIGH

1 9 8 2

APPROVED BY

_____ _____

_____ _____

_____

Chairman of Advisory Committee

BIOGRAPHY

Kaye Woodroof Wolf was born on [redacted] in [redacted] She received her elementary and secondary education here, graduating from Roanoke Rapids Junior-Senior High School in 1973. She entered North Carolina State University at Raleigh in that same year and graduated magna cum laude with a Bachelor of Science in Mathematics in August, 1976. She began her graduate program at the same institution in January, 1977 and received a Master of Science in Textile Materials and Management in December, 1979. At that time she was enrolled in the Fiber and Polymer Science program. Upon completion of her doctorate she will be employed by Monsanto Textiles Company in Pensacola, Florida.

The author is the daughter of Mr. and Mrs. R. A. Woodroof, Jr.

ACKNOWLEDGEMENTS

The author wishes to express sincere appreciation and gratitude to Dr. R. E. Fornes, Chairman of her Advisory Committee, for guidance and advice throughout this program of study. She also wishes to thank the other members of her Committee, Drs. R. D. Gilbert, J. D. Memory, W. K. Walsh, and A. A. Fahmy, for their helpful suggestions.

Special thanks are extended to Dr. A. W. Waltner of the Department of Physics for assistance with proton irradiation and to Dr. R. W. Linton and Mr. D. P. Griffis of the Department of Chemistry, University of North Carolina at Chapel Hill for performing the electron spectroscopy for chemical analysis. The author also thanks Dr. E. R. Long of NASA Langley Research Center for supplying samples.

The author expresses deep gratitude to Mr. G. G. Floyd and Mr. K. K. Crabtree for many hours of assistance with electron irradiation. Sincere thanks are due Ms. Carol Carrere and Ms. N. Naranong for assistance in physical testing, Mr. M. Bowen for graphic art work, and Mr. G. M. Kent for photography.

The author also wishes to express deep appreciation to her family for their patience and moral support throughout this entire study.

The author gratefully acknowledges NASA for financial support during the course of this study.

TABLE OF CONTENTS

TABLE OF CONTENTS (cont'd)

TABLE OF CONTENTS (cont'd)

LIST OF TABLES

LIST OF TABLES (cont'd)

LIST OF FIGURES

LIST OF FIGURES (cont'd)

LIST OF FIGURES (cont'd)

1. INTRODUCTION

Over the last two decades there has been considerable interest in the technology of composite materials. Graphite fiber reinforced composites are of particular interest because they have many properties which make them attractive candidates for aerospace applications. These properties include high modulus, high strength-to-weight ratio, low density, exceptional fatigue resistance, and near-zero coefficient of thermal expansion [1-5]. In aerospace applications, these composites will be exposed to ionizing radiation so it is important to understand the effects of irradiation on composite integrity, particularly ultimate stress and modulus.

In order to do this, the initial phase of this investigation was designed to examine the long-term effects of radiation on the mechanical properties of graphite fiber composites. Based on the results of this experiment, the focus of the investigation was directed to interfacial aspects of composites.

The interface between fiber and matrix plays a profound role in the behavior of composites. The interfacial bond can influence composite strength, modes of failure, Young's modulus, interlaminar shear strength, compressive strength, and critical fiber length. In addition, load transfer mechanisms are predicated on a strong interfacial bond and structural stability at elevated temperatures is a function of reactions which occur at the interface. The interface also plays an important role in the fracture behavior of composite materials [6-10].

The objective of this study was to determine the effects of radiation on the interfacial properties of graphite fiber composites. The techniques used to characterize the interface were scanning electron microscopy, transverse tensile test, interlaminar shear test, and electron spectroscopy for chemical analysis (ESCA).

2. REVIEW OF LITERATURE

2.1 Introduction

The interface region in fiber-matrix composites is difficult to define and even more difficult to study. As with any mixture of two distinct homogeneous phases, the fiber-matrix interface is not to be regarded as a simple geometrical plane with a homogeneous phase extending on either side of it, but rather as a "surface phase" with characteristic thickness. Macroscopically, this "surface phase" consists of a surface which is common to both fiber and matrix and the region immediately surrounding this surface. It has physical and mechanical properties which are different from those of the two homogeneous phases. Microscopically, this region consists of surface atoms and subsurface atoms. It is not known how many atomic layers below the surface influence the properties of the interface. The distance between atoms of the two homogeneous phases is also uncertain but varies depending on chemical affinity, steric requirements, and mechanical restrictions placed on the interface due to cooldown of the composite after fabrication. At least three types of bonding--chemical, electrical, and mechanical--are thought to exist at the interface [7,11-13].

Various interfacial phenomena are discussed in this review. Interfacial bonding has been approached both theoretically and experimentally. In view of the theoretical approaches, theories of adhesion which are based on surface properties and treatments of the fibers, surface energy, and wettability are discussed. The quantitative parameters most frequently used to assess the interface

are shear strength and modulus. Experimental techniques used to determine these are discussed. Environmental effects (e.g. moisture, ambient aging) on the interface and the role of the interface in fracture are also discussed.

2.2 Surface Properties and Treatments of Graphite Fibers

2.2.1 Formation of Graphite Fibers

Graphite fibers are produced by the controlled pyrolysis and graphitization of certain organic fibers, principally rayon and polyacrylonitrile. These fibers lose much of their non-carbon content as gases and change to forms of carbon when heated above 300°C in an inert atmosphere. This process is called carbonization. Carbon formed at these low temperatures contains many grown-in defects because thermal energy is not sufficient to break already-formed carbon-carbon bonds. Because of these grown-in defects, carbon is stable up to very high temperatures before changing to graphite. Graphitization, which is defined as the establishment of a regular stacking of graphitic sheets, does not occur until "graphitizable carbons" are annealed above 2500°C. It is presumed that at this temperature vacancies in the graphite sheet become mobile enough to remove grown-in defects. The overall morphology of the graphite sheets is determined during carbonization. During the graphitization process, the multifilament fibrous nature of the organic precursor is retained, but the chemical and mechanical properties are those of graphite [3,14-16].

A single crystal of graphite is composed of a series of parallel planes of carbon atoms arranged in benzenoid geometry. The intraplanar carbon-carbon bond length is 1.42 Å and the distance

between planes decreases with graphitization temperature, the minimum value being 3.35 Å for natural graphite. The planes are held together by van der Waals forces which allow them to be readily displaced with respect to one another in a lateral direction. This structure is the basis of graphite's lubricity and anisotropic nature [12,16,17].

Graphitic lamellar ribbons composed of graphitic crystallites are the main structural elements of graphite fibers. These ribbons undulate and twist along the fiber axis. In the core of the fiber, ribbon orientation is slightly radial and in the outer sheath, the ribbons are circumferentially oriented as shown in Figure 2.1. The crystallite size varies with graphitization temperature. For example, crystallites in a fiber graphitized at 1500°C were 13 graphitic layers thick and 40 Å wide while those in a fiber graphitized at 2600°C were 20 layers thick and 70 Å wide. The degree of alignment also varies with the graphitization conditions [4,18,19].

2.2.2 Surface Properties of Graphite Fibers

Carbon and graphite fibers have a similar surface appearance but the graphite surface is much less porous. The porosity present results from a 70-80% weight loss in the precursor upon graphitization. Carbon fiber densities range from 62 to 88 percent of those of pyrolytic graphite. Scanning electron photomicrographs of graphite fibers often show a smooth surface with striations parallel to the filament axis [12]. Some graphite fibers, however, do not show the presence of striations.

Specific surface area and surface roughness are the principal features of physical structure relevant to adhesive bond formation

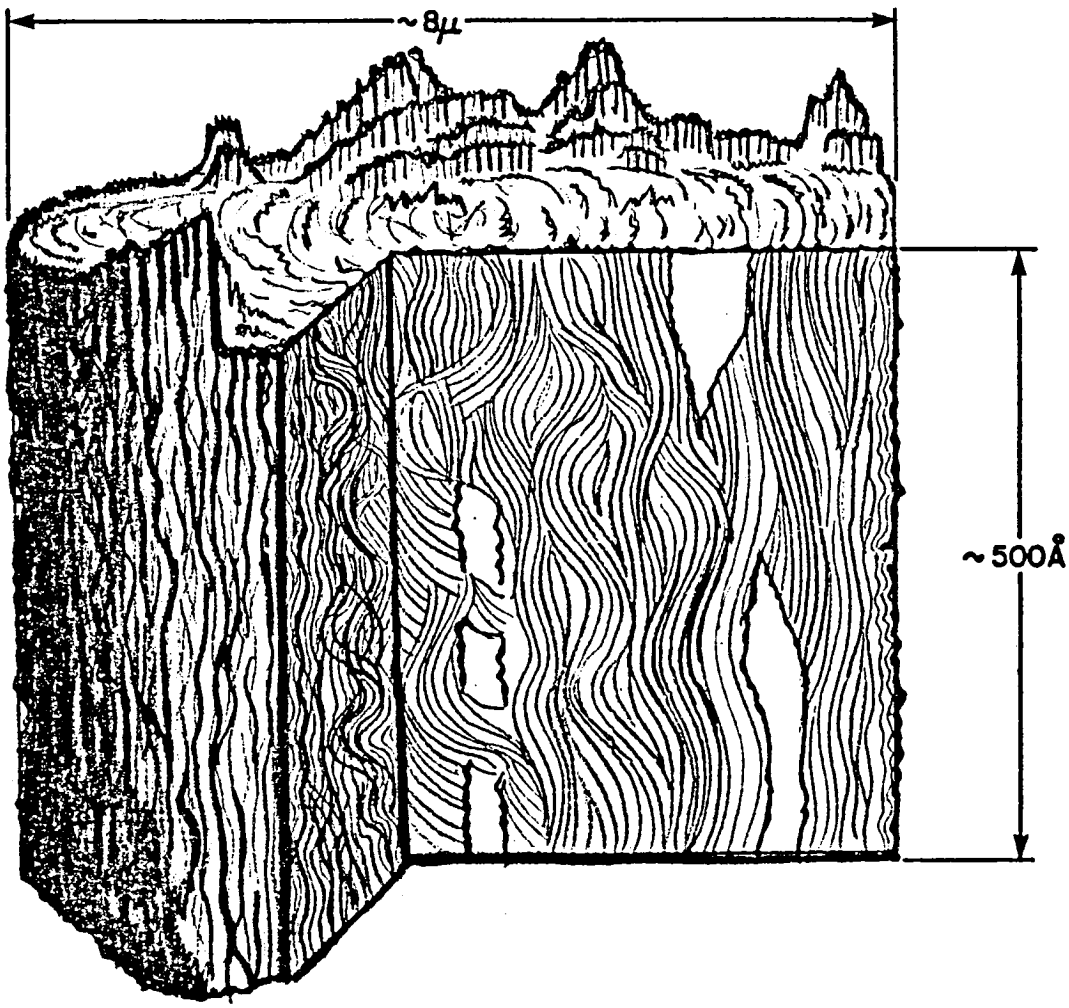

Figure 2.1 Core-sheath structure of graphitic lamellar ribbons in graphite fibers [19].

between fiber and matrix. These aspects of surface topography are important because they determine the amount of physical interfacial area available for formation of fiber-matrix bonds [7]. Scola and Brooks [20] found that the specific areas of graphite fibers (Thornel 50, Hitco HMG-50, and Morganite I) were much greater than those of boron and silicon carbide, which was consistent with the fiber size and surface roughness revealed by electron micrographs. They calculated surface areas based on fiber size and density and found them to be very close to their experimental values, which indicated a low order of surface roughness. The specific surface area of carbon fibers was found to be greater than that of graphite fibers [3]. This is reasonable given the differences in pore content. This lower interfacial area may also be a factor in the lower shear strength exhibited by graphite fiber composites compared with carbon fiber composites. It should be noted however, that not all the surface area determined by nitrogen adsorption is available to the resin [3]. Ouackenbush and Thomas [21] found the average pore diameter of carbon fiber to be 8 Å, which is too small for resin molecules to enter and thus probably makes little contribution to the mechanical interlocking of fiber and resin.

Hydrogen and oxygen are the most common species other than carbon on the graphite surface [7]. Scola and Brooks [22] detected oxygen at depths of 3μm using electron microprobe techniques. Herrick [23] and other workers [24-26] have differentiated the types of oxygen-containing functional groups on the graphite fiber surface. These

include carboxyl ($-CO_2H$), aromatic and aliphatic alcohols ($-\overset{H}{\overset{|}{C}}-OH$), carbonyl ($\overset{|}{C}=O$), and lactone ($-\underset{O}{\overset{|}{C}}=O$). As will be discussed later, these functional groups can react with the resin and form a chemical bond at the interface. The surface composition of graphite is influenced by the nature of the precursor fiber, the processing conditions, and the reactive nature of carbon [7].

2.2.3 Surface Treatments of Graphite Fibers

Despite the fact that early graphite fiber composites had uniquely high specific strengths and moduli, the fiber-resin interaction was poor, which led to low interlaminar shear strengths [3,7,18]. In an attempt to enhance the chemical bond between fiber and matrix, many different fiber surface treatments have been used to establish an active fiber surface. Values of interlaminar shear strength are used to compare the effects of different treatments.

A treatment of graphite fibers which gives a dramatic increase in the interlaminar shear strength of plastic composites is the "whiskerizing" process [3]. This process involves the growth of single crystal silicon carbide whiskers perpendicularly from the graphite surfaces, which produces a real mechanical tie between adjacent fibers and layers in the composite. Interlaminar shear strengths of 6.9-7.6 x 10^7 N/m^2 (10,000-11,000 psi) were reported [3] as compared to values of 2.1-2.4 x 10^7 N/m^2 (3,000-3,500 psi) for untreated fibers. Whiskerizing, however, has two drawbacks --a weakening effect on the fibers and the expense of the process.

It is well documented in the literature that silane coupling agents improve the glass-resin adhesive bond [6,7,12]. Coupling agents act as an intermediate, flexible, low-modulus layer between the matrix and the reinforcement and improve composite tensile and compressive strength [6]. It was thought that perhaps coupling agents could also be used successfully with graphite fibers. Theoretically, isocyanate groups in a urethane prepolymer could react with carboxyl and phenolic groups on the surface of oxidized graphite while other isocyanate groups reacted with the resin. However, composites made from fibers treated with this polyisocyanate coupling agent exhibited no significant improvements over those made from oxidized fibers with no coupling agent. Similarly, Ray et al. [27] found that applying a silane coating to heat-treated graphite fiber was ineffective in improving interlaminar shear strength. Harris and Beaumont [28] obtained the same results by application of a silane coating to an oxidized graphite fiber. On the other hand, oxidized graphite fibers treated with the glass coupling agent gamma-aminopropyltriethoxysilane yielded composites with slightly higher shear strength than those made from oxidized fibers without coupling agents. It was speculated that the phenolic hydroxyl groups on the oxidized graphite surface reacted with the coupling agent in a fashion similar to that of the silanol groups on the glass surface [3].

Goan and Prosen [3] used various wet and dry oxidizing systems to activate the graphite fiber surface. The wet treatments were carried out in various oxidizing solutions, the primary one being 60% aqueous nitric acid. The dry treatments included air oxidation at 400°C,

heating the fibers in a mixture of dry oxygen and ozone, and exposure of the fibers to oxygen under reduced pressure in the presence of an RF discharge.

The nitric acid treatment was the most effective of those studied in increasing interlaminar shear strength. It also produced the least fiber tensile strength loss. The shear performance of composites made from fibers oxidized in air was similar to that of those oxidized in RF gaseous discharge. The ozone treatment had little effect on the interlaminar shear strength.

Oxidation increases the fiber surface area, which would tend to improve the mechanical bond between fiber and resin, and also alters the nature of the surface [3,4]. Rivin [29] and Boehm [30] proposed the following scheme for the oxidation of graphite:

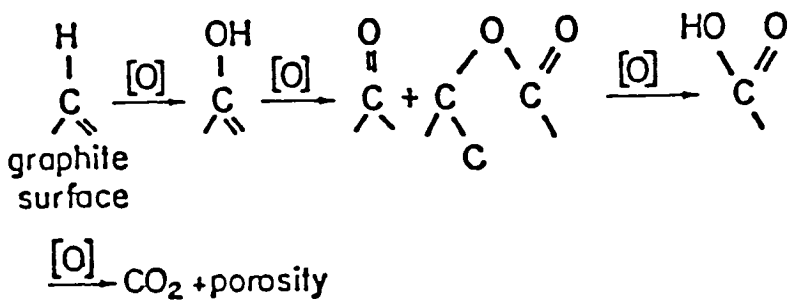

It should be noted that the first step in this scheme is not favorable since vinylic hydrogen abstraction is an inherently slow reaction due to the high bond energies of these carbon-hydrogen bonds [31]. However, the oxidation temperature may be sufficiently high to cause the reaction to proceed at a reasonable rate.

Due to the oxidation process, the surface of graphite has functional groups which can act as "handles" to the resin by reacting

with epoxy, amine, or other chemical groups in the resin [3,7,32]. Herrick [23] showed experimentally that surface chemical functionality was a more important influence than surface area on composite shear strength. He oxidized graphite fiber with nitric acid to increase both surface area and surface chemical activity. He then used hydrogen furnace reduction of the surface to eliminate the chemical activity yet leave the surface area unchanged. Composites made from fibers treated in this manner had shear strengths comparable to those of composites containing untreated fibers. Hence, Herrick concluded that surface chemical functionality played a more significant role than surface area with regard to shear strength.

Dauksys [32] experimented with three graphite fiber treatments which increased the values of composite interlaminar shear strength relative to the initial polyvinyl alcohol (PVA)- or H_2O-sized fibers. One method involves subjecting the fibers to a thermal-oxidative treatment then to a polymeric coating prior to epoxy impregnation. The other two methods are low temperature, wet chemical oxidations that induce carbonyl specificity to the graphite surface. These carbonyl groups react with $SnCl_4$ to form an intermediate complex which reacts with the epoxy molecules.

The heat treatment (propane torch, ~ 1925°C) and polymeric coating were found to improve the composite shear strength of PVA- or H_2O-sized Thornel graphite composites by a factor of approximately two or more without significant adverse effects on fiber mechanical properties. However, neither of these processes alone resulted in a

significant improvement. Ease of production and economic considerations make this method an attractive one.

It is believed that the heat treatment serves several purposes in addition to fiber oxidation. The temperature and gaseous pressure generated may decompose foreign contaminants and remove them from the fiber surface, thereby enhancing more intimate contact between the fiber and matrix. The heat treatment also increases porosity due to sublimation or volatilization of absorbed low molecular weight material within the pores of the fiber.

In one of the wet chemical methods the graphite fibers are oxidized in an aqueous sodium iodate ($NaIO_4$) solution which imparts carbonyl functionality to the fiber surface. The proposed reaction is as follows:

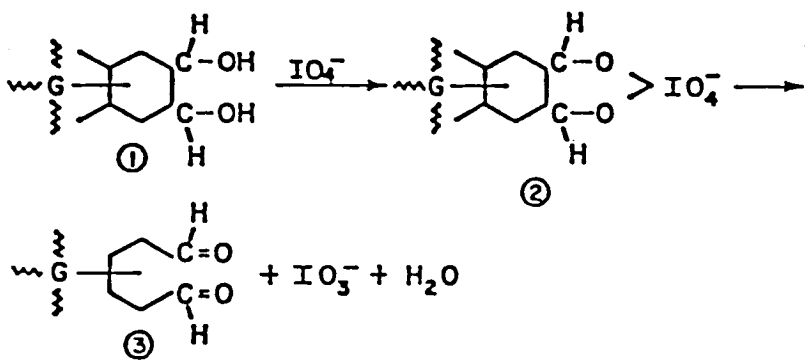

where (1) represents the graphite fiber with adjacent hydroxyls on the surface, (2) represents the iodate complex, and (3) represents the carbonyl-substituted fiber with reduction by-products. The degree of carbonyl substitution is a function of time and temperature. A coarse-grained fiber surface results after exposure to $NaIO_4$ for moderate periods of time or high temperature.

In the other wet chemical process carbonyl functionality on the graphite fiber surface is achieved by reaction in an aqueous dioxane osmium tetroxide solution. The proposed mechanism, which is given below, shows OsO_4 reacting with the graphite surface (4) to form the osmate ester complex (5). This reverts to a surface containing 1,2-diols (1) and OsO_4 is reduced to the higher valence state metal. The hydroxyls are oxidized to carbonyls (3) by $NaIO_4$ (as in the preceding method) and as an important secondary reaction, Os is oxidized to OsO_4, thus forming a regenerative cycle.

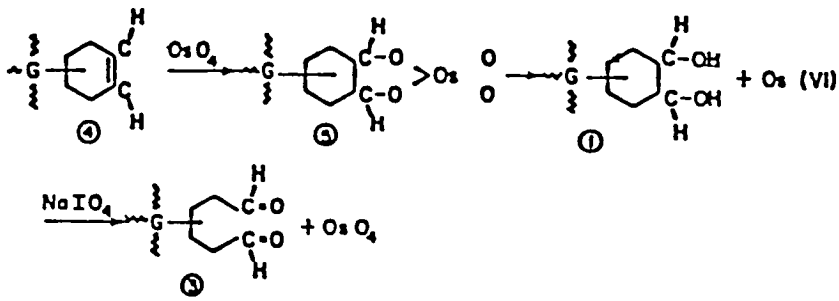

Dauksys also proposed a mechanism by which the carbonylated graphite surface is coupled to the oxirane ring of the epoxy molecule. This reaction involves formation of a stannic chloride ($SnCl_4$) intermediate by reacting $SnCl_4$ (in 2-butanone) with the carbonylated graphite surface (3) to form a complex. This reaction proceeds as follows:

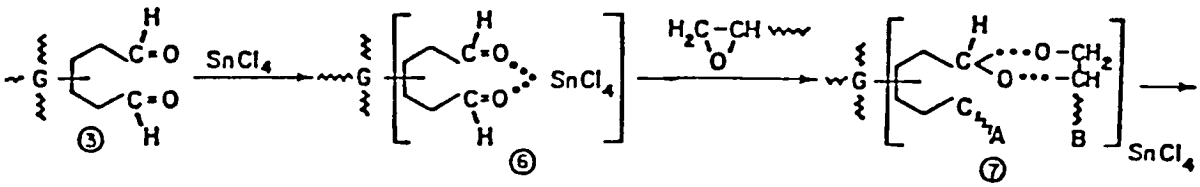

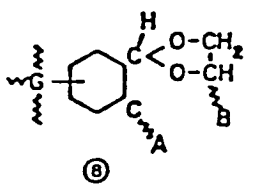

"A" indicates that carbonyl may remain unreacted, proceed as adjacent carbonyl, or is further reacted to carboxyl.

"B" indicates the rest of expoy polymer.

As can be seen from scanning electron photomicrographs of fractured surfaces, both wet chemical oxidation processes enhance graphite fiber-epoxy resin adhesion. Both treatments improve the composite interlaminar shear strength with only minor degradation of the fiber properties.

Scola and Roth [33] increased the specific surface area of the fiber by increasing oxidation exposure. As illustrated in Figure 2.2, they reported that shear strength increased with the surface area of graphite fiber. Composites made from nitric acid-oxidized graphite fibers had shear strengths of 5.9×10^7 N/m^2 (8,500 psi) compared to 2.4×10^7 N/m^2 (3,500 psi) for those with untreated fibers. Figure 2.2 also shows an increase in transverse tensile strength with surface area, but the degree of the increase is not as great.

Many of today's commercial graphite fibers are treated but the exact nature of the treatment is not divulged for proprietary reasons. Table 2.1 [20] compares the surface areas and composite shear strengths of a series of untreated fibers and fibers treated by Union Carbide, Hitco, Courtaulds, and Morganite. Given the large increases in composite shear strength with fibers treated by the latter three

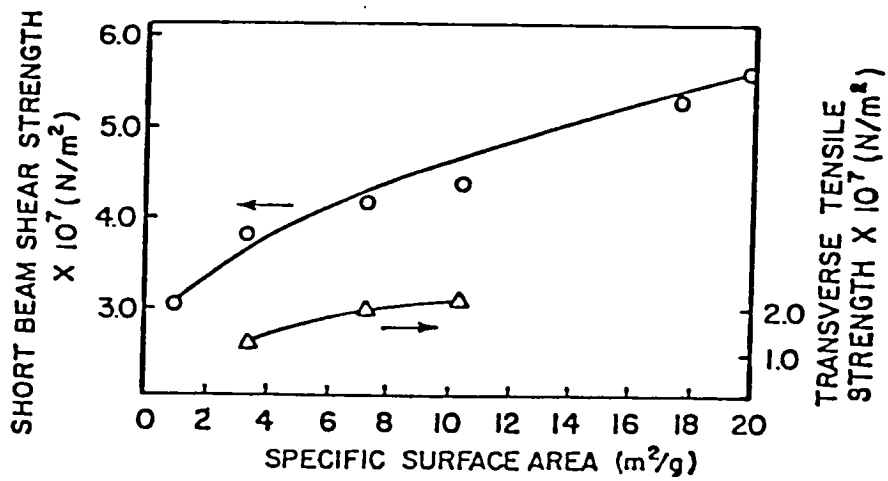

Figure 2.2 Shear and transverse strengths of unidirectional graphite-fiber-reinforced epoxy-resin composites [33].

TABLE 2.1
Comparison of fiber surface areas and composite shear strengths[a] [20]

Fiber	Treatment	Fiber specific surface area[b] (m^2/g)	Composite short-beam shear strength[c,d] ($N/m^2 \times 10^7$)	(psi)
Thornel 50	H_2O size	0.55	2.55	3700
Thornel 50	PVA size	0.59	2.76	4000
Thornel 50	Oxidation	2.5	4.83	7000
Hitco HMG-50	None	0.87	3.31	4800
Hitco HMG-50	By manufacturer	0.66	4.48	6500
Hitco HMG-50	Oxidation	7.3	5.86	8500
Morganite I	None	0.11	2.76	4000
Morganite I	By manufacturer	0.13	6.21	9000
Courtaulds B	None	0.31	2.76	4000
Courtaulds B	By manufacturer	0.39	6.21	9000

[a]Scola and Brooks (1970).
[b]Measured by low-temperature adsorption of krypton (Beebe et al., 1945).
[c]Unidirectional graphite fiber-2256-0820 epoxy resin composites, ~55 vol% fiber. Cure cycle, 2 hr at 80°C (200 psi) + 2 hr at 150°C.
[d]Shear strength measured at a span-to-depth ratio of 5/1.

manufacturers as compared to their untreated fibers, it is more likely that these increases are dependent on surface reactivity rather than surface area. Similarly, Drzal and co-workers [18,19] found that the surface area of graphite fibers treated by Hercules increased only slightly (7-10%) after treatment. They concluded that the increase in surface area alone could not be responsible for the improved strength characteristics of the surface-treated fiber composites.

From these investigations, it is apparent that both increased fiber surface area and surface reactivity contribute to improved composite shear strength, however it is difficult to obtain a quantitative correlation. The adhesive bond strength is also affected by other factors such as fiber contamination, variability in fiber quality, and fabrication parameters. Even considering these factors, the type of failure -- fiber, matrix, or fiber-matrix interface -- must be determined in order to make a quantitative assessment of the roles of surface area, surface reactivity, and wettability in adhesive bonding [7,19,32,34,35].

Williams and Kousiounelos [36] reported a new advanced fiber composite concept in which thermoplastic fibers and fiber coatings enhance the mechanical properties of continuous graphite fiber epoxy composites. The thermoplastic fibers assist in the intralaminar load distribution and improve interlaminar strength and toughness. The coatings behave as substantial bonding control layers applied to the fiber surface and should not be interpreted as a "treating". They control fiber and matrix debonding, contain individual fiber fractures which decreases fiber-fiber flaw communication, and control fiber

pull-out. Fiber coatings tested in this study were polyvinylalcohol and polysulfone. Both of these coatings significantly enhanced the notched fracture toughness and unnotched tensile strength of the fiber laminates.

2.3 Adhesion and Cohesion

2.3.1 Surface Energy and Wettability of Graphite Fibers

2.3.1.1 Qualitative aspects

Zisman [37] and others [38-40] have shown that the general requirements for a good adhesive are as follows:

(1) The adhesive must completely wet the adherend surface in order to obtain intimate contact.

(2) The adhesive must become viscous or solidify during the bonding stage.

(3) The adhesive must have the ability to deform during solidification to relieve internal stresses caused by thermal and cure shrinkage.

These requirements, however, place certain conditions on surfaces to be bonded. The first condition is that the surface must be free of foreign particles and easily wetted by the adhesive. The second condition is that a large interfacial area of intimate contact is a prerequisite whether the adhesive bond is due primarily to van der Waals physical adsorption forces or to chemical bond formation.

Thermodynamically, a high-surface-energy solid surface is the most conducive to good wetting, particularly if the adhesive contains polar functional groups. In order for the adhesive to wet the surface, the surface energy of the adherend must be greater than the

adhesive surface energy [7,41]. For spontaneous spreading, the fiber surface tension should be about 45 dynes/cm so that it exceeds that of the adhesive (35-45 dynes/cm) for polar organics.

The chemical composition and structural features of the fiber surface determine the magnitude of surface free energy. Graphite fibers have appreciable numbers of surface oxides which produce a high-energy surface but the presence of contaminants such as adsorbed water vapor can lower the surface tension and lead to incomplete wetting. Poor wetting can produce voids at the interface which may concentrate stresses and initiate cracking. If complete wetting is obtained, it is theoretically possible that resin adsorption on high-energy surfaces can provide adhesive strength far in excess of the cohesive strength of the resin [7,42,43].

The geometry of the surface roughness can help or hinder wetting. The porosity of the coating permits interlocking with the polymer to take place, changing the locus of any failure process and making it a mostly cohesive one. Wetting flaws that exist with a plane surface are all lined up in one plane, facilitating crack propagation from any one flaw. This is not the case for a rough surface. The pores should be funnel-shaped and have as few sharp edges as possible since these give rise to stress concentrations. Pore penetration should be as complete as possible to prevent air pockets. The polymer should set slowly to reduce thermal stresses. Provided that roughnesses are not conducive to pocket formation, and particularly when interlocking occurs, rugosity of a surface can be an effective factor in the formation of a strong adhesive bond [44].

2.3.1.2 Quantitative aspects

The interfacial free energy (or tension) can be expressed in terms of the surface tensions of the two homogeneous phases which are in contact [35]:

$$\gamma_{12} = \gamma_1 + \gamma_2 - 2\sqrt{\gamma_1^d \gamma_2^d} \qquad (2.1)$$

The geometric mean in the last term is based only on the dispersion part of the surface free energies and is not unusual in physical interactions. Consider phase 1 prior to contact with phase 2. Surface concentration of the molecules is lower than that of the bulk due to the inward force of the surface tension γ_1. When phases 1 and 2 are brought in contact, the surface tension γ_1 is reduced by the force across the interface in the opposite direction. This tension depends almost entirely on the dispersion force interaction and is expressed as the geometric mean $\sqrt{\gamma_1^d \gamma_2^d}$. Hence, the surface tension γ_1 is reduced to $\gamma_1 - \sqrt{\gamma_1^d \gamma_2^d}$. A similar argument can be given for phase 2, reducing its surface tension to $\gamma_2 - \sqrt{\gamma_1^d \gamma_2^d}$. Adding these two expressions yields Equation 2.1, the interfacial tension.

Good, working with Girifalco [45] and later co-workers [46,47], introduced an "interaction efficiency" parameter ϕ to account for inefficiencies in interfacial force interactions. They believe that these inefficiencies arise because not all forces in material 1 can interact with all forces in material 2 since some force components have no counterpart in the other material. Also, poor lattice fit at

the interface can decrease the number and intensity of interfacial force interactions. Good expressed the effective interaction term as

$$A_{12} = \phi \sqrt{A_{11}A_{22}}$$

and the corresponding expression for interfacial tension as

$$\gamma_{12} = \gamma_1 + \gamma_2 - \phi\sqrt{\gamma_1\gamma_2}$$

where $\phi = \phi_A\phi_V$

$$\phi_V = \frac{4(V_1V_2)^{1/3}}{(V_1^{1/3} + V_2^{1/3})^2}$$

V_1, V_2 = molar volumes of phases 1 and 2

ϕ_A = ratio of force components which can interact across the interface to the total internal force components.

Huntsberger [48] reasoned that selecting adhesives which satisfy the sole criterion $\gamma_1 < \gamma_c$ ($\gamma_1 \equiv$ surface tension of adhesive; $\gamma_c \equiv$ critical surface tension of adherend) limits the selection to low-energy adhesives which will fail cohesively. If an adhesive with surface tension $\gamma_1 > \gamma_c$ is used, the predicted work of adhesion can exceed $2\gamma_c$, however, interfacial contact may be incomplete. Huntsberger also showed that, in general, the spreading rate for adhesives having $\gamma_1 > \gamma_c$ is positive so with sufficient time, good interfacial contact should be produced unless the adhesive solidification rate is very rapid or the value $\gamma_1-\gamma_c$ is unusually large.

2.3.1.3 Methods of measuring surface tension

The most direct method of obtaining values for surface tension is by measuring the contact angle of various liquids to the surface. However, because of the geometry and small filament diameter of graphite fibers, it is difficult to obtain accurate measurements [3,7]. Bobka and Lowell [49] report the contact angle between water and graphite fiber to be 36° and it is not altered by treatment for 15 minutes at 500°C in an air stream. However, as shown in Table 2.2, the wettability of the graphite fiber for two epoxy resins appeared to improve considerably with this treatment.

The flotation method is another technique which can be used to determine critical surface tension γ_c. Due to irregular surface structure, small filament diameter, and small difference in density between filament and flotation liquids, it is difficult to obtain unequivocal estimates of γ_c on graphite fibers [7].

Using the wicking technique, Chwiastiak [50] found the surface tension of mild gas-phase of nitric acid-oxidized Thornel 50 graphite fiber to be 20-30 dynes/cm while ozone-oxidized Thornel 50 had a value of 50-56 dynes/cm. He reported the value for untreated Thornel 50 to be ≤ 0. The increase in total surface free energy due to fiber treatment is the result of an increase in the polar component of the fiber surface free energy [4]. He concluded, however, that this increase in surface tension or wettability of the fiber was not sufficient to account for the increased shear strength of composites made from oxidized fibers.

TABLE 2.2

Contact angles between several liquids and graphite fibers [7]

Fiber	Treatment	Liquid phase	Contact angle (deg)	Method
Graphite (Thornel 25)	Untreated	H_2O	36	Photomicrograph[b]
		ERLA-0400	12 ± 7	
		ERLA-2744	32 ± 8	
Graphite (Thornel 25)	Heated in 2 cm^3/min O_2 stream for 15 min, 500°C, followed by thermal desorption	H_2O	38 ± 8	Photomicrograph[b]
		ERLA-0400	4.3 ± 0.6	
		ERLA-2774	5.4 ± 0.7	

[a]Jones and Porter (1966).
[b]Bobka and Lowell (1966).

2.3.2 Theories of Adhesion

It is now recognized that ordinary dispersion or van der Waals' forces can be responsible for adhesive strengths far greater than experienced in practice if sufficiently intimate contact is achieved. In many cases only dispersion forces interact across an interface -- dipole and induced dipole forces contribute little or no interactions. However, hydrogen bonding can enhance adhesion. Chemical bonding and/or chemisorption may provide the links across the interface in some cases [35].

2.3.2.1 Polymer adsorption

Given a polymer adhesive that wets a surface and advances over it, it is important to consider on a molecular scale the manner by which the polymer becomes attached. Eirich [44] and Stromberg [51] reported that polymer molecules are absorbed from solution more or less as random coils, anchoring segments of their length to the interface at intermittent intervals. Other polymer molecules can become entangled in the intervening loops, creating a system of interpenetrating coiled molecules in an adsorbed layer of approximately bulk density. They had no reason to believe that adsorption from the melt would be qualitatively different. Since polymer molecules are adsorbed at various points 100 Ångstroms or more apart, their attachment to the interface is rather insensitive to surface variations. Eirich also pointed out that a unique aspect of polymer adsorption is its very slow reversibility due to the required simultaneity of desorption of the various anchor points. Another attractive feature of polymer adsorption is that, since polymers have

smaller volume contractions during cooling than most other organic substances, they generally maintain better molecular contacts during solidification.

As an adhesive polymer wets a surface, it does so in competition with any impurities which are at the original interface. There are also impurities in the polymer which may have an affinity for the polymer-substrate interface, form an interlayer, and thus sever the polymer-substrate bond. External impurities such as water or organic vapors may collect at the interface and, unless the adhesive has good barrier properties, can lead to rapid destruction of the bond even if it was initially strong. The presence of certain agents such as nitriles, ketones, multihydric acids, alcohols, or amines at the interface may prevent polymer adsorption completely [42,44].

In cases where chemisorption occurs, an extensive chemical attack converts the original substrate into a porous surface to allow interlocking with the polymer. The pore walls may be primed to reduce the contact angle and enhance interpenetration. It is critical that there be no adhesive contamination within the pores during the wetting process [44].

2.3.2.2 Improbability of adhesion failure

Several authors [41,42] have argued both theoretically and with extensive experimental data that the formation of specific interfacial bonds across an adhesive-adherend interface is neither necessary nor essential to form a good bond. They contend that every material adheres to every other material, provided that good interfacial contact is achieved. This close contact alone should yield an

adhesive bond strong enough to cause failure in either the adhesive or the adherend, but not at the interface. Tensile and peel strength tests of adhesive joints by Bolger and Michaels [43] never failed to show small quantities of either the adhesive or the adherend phases remaining on one or the other of the fractured surfaces, indicating cohesive failure.

Bikerman [42] claims that rupture almost never takes place between two different materials; instead, one of the materials making up the adhesive bond breaks down. He postulated that interfacial attractive forces between two phases never deviate appreciably from the approximation

$$A_{12} \approx \sqrt{A_{11}A_{22}}$$

where A_{11} and A_{22} are the intermolecular attractive forces in phases 1 and 2, and A_{12} is the intermolecular attractive force across the interface. Assuming this approximation holds, then unless A_{11} and A_{22} are equal, A_{12} will always be larger than one or the other of the cohesive force terms, rendering cohesive rather than adhesive failure.

Bikerman also bases his argument for cohesive failure on probability. In most systems, an interphase of variable composition exists between the adhesive and the adherend, rather than an atomically sharp interface. However, if a sharp interface exists, mechanical separation does not proceed along it since the probability becomes small that the loci of separation will lie entirely along the interface. Consider a crack which begins between an atom of the

adhesive and an atom of the adherend. For adhesive failure to occur, the crack must grow between the next pair of adhesive and adherend atoms. The only alternatives are for the crack to advance either between two atoms of the adhesive or between two atoms of the adherend. Assuming each atom occupies an approximately cubical space, it can be seen that there are three adhesive-adhesive paths and three adherend-adherend paths for every adhesive-adherend path. Thus, if the probabilities of all paths are equal, there is a one-in-seven chance that the crack will progress between two different materials. The same possibilities for separation exist at each interfacial atomic diameter, hence the probability of a crack growing along the interface for the space of n atoms is $(\frac{1}{7})^{n-1}$. In reality, however, the probability of interfacial cracks is smaller because not all paths are equally probable.

Bikerman [42] gives the following equation as an approximation of the breaking stress f_m of the adhesive bond:

$$f_m = \frac{1}{\alpha} (\frac{\xi}{\beta} - s)$$

where ξ = theoretical cohesive stress of the adhesive material

β = stress concentration factor due to heterogeneity of all solids

α = stress concentration factor caused by the rheological difference between adherend and adhesive

s = "frozen" stress (usually due to shrinkage) in the adhesive.

This equation applies as long as the adherend is stronger than the adhesive and there is no weak boundary layer at the interface. The

ratio $\frac{\xi}{\beta}$ is often approximately equal to the tensile strength of the adhesive in bulk. Thus, when α is approximately one and s is small, $f_m \approx \frac{\xi}{\beta}$; in other words, the breaking stress of the adhesive bond is nearly equal to the tensile strength of the adhesive. Several investigators [52-54] have noticed this equality.

2.4 Role of the Interface in Composite Integrity

The transmission of stress between fiber and matrix depends on a strong interfacial bond which resists failure [32,55]. For this reason, the degree of contact and the cohesive forces at the interface are of considerable importance [7]. Inherent tangential stresses due to thermal effects are present at the interface and these affect bond strength. The bond strength can be measured by several techniques. The fracture mode of the composite also depends on the strength of the interface. These interfacial aspects will be discussed in this section.

2.4.1 Requirements of the Interface

The interface must be able to withstand mechanical and thermal deformations in a more or less reversible manner. In order to do this it must combine reasonable strength with the ability to absorb mechanical energy. Tangential stresses, which will be discussed in detail later, arise at the interface due to inevitable differences in the coefficients of thermal expansion, moduli, and Poisson ratios of the two materials. These stresses can lead to dewetting or crack formations along the interface and hence weaken the composite since interfacial flaws act as stress concentrators. The presence of an

elastomeric interphase rather than a mere interface helps reduce these stresses. The interphase is a transition layer in which there is a gradual change in properties from the bulk phase. Figure 2.3 illustrates this concept. Also, stresses are reduced during bond formation if one of the materials has a wide softening range rather than a sharp phase transition. Another advantage is for the adhesive to undergo small volume changes during the solidification process. Also, selecting materials with relatively high stiffness ratios will minimize the shear stress concentration [7,32,44].

If the interphase is constructed successfully, the failure locus moves into the polymer, thus the polymer strength becomes the limiting factor governing composite strength. Other polymer properties affect interface properties so the polymer should have good adhesive and barrier properties, slowly varying properties with temperature, and sufficient modulus, strength and deformability. Obviously, a simple polymer cannot fulfill all these requirements so block and graft copolymers and factors such as crystallinity and cross-linking must be considered [7,44].

2.4.2 Bond Characteristics of the Interface

To assume a surface or interface is smooth on a molecular scale is a gross oversimplification. All surfaces are rough and, except in rare cases, have foreign molecules adsorbed on them. By using refined techniques, it has been found that the vertical distance between the highest peak and the deepest trough is on the order of 100-1000 Å for the flattest surface possible. The values for normal surfaces are much higher--on the order of microns or greater. Bonding of the two

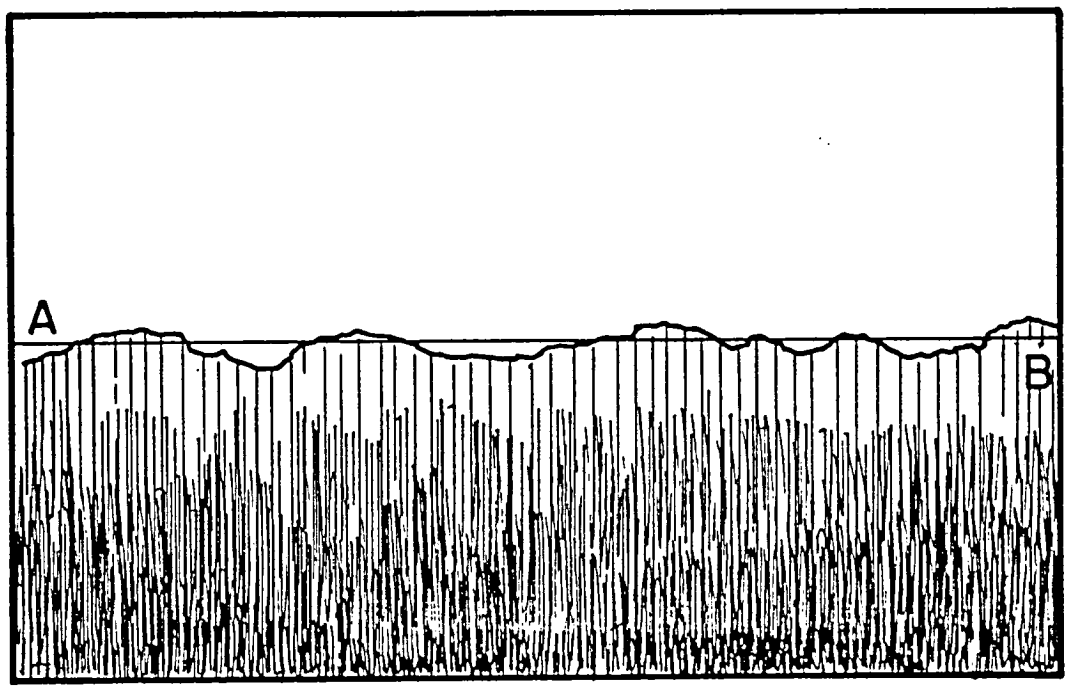

Figure 2.3 Cross-section of a typical solid surface. The solid is shaded, and the gradation of shading indicates gradual change of properties on nearing the interface with air (white) [12].

phases in the interphase may be due to primary or secondary bonds, assuming there is no entrapped air, foreign adsorbed molecules, or impurities. Covalent bonds have the smallest range of action (~1 Å) and van der Waals' have the greatest (~5 Å). Hence, the two phases must approach to within this sort of distance to obtain a strong boundary layer or interface [12].

As with bulk materials, there is considerable difference in the theoretical and actual values of interface strength. Using atomic bonding forces, the theoretical strength is calculated to be in the range $1\text{-}10 \times 10^6$ psi. This is within an order of magnitude of the modulus (E/10) for many materials. Actual strength values observed are in the range $1\text{-}100 \times 10^3$ psi. This large difference may be due to the presence of flaws or voids which give rise to stress concentrations. The relative importance and magnitude of different types of interatomic and intermolecular bonding forces can also contribute to these differences [12].

2.4.3 Microresidual Stress Effects on Interfacial Bond Strength

During the fabrication process microresidual stresses are inherently produced at the interface. This is illustrated in Figure 2.4. The curing temperature is above the glass transition temperature of the resin which means the resin is in the rubbery and minimum stress state. As the resin cools and reaches T_g, it solidifies and is able to support a load. If the resin cools unrestrained it will contract; however, if the fiber-resin bond formed is strong it will prevent contraction at the interface and the resin

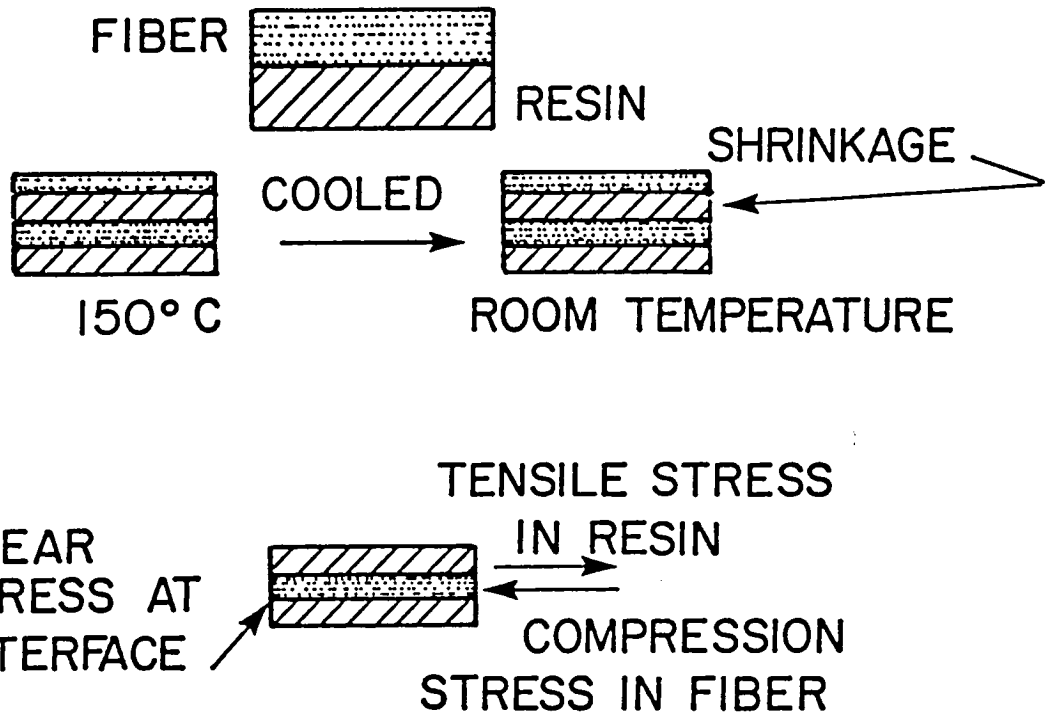

Figure 2.4 Schematic diagram of resin shrinkage in reinforced fiber-resin composites; thermally induced longitudinal stresses [7].

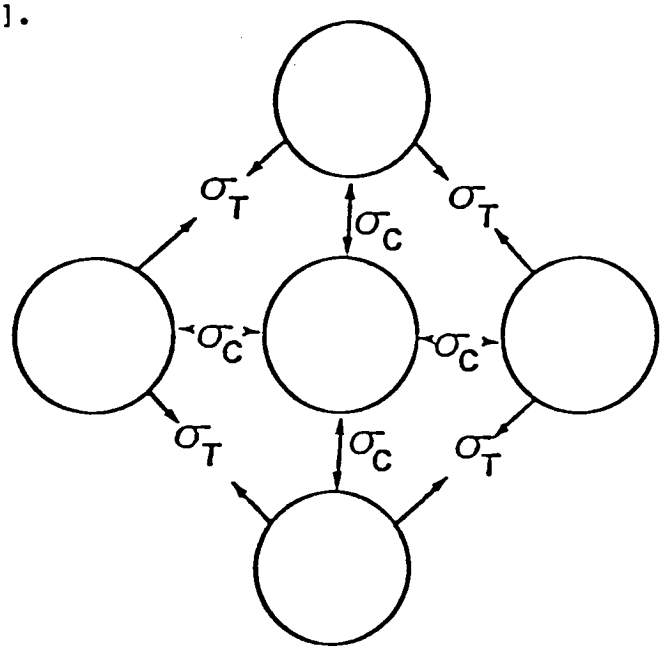

Figure 2.5 Thermally induced radial stresses in a square array of fibers in a resin matrix [56].

will be in a state of stress. This room temperature stress for a graphite-epoxy composite can be calculated as follows [7]:

$\Delta\alpha = \alpha_r - \alpha_f = (4.8 \times 10^{-5} - 0.1 \times 10^{-5})$ m/m/°C $= 4.7 \times 10^{-5}$ m/m/°C

$\Delta T = 135°C - 25°C = 110°C$, from T_g to room temperature

strain $= \Delta\alpha\Delta T = (4.7 \times 10^{-5}$ m/m°C$)(110°C) = 5.17 \times 10^{-3}$ m/m

stress = modulus x strain $= (3.45 \times 10^9$ N/m$^2)(5.17 \times 10^{-3}$m/m)

$= 1.78 \times 10^7$ N/m^2

where α = coefficient of thermal expansion.

Since the fiber-resin interface is already in a state of thermally-induced shear stress, the load required to fail the specimen will be lower than if the sample were not prestressed.

As shown in Figure 2.5, there are also stresses normal to the fiber direction which can be either tensile or compressive. The fiber-resin interface is strengthened by the compressive stresses but weakened by those which are tensile. These stresses, which are induced by thermal cure shrinkage, increase as the relative stiffness ratio E_f/E_m decreases and the fiber volume ratio increases. In the case of a graphite-epoxy composite the compressive stresses are approximately 1.4×10^7 N/m^2 (2000 psi) and the radial tensile stresses are approximately 3.4×10^6 N/m^2 (500 psi). The effect of this latter stress is to reduce the transverse tensile strength of the composite. The compressive stresses tend to increase the composite longitudinal tensile strength and shear strength. The effect on the composite of the interaction of all residual stresses is difficult to predict, especially when the interface is subjected to various environments [56-58].

2.4.4 Methods for Measuring Interface Bond Strength

The interfacial stress state and bond strength can be obtained by several methods which are either direct or indirect. The direct methods involve model studies with either single fibers cast in a matrix or multifibers. The photoelastic method of multifiber inclusion is the most reliable method to determine point stress states. The most common and convenient test used to measure average bond strength is the fiber pullout test. The short-beam shear and transverse strength tests can be used to indirectly assess the interface bond strength. The short-beam shear test is convenient for quality control and for determining environmental effects. The indirect methods can be viewed as qualitative but when interpreted properly can serve as quantitative tests [7].

2.4.4.1 Single fiber pullout model

Single fiber pullout tests to measure shear strength can be conducted in two ways. In the first case, a single fiber is embedded in a polymer matrix and is failed by loading the resin matrix. In the second case, the fiber is partially embedded and is failed by loading the fiber. This method is believed to have the following advantages [1]:

(1) more similar geometrically to an actual composite

(2) residual stresses produced in the specimen due to resin curing are similar to those in an actual composite

(3) failure initiation is more realistic.

The expression for shear stress is as follows, assuming there is a uniform distribution along the interface [6]:

$$\tau = \frac{P_m}{2\pi r \ell} = \frac{\sigma_m r}{2\ell}$$

where τ = average shear strength of bond

P_m = maximum load applied to fiber

r = radius of fiber

ℓ = embedded fiber length

σ_m = maximum stress applied to fiber.

Fiber strength influences the embedded fiber length since the fiber will fail in tension before pullout occurs if the embedded length exceeds the maximum embedded length which is given by

$$\ell = \frac{\sigma_{ult} r}{2\tau}$$

where σ_{ult} = ultimate fiber strength.

An experimental technique frequently used to evaluate shear strength involves measuring the failure load as a function of embedded fiber length and plotting P_m versus ℓ. The shear strength is then determined from the slope of this straight line relationship. Shear strength values determined in this manner are only an average value since stress concentrations exist at the fiber ends and exit points from the matrix [6].

Two types of single filament specimens were developed to test fiber bond strength. The trapezoidal specimen was designed so that the interface fails in shear when the specimen is axially loaded in compression since the sloping sides produce a sharply changing axial stress. The curved neck specimen was designed to fail by tensile debonding rather than shear failure. A compressive axial load on this specimen produces radial expansion since Poisson's ratio of the matrix

is greater than that of the fiber. Consequently an interfacial tensile stress given by the following expression is created [6]:

$$S = \text{debonding stress} = -\frac{\sigma_m(\mu_m - \mu_f)E_f}{(1+\mu_m)E_f + (1-\mu_f-2\mu_f^2)E_m}$$

where σ_m = axial stress on minimum section

μ = Poisson's ratio

E = elastic modulus.

Bond failure can be visually observed in these specimens as a separation at the fiber-matrix interface which begins at the neck or area of minimum cross-section where the stress is highest.

Mozzo and Chabord [59] suggested an alternative method for analyzing the data of the curved neck specimen. Instead of using the maximum load or axial stress at bond failure initiation, they used the area under the force-deflection curve. This method is advantageous when the resin matrix exhibits nonlinear elastic behavior.

For fiber diameters less than 10 mils tensile debonding or shear debonding methods should be used, depending on which mode of failure is of the greatest interest. The tensile debonding test is more reproducible and bond failures are easier to observe [6].

Mullin et al. [60] used an optical microscope to observe the fracture modes of single filaments embedded in epoxies. A single fracture plane in the resin normal to the fibers and emanating from the point of fiber failure was the most common form of fracture observed. Bond failure occurred at the interface in specimens with a ductile matrix capable of resisting the initial tendency to crack. By

observing which mechanism takes precedence, the tensile strength of the matrix can be compared to the bond strength.

2.4.4.2 Short-beam shear test

The short-beam shear test consists of subjecting a rectangular bar having a span-to-depth ratio of approximately four to symmetric three-point bending. Two stationary circular rods called reaction noses support the specimen and a third circular rod called the loading nose, moving at a constant rate, applies the external load by making contact with the specimen. According to the Euler-Bernoulli assumptions, the shear stress τ_{xy} is parabolically distributed across the face of the specimen with a maximum at the center of the face given by [61,62]

$$\tau_{xy_{max}} = \frac{3P}{4db} \qquad (2.2)$$

where P = load applied at center of beam

b = width of beam

d = depth of beam.

τ_{xy} represents the composite shear strength when $P = P_c$, the fracture load of the composite.

Studying unidirectional graphite-epoxy composites, Daniels et al. [62] observed non-linear deformation and yield which they attributed entirely to shear. They concluded that most of the apparent initial linear deformation was due to machine compliance and loading nose indentation. Their experimental data showed a strong dependence of short beam shear strength on the span-to-depth ratio, namely decreasing shear strength with increasing L/d. They also observed a

sudden drop in the short beam shear strength around the glass transition temperature.

Despite the fact that the short-beam shear test has been widely used to determine the interface bond strength, several workers [61,63] have pointed out that it is not a true shear test and that interpretation of the experimental data using Equation 2.2 is not completely accurate. Bader et al. [63] observed broken test-pieces and found that in most cases failure was flexural rather than interlaminar. Therefore, they concluded that the short-beam shear test was not a satisfactory measure of the interface strength. Berg et al. [61] pointed out that the Euler-Bernoulli hypotheses of beam bending apply only to a beam with a large span-to-depth ratio. Also, according to classical theory on which Equation 2.2 is based, the stress distribution is the same on all transverse faces regardless of position along the beam axis. On the contrary, the vertical plane lying directly under the concentrated central load is a plane of symmetry and thus has no shear stresses acting on it. Because of these deviations, they recommended that the short beam shear test be used only as a screening test for composite materials.

2.4.4.3 Transverse tensile strength

The transverse tensile strength of the composite is directly affected by the strength of the interface. It is also affected by the tensile strength of the matrix. Regarding transverse strength, there are two limiting cases [8]:

(1) fiber and interface are very strong

(2) interface is very weak.

In the first case, failure is expected to occur in the matrix with the failure crack avoiding the fibers. In the second case, failure occurs at points of minimum thickness of the matrix, i.e. points of closest approach of fibers. A simple statistical estimate of the mean minimum distance between fiber axes is $L = 1/\sqrt{N}$, where N is the number of fibers per unit area of composite surface when viewed normal to the fiber axis. Thus, the mean closest approach for fibers having radius a is $d = \frac{1}{\sqrt{N}} - 2a$. Expressing this in terms of the fiber volume fraction V_f, $d = a\left(\sqrt{\frac{\pi}{V_f}} - 2\right)$. For a weak fiber-matrix interface (i.e. interfacial stress $<<\sigma_m$), the transverse strength will be reduced by the ratio $\frac{d}{L}$; hence,

$$\sigma_t = \sigma_m \left(1 - \sqrt{\frac{4V_f}{\pi}}\right)$$

where σ_t = composite transverse tensile strength

σ_m = matrix tensile strength [8].

For the case where interface strength is greater than the matrix strength, the situation is complicated but it is reasonable to assume a rule of mixtures. Applying this rule, the composite transverse tensile strength is given by the following expression [8]:

$$\sigma_t = \sigma_m \left(1 - \sqrt{\frac{4V_f}{\pi}}\right) + \sigma_i' \left(\sqrt{\frac{4V_f}{\pi}}\right)$$

where σ_i' = average tensile stress necessary to separate the fiber from the matrix under transverse loading.

In a study of Thornel 50-epoxy composites, Elkin et al. [64] found that the transverse strength decreased as the fiber content

increased. From their results they concluded that the transverse tensile strength test is a sensitive one for assessing the condition of the interfacial bond.

2.4.5 Influence of Interfacial Bond Strength on the Composite Failure Modes

The bond quality at the interface plays a predominate role in determining the type of fracture surface that a composite will exhibit when loaded in the fiber direction. A strong interfacial bond generally yields a sharp, well-defined break while a poor bond results in progressive fracture, that is, bond failure, followed by matrix failure, and finally fiber failure [7,9].

Chamis [65] studied photomicrographs of graphite-epoxy composite fracture surfaces and observed that a strong, an intermediate, and a weak bond each result in a distinctly different fracture surface. Figure 2.6 schematically illustrates the three failure modes. Using optical and scanning electron microscopy, Bader et al. [63] observed the same three failure modes as Chamis but termed them "brittle," "progressive," and "multiple shear." Brittle fracture, characterized by a near planar fracture surface (Figure 2.6a) and very little fiber pullout, is associated with high interfacial strength, low fiber volume fraction, and low energy absorption. Composites exhibiting brittle fracture have high stiffness and static strength but tend to be notch-sensitive [7,32]. The specimen with intermediate bond strength, shown in Figure 2.6b, has an irregular fracture surface and some fiber pullout. This progressive mode is associated with moderate fiber volume fraction (0.4-0.6) and intermediate energy absorption. The

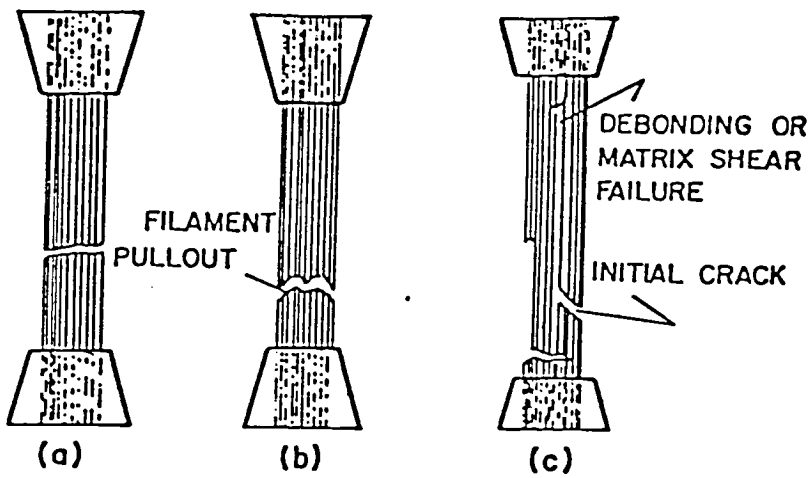

Figure 2.6 Longitudinal tensile failure modes. (a) Brittle, (b) brittle with filament pullout, (c) irregular [65].

fracture surface of the composite with a very poor interface bond is shown in Figure 2.6c and is characterized by pronounced irregularity and fiber pullout. This multiple shear mode shows extensive delamination and is associated with high energy absorption. Wadsworth and Spilling [66] observed that broken fibers recede within the matrix in composites having a weak interfacial bond.

When a composite is subjected to bending stresses, interface failure or overall composite failure may occur. Interface failure is undesirable because it does not allow the fibers to develop their full load-carrying ability. For a composite beam subjected to three-point bending, Greszczuk [9] reported that the interface strength required to obtain overall composite failure rather than interface failure is given by

$$\tau = \left(\frac{r}{L}\frac{E_f}{E_L}\right)\sigma$$

where r = fiber radius

L = span length

E_f = fiber modulus

E_L = composite modulus [given by rule of mixture $E_f k + E_m(1-k)$]

k = volume fraction of fibers

σ = maximum composite stress.

2.4.6 Mechanism of Load Transfer at the Interface

Figure 2.7 gives a mechanistic representation of load transfer in a short fiber composite under tensile stress for both an elastic and an inelastic matrix. In the case of an elastic matrix, interfacial shear stress increases rapidly to its maximum value then decays

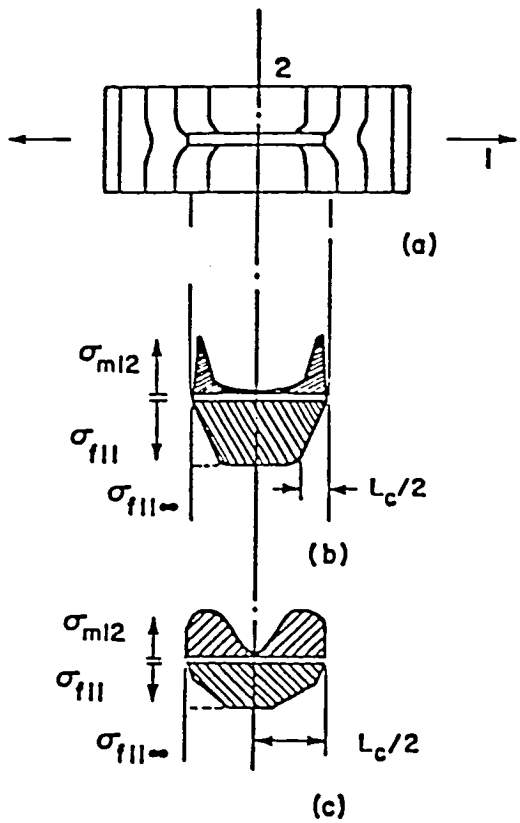

Figure 2.7 (a) Deformation model. Stress distribution at the interface produced by (b) elastic and (c) inelastic matrix. $\sigma_{m_{12}}$ denotes interfacial shear stress; $\sigma_{f_{11}}$ denotes fiber tensile stress [7].

rapidly away from the fiber end. The fiber axial stress increases rapidly to its average value and then remains constant. In the case of an inelastic matrix, interfacial shear stress increases to a value that will cause the interface or matrix to behave inelastically (plastically). The shear stress remains at this value for a distance along the fiber until the major portion of the load has been transferred to the fiber, then it decays rapidly [7,67].

The strength of the interface also affects the load transfer mechanism. If the interface is weak, when a fiber breaks the interface fails and the fiber ends recede in the hole in the matrix. The load is then transferred to other fibers over a long frictional transfer length. This length is much longer than the elastic transfer length required when interface failure does not occur. Neighboring fibers can shed almost all their increase in load to other fibers which are further away. Thus, a break in one fiber causes little increase in the load in others, and the crack does not spread. In this case, cracks in neighboring fibers are not correlated. In the case of a strong interface, load is transferred to nearby fibers over the same elastic transfer length as they need to shed it. This creates a large stress concentration and the crack is likely to propagate into adjacent fibers. Because of this, a different failure mode may result in composites with high fiber contents [66,67].

The critical fiber length is the length which is required for the fiber to develop its fully stressed condition in the matrix. This length is affected by the shear strength of the fiber-matrix interface, τ_i, and is defined as

$$\ell_c = \frac{\sigma_f r}{2\tau_i}$$

The ratio of the fiber length to the critical length is important since short fibers tend to be pulled out during fracture whereas long fibers will be broken. Critical fiber length can be determined by plotting load versus length/diameter (L/d_f) data from fiber pullout strength tests. Tensile failures denote fiber breaks while shear failures denote fiber pullout from the matrix. The intersection of the lines connecting these groups of points represents the critical fiber length. It should be noted that this length is very, very small — on the order of three fiber diameters [7,8].

2.5 Environmental Effects on the Fiber-Matrix Interface

One problem limiting the use of polymer-matrix composites is their poor reliability in wet environments, especially at elevated temperatures [7,68]. Moisture-induced composite failure involves both surface chemistry and fracture mechanics and is due to a decrease in interlaminar shear strength. Fiber composites also undergo strength reduction on aging in ambient conditions for extended periods of time. Like moisture-induced failure, this effect manifests itself mostly at elevated temperatures, and both resin and interface appear to contribute to the reduction in mechanical properties. The effect of temperature on composite interlaminar shear strength has also been investigated.

2.5.1 Moisture Sensitivity of Graphite Fiber Composites

It is well-documented that moisture has adverse effects on adhesive bonding [68-72]. Tests have shown that many variables such

as temperature, pH and ionic strength of the water, resin formulation, and surface constitution of the adherend influence the rate of bond degradation. Several investigators [70-72] have identified three general areas of water attack: the oxide surface of the adherend, the polymer immediately adjacent to the adherend, and bulk polymer away from the interface. Interfacial and bulk polymer are distinguished since the polymer near the adherend may have a different structure from the bulk.

A distinction should be made between the effect of water on the matrix alone and the effect of water on the interfacial region. This is difficult to do in an experimental study and many researchers tend to emphasize the interfacial attack. For example, using scanning electron microscopy, Patrick and co-workers [73] studied interfacial fracture surfaces and reported that the moisture-induced fracture appeared to have propagated at the resin-adherend boundary. It should be noted, however, that water sorption by the resin and the ensuing swelling can destroy the composite [7]. Whitney and Ashton [74] calculated that matrix swelling due to long-term moisture exposure could significantly affect laminate properties.

Ashbee and Farrar [75] and Farrar et al. [76] used an optical interference technique to detect changes in the physical state of the fiber-matrix interface due to water uptake. In this technique, a beam of light is internally reflected from the interfaces and interfacial changes are manifested by changes in transmitted light intensity. For opaque fibers such as carbon fibers, the resin is the transmission medium.

Water molecules can enter the epoxy resin either by activated diffusion or by flow in microcracks and capillaries. The presence of water is accompanied by swelling and plasticization, the latter evident by a reduction in the glass transition temperature of the resin. Elastic and possibly plastic strain builds up in the resin immediately adjacent to the fibers due to resin dimensional changes. Resin swelling, i.e. strain and rate of water uptake, may be deduced from measurements taken from photographs of the interference pattern of Newton's rings. The rate of chemical degradation due to moisture is slow if no free active groups or low molecular weight materials are present. In order for this to occur, however, the matrix must be cured completely and this is rarely achieved in practice. Dissolution of unreacted molecules and/or impurities can create pockets of pressure within the resin which can be sufficient to stabilize the growth of flat disc-shaped cracks. Farrar et al. [76] pointed out that the occurrence of these interfacial pressure pockets signals the onset of loss of load transfer.

Ashbee and Farrar [75] found that a significant concentration of diffused water had collected at the fiber-resin interface after 550 hours of exposure to distilled water at 95°C. This presumably implies the presence of solute at the interface or else there would be no thermodynamic driving force to cause precipitation of diffused water since carbon is normally hydrophobic.

It was initially believed that moisture would not cause strength reduction in graphite-epoxy composites at room temperature [77,78]. However, early experimental work involved composites with initially

low shear and flexural strengths. Later Scola [78] conducted boiling water experiments on high-shear-strength composites containing surface-treated fibers. When subjected to a 2-hour water boil, these composites suffered losses in room-temperature shear strength ranging from 14 to 27%. Farrar et al. [76] found that debonding of joints in boiling water is faster by a factor of 40 than debonding of joints in room temperature water.

When considering water sorption in the resin itself, it should be pointed out that microscopical studies [80,81] have shown that most resins are not homogeneous. Instead, they consist of regions of high-density polymer separated by narrow boundary regions of lower molecular weight material. This structure arises because polymerization initiates from random points and proceeds radially. As these regions approach each other, it is difficult for them to coalesce into a homogeneous network; hence, polymerization terminates, leaving unreacted or partially reacted material at the periphery, thus giving rise to the high-density regions. This low-molecular-weight material can exist at an interface as a thin film or as a channel between high-density regions, in either case, offering pathways for the easy entry of water into the interfacial region. When graphite fiber composites are exposed to high humidity or water immersion, the state of the interfacial bond depends on the degree of equilibration to the adverse environment [68].

Many commercial adhesives are able to resist loss of adhesion in the presence of moisture by maintaining non-equilibrium conditions at

the interface. They retain their useful lifetimes because of rate-limiting factors which include the following [43]:

(1) diffusion rate of water through the resin to the interface

(2) solubility of water in the resin

(3) elastic modulus of the resin, particularly in the region immediately adjacent to the interface

(4) surface topography (i.e. degree of roughness).

These factors are affected by the resin crosslink density. In general, diffusivity and solubility decrease with an increase in crosslink density while elastic modulus increases.

Voids created by entrapped air during composite fabrication are another cause for poor reliability in wet environments. When the composite is stressed, voids can initiate internal cracking, creating paths for the entry of moisture. While void size can be controlled by fabrication techniques, voids cannot be eliminated altogether. Bascom and Romans [82] report that microvoids are inherent whenever a viscous resin impregnates a strand or cloth of filaments since the resin is unable to completely displace the air between the filaments at normal rates of impregnation. Even in the absence of moisture voids have a detrimental effect on composite integrity and strength since they weaken the interfacial bond strength [7].

The results of Kaelble et al. [68] indicate that moisture degradation of interfaces in graphite-epoxy composites is essentially irreversible. Fiber-matrix bonding occurs before the epoxy matrix is crosslinked, therefore local stress relaxation processes allow rheological equilibrium at the bonded interface. After curing, the

matrix remains crosslinked and residual elastic stresses prevent rebonding of a damaged interface -- even when the resin temperature is raised above its glass transition point.

2.5.2 Interlaminar Shear Strength Degradation Due to Water Immersion

Kaelble et al. [68] used a dispersion-polar interaction model as the basis for predicting bond strength degradation upon water immersion of the fiber-matrix interface. Surface energy parameters which define this three-phase model were given by the following expressions:

$$\gamma_1 = \gamma_1^d + \gamma_1^P = \alpha_1^2 + \beta_1^2$$

$$\gamma_2 = \gamma_2^d + \gamma_2^P = \alpha_2^2 + \beta_2^2$$

$$\gamma_3 = \gamma_3^d + \gamma_3^P = \alpha_3^2 + \beta_3^2$$

where the subscripts 1, 2, 3 represent the matrix, environmental immersion phase, and the fiber, respectively, and the parameters $\alpha = (\gamma^d)^{1/2}$ and $\beta = (\gamma^P)^{1/2}$ were introduced for notational convenience. These six surface energy terms are included in the Griffith relation for critical stress σ_c for crack initiation as defined by

$$\sigma_c \left(\frac{\pi c}{2E}\right)^{1/2} = \gamma_G^{1/2} = (R^2 - R_o^2)^{1/2}$$

where γ_G = Griffith surface energy

$$R_o^2 = 0.25\ [(\alpha_1-\alpha_3)^2 + (\beta_1-\beta_3)^2]$$

$$R^2 = (\alpha_2 - H)^2 + (\beta_2 - K)^2$$

$$H = 0.50\ (\alpha_1 + \alpha_3)$$

$K = 0.50\ (\beta_1 + \beta_3)$

E = Young's modulus

c = crack length.

Assuming that changing the immersion environment from air to water did not significantly affect the modulus E or crack length c (i.e. $\pi c/2E$ constant), Kaelble et al. found the ratio of fiber-matrix debonding to be

$\sigma_c(H_2O)/\sigma_c(air) = 0.46$ for HTS-BP-907 composite. Hence, water substantially reduced the interfacial bond strength.

Kaelble et al. also postulated that fracture in interlaminar shear produced shear stresses which simultaneously fracture the fiber-matrix interface and the matrix itself. The composite interlaminar shear strength λ_b was obtained from the rule of mixtures

$$\lambda_b = f_I\lambda_I + f_m\lambda_m \qquad (2.3)$$

where λ_I = interfacial failure

λ_m = matrix failure

f_I = fractional area for interfacial failure

f_m = fractional area for matrix failure

and $f_I = 1 - f_m$. Assuming

$\lambda_{bo} = \lambda_{Io} = \lambda_{mo}$

$\lambda_{m\infty} = \lambda_{mo}$

then

$$\lambda_{I\infty} = \lambda_{Io}\,\frac{\sigma_c(H_2O)}{\sigma_c(air)}$$

where the zero subscript indicates no exposure to water and ∞

indicates infinite underwater immersion and substituting these into Equation 2.3, they obtained the following relation:

$$\frac{\lambda_{b\infty}}{\lambda_{bo}} = (1 - f_I) + f_I \frac{\sigma_c(H_2O)}{\sigma_c(air)}$$

This relation was used to predict the degradation of composite interlaminar shear strength due to water immersion. The analysis and experimental data indicate that exposure to moisture merely weakens rather than destroys the fiber-matrix shear bond strength. Kaelble et al. report that exposure to 95% relative humidity or water immersion at 100°C for times greater than 200 hours results in a 30 to 50% reduction in interlaminar shear strength.

2.5.3 Effect of Ambient Aging on Composite Strength

Forest [83] was the first to report the phenomenon of flexural and shear strength loss in composites due to aging under ambient conditions. He noticed that graphite-epoxy and boron-epoxy composites only showed degradation at elevated temperatures (>200°F) while glass-epoxy composites lost strength at room temperature. Tables 2.3 and 2.4 illustrate the flexural and shear strength losses for graphite- and boron-epoxy composites.

Scola [79] measured the short-beam shear strength of four ambient-aged graphite-polyimide composites at room temperature, 500°F, and 600°F. At room temperature, these composites suffered a maximum of 10% reduction in strength and some composites were not affected by ambient aging. The 500°F results were difficult to interpret. Some composites showed a 2-16% decrease while others showed a 10-21% increase in shear strength. Similarly, shear strength changes at

TABLE 2.3

Summary of selected literature data[a] on longitudinal flexural strength of ambient-aged graphite-epoxy resin composites [83]

Composite system fiber-resin[b]	Ambient aging (weeks)	350°F Flexural strength (ksi) Initial	After ambient aging	Percent decrease
HTS (c)-X-904[c,d]	1	115.1	117.0	None
HTS (s)-X-904[c,d]	2	104.7	63.7	39
HTS (s)-X-904[c,d]	5	155.2	112.0	38
HTS (s)-X-904[c,d]	30	123.5	69.7	44
GY-70 (c)-X-904[c,d]	6	69.2	48.6	30
HTS (c)-3002[d,e]	6	158.1	100.0	37
HTS (c)-3002[d,e]	6	158.0	161.0	None
HTS (c)-3002[d,e]	20	149.0	75.7	49
HTS (c)-1004[d]	15	151.8	120.2	21
GY-70 (c)-1004[d]	52	99.0	45.0	55
GY-70 (c)-1004[d]	10	69.2	48.6	30
HMS (c)-BP-907[f]	20	155.0	130.0	16
HTS (s)-experimental resin	6	192.5	186.8	3.4
HTS (s)-experimental resin	20	105.0	89.0	15
Morganite I (short)-E-293[d]	36	78.0	87.0	11.5
	36	93.0	84.0	9.7

[a] Forest (1970).
[b] (s) = staple, (c) = continuous.
[c] Tetrafunctional aromatic resin.
[d] Proprietary commercial resin.
[e] Cycloaliphatic plus epoxy novalak.
[f] Standard bisphenol-A epoxy resin, dicyandiamide, and polyvinylformal flexibilizer.

TABLE 2.4

Summary of selected literature data of shear strength of ambient-aged graphite-epoxy and boron-epoxy resin composites[a] [83]

Composite system fiber-resin	Ambient aging (weeks)	350°F Short-beam shear strength (Ksi)		
		Initial	After ambient aging	Percent decrease
HTS-3002[b]	3	9.0	3.2	66
	20	6.7	4.8	31
HTS-X-904[b,c]	6	5.7	4.7	18
B-epoxy	13	7.0	4.2	46

[a]Forest (1970).
[b]Proprietary commercial resin.
[c]Tetrafunctional aromatic resin.

600°F were erratic, with decreases ranging from 10-32% and increases from 9-55%. He suggested that differences in the void content of the composites may account for the inconsistencies in the data.

Scola also exposed ambient-aged graphite-polyimide composites to boiling water for one week. The results indicated that this treatment did not alter the room-temperature shear strength properties of the composite. Both ambient aging and boiling water affect the high-temperature strength of the composite but the extent of each varies from composite to composite. Comparing the high-temperature strength data for composites which had been aged 4 and 13 months to that of those aged 13-19 months indicated that a time period of at least one year was required for ambient aging to cause a strength reduction in graphite-polyimide composites.

There are several factors which may account for the variation in ambient-aged and boiling water strength losses of the various graphite-polyimide composites. One of these may be differences in the chemical composition of the polyimide resins, for example, polyimide 709 contained a silica filler. Another factor may be differences in the void content of the composites [7].

Scola proposed that three processes -- resin property changes, interface and fiber degradation, and resin stress relaxation -- are responsible for the ambient aging degradation of fiber-reinforced resin systems. First consider the resin property changes. The resin may simply become weaker due to ambient exposure. Moisture absorption by the resin would also affect its properties and thus any composite properties which require the matrix to carry a large portion of the

applied load. Strength reduction due to these factors would be expected to affect both room-temperature and elevated temperature composite properties, although not necessarily to the same extent. Another possible resin change is plasticization caused by water absorption. This may not cause a significant change in room-temperature resin properties but there would be a tendency for a decrease in modulus and an increase in elongation.

The magnitude of the effect of interface and fiber degradation depends strongly on the resin and fiber types. Moisture may reach the fiber-matrix interface either by diffusion through the resin or by migration along the fiber surface. In cases where the former mode is more detrimental to the composite strength than the latter, moisture-resistant resins would prevent or delay the degradation process.

As mentioned previously, residual stresses are produced at the interface during the fabrication process because of differences in thermal contraction between the fibers and the resin. These stresses can be compressive or tensile, depending on the expansion coefficients and the fiber volume fraction. Relaxation of the compressive stresses could be detrimental to the composite, particularly if they play an important role in aiding stress transfer. The process of resin stress relaxation as a factor contributing to the ambient-aging strength reduction of fiber composites appears to be real and should be investigated further to determine its relative importance in the degradation process.

2.5.4 Effect of Temperature on Graphite Fiber Composites

Daniels et al. [62] investigated the effect of temperature on interface bond strength by measuring the interlaminar shear strength. For a graphite-epoxy composite with fiber content of 50%, they found that the interlaminar shear strength remained approximately constant in the temperature range of -65 to 180°F then decreased rapidly and approached zero at 350°F. They concluded that interlaminar shear strength was insensitive to temperature rises to about one-half the composite cure temperature. The interface bond became progressively weaker above this temperature. Tests showed similar behavior for other parameters such as longitudinal compressive and flexural strength. The effects of temperature in combination with moisture have already been discussed in this review.

2.5.5 Effect of Radiation on Graphite Fiber Composites

Bullock and co-workers [84,85] conducted several studies on the effects of neutron radiation on the mechanical properties of graphite/epoxy composites. Graphite/epoxy composites were irradiated for 600 hours in air at ambient temperature in a mixed radiation (gamma and neutron) Ground Test Nuclear Reactor. Gamma doses of 2.7×10^{11} ergs/g (2700 Mrad) and 5.8×10^{11} ergs/g (5800 Mrad) had no effect on the tensile strength of the composites [84].

Unidirectional graphite/epoxy composites (HT-S*/ERLA 4617) irradiated to 2700 Mrad in air at ambient temperature and in liquid nitrogen at -196°C had lower longitudinal flexural strength (20%) and transverse strength (85%) than the unirradiated specimens when tested at room temperature. After further radiation exposure (to 5800 Mrad),

longitudinal flexural strength decreased to a level 70% lower than the control, but transverse strength did not undergo any further change. Bullock [85] concluded that only moderate transverse flexural strength was required for good translation of fiber strength into composite longitudinal strength and that matrix strength was not as critical to composite strength as fiber-matrix bonding. On the other hand, Bullock found that the longitudinal flexural strength of the composites increased 80% after exposure to 8900 Mrad in liquid nitrogen at -196°C when tested at this same temperature. He suggested that the increase was probably caused by a radiation-induced lowering of the interlaminar shear strength which was too high for specimens in liquid nitrogen prior to irradiation.

Arrington and Harris [86] exposed unidirectional carbon fiber/epoxy composites to a 300 rad/s gamma flux for 16 days then measured the interlaminar shear strength using a three-point bending test. They found a slight increase in strength with radiation exposure but the average work of fracture was reduced. They suggested that radiation increased the matrix crosslink density, thus stiffening it.

After exposing unidirectional graphite/epoxy composites (AS/3002) to nuclear radiation (neutron and gamma) up to 2.6 Mrad, Lackman et al. [87] concluded that there was no degradation in longitudinal flexural strength, transverse strength, or horizontal shear strength.

Naranong et al. [88] and Fornes et al. [89] found that electron radiation in doses up to 5×10^9 rad in the absence of oxygen had no

adverse effects on the ultimate stress and modulus of unidirectional graphite fiber composites. In the latter investigation, scanning electron microscopy revealed very little morphological differences in ruptured control and irradiated samples.

The components of graphite/epoxy composites have been shown to be radiation-resistant as separate entities. Parkinson and Sisman [90] reported that polymers containing aromatic rings are highly resistant to radiation because of their ability to absorb and dissipate energy without bond disruption. They found that aromatic amine-cured epoxy retained more than 80% of its initial strength when irradiated in air with gamma radiation and neutrons up to 100 Mrad from a nuclear reactor. Bullock [91] found an increase of 30% in the tensile strength of graphite fibers after neutron irradiation. He also demonstrated that this enhanced property translates into epoxy laminates reinforced with these fibers and irradiation improves the strength of the fiber-matrix interface as indicated by increased short-beam shear strengths [92].

3. EXPERIMENTAL PROCEDURE

Two types of graphite fiber reinforced composites were used in this study, namely T300/5208 and C6000/PMR 15. The T300/5208 samples were available in four different constructions - uniaxial with the fiber axis lying in the longitudinal direction of the composite, uniaxial with the fiber axis lying in the transverse direction of the composite, 0/± 45/0 crossply, and 90/±45/90 crossply. The C6000/PMR 15 samples were available in both the longitudinal and transverse uniaxial constructions. The sample dimensions were approximately 2.54 cm x 1.27 cm x 0.053 cm. All samples were fabricated, cured, and cut at NASA Langley Research Center, Hampton, Virginia. The samples were exposed to various levels of 0.5 MeV electron radiation with the maximum dose being 10,000 Mrad. A few samples were exposed to 1.6 MeV proton radiation and received doses of either 10,000 or 40,000 Mrad. The effects of electron irradiation on the mechanical properties (ultimate stress and Young's modulus) of the composites were evaluated using a three-point bending test as prescribed by ASTM D-790 and adapted to an Instron testing machine. The interlaminar shear strength of the composites was determined by the interlaminar shear test described in ASTM D-2733. Scanning electron microscopy was used to assess any visual differences between ruptured control samples and those exposed to radiation. Electron spectroscopy for chemical analysis (ESCA) was also used to examine the composite samples.

3.1 Materials

3.1.1 T300/5208

This graphite/epoxy composite is composed of Union Carbide Thornel 300 graphite fiber and NARMCO 5208 epoxy resin. Thornel 300 is a 3000-filament strand with each filament having a diameter of 7 microns. The strand breaking strength is reported to be 408 x 10^3 psi and the elastic modulus is 33.2 x 10^6 psi. The fibers have been treated with an epoxy compatible sizing to develop high interlaminar shear strength in resin matrix composites [93]. NARMCO 5208 consists of tetraglycidyl-4,4'-diamino diphenyl methane (TGDDM) cured with 4,4'-diamino diphenyl sulfone (DDS) [94,95]. The structures of these components are as follows [95,96]:

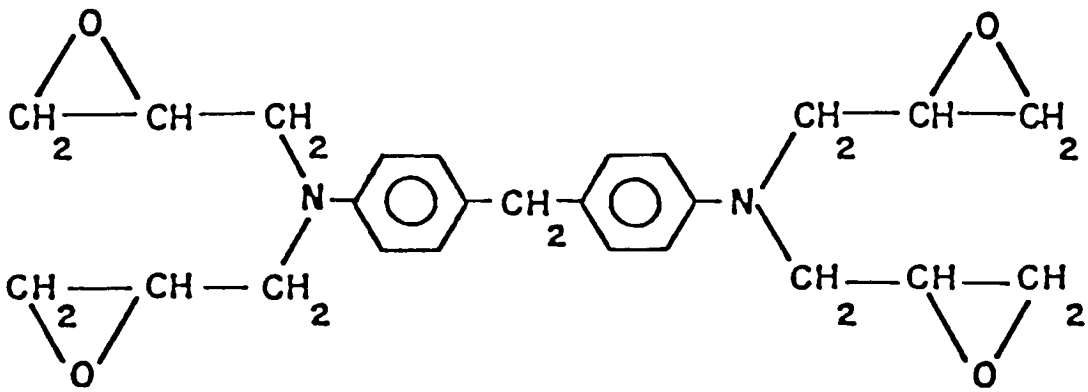

Tetraglycidyl-4,4'-diamino diphenyl methane (TGDDM)

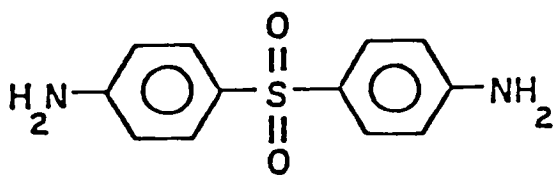

4,4'-diamino diphenyl sulfone (DDS)

Carter et al. [97] reported the glass transition temperature of NARMCO 5208 to be 196°C while Bascom et al. [94] found it to be 260°C.

By monitoring the tensile mechanical properties of the TGDDM-DDS epoxy system as a function of temperature in the range of 23°-250°C, Morgan and O'Neal [96] concluded that a broad glass transition exists in the 200°-250°C temperature range. They also measured Tg as a function of initial DDS concentration and for 27 wt% DDS they found Tg to be about 240°C.

3.1.2 C6000/PMR 15

This graphite/polyimide composite is composed of Celanese Celion 6000 graphite fiber and PMR 15 polyimide resin matrix. PMR 15 is a thermosetting resin developed by NASA and manufactured by Ciba Geigy Corporation [94]. The general structure of polyimide is given below [95]:

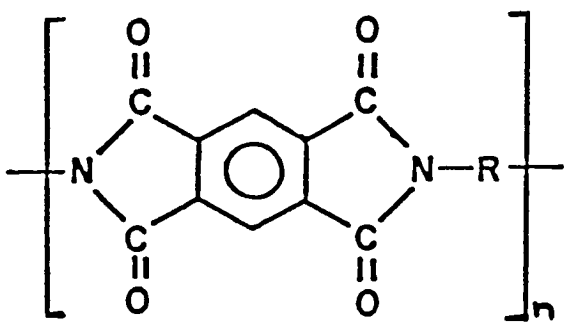

PMR 15 is prepared from 5-norbonene-2,3-dicarboxylic anhydride (NBA), 3,3',4,4'-benzophenone tetracarboxylic dianhydride (BTDA) and 4,4'-methylene dianilene (MDA). The NBA and BTDA are dissolved in methanol. The MDA is dissolved in methanol then added to the anhydride mixture. Most of the methanol is removed by vacuum evaporation at low temperature (30-40°C). The remainder is removed by heating at higher temperatures (130-145°C) for one hour in an evacuated oven. This produces a glassy foam which should be post-cured for 16 hours at 316°C to form the cured polyimide matrix [94,95].

Bascom et al. [94] report the glass transition temperature of PMR 15 to be 350°C.

3.2 Pre-Conditioning

In order to most nearly simulate the vacuum environment of space, samples were pre-conditioned and packaged in the following manner. First the samples were placed in Petri dishes and pre-vacuumed for one week in a heated vacuum desiccator at 80°C. Then they were placed in rows on aluminum foil (Heavy Duty Reynolds Wrap®) and held in place with narrow strips of masking tape. As shown in Figure 3.1, the foil was then folded to form a package and the edges were sealed with epoxy glue. Prior to sealing the package a glass tube was extended from it to allow a direct vacuum line to be connected later. The foil packages were pre-vacuumed for one week in a heated vacuum desiccator at 80°C. Immediately prior to irradiation the packages were vacuumed directly through the glass tube then heat-sealed.

The samples to be used in the electron spectroscopy for chemical analysis (ESCA) examination were thoroughly washed with acetone prior to the pre-vacuum treatment to remove surface contamination. After this the samples were handled only with tweezers with care being taken not to touch them.

3.3 Irradiation Procedures

3.3.1 Electron

The radiation source was an electron accelerator manufactured by High Voltage Engineering Corporation and located in the School of Textiles, North Carolina State University. It was operated at 500 kilovolts (from an insulated core transformer) with a beam current of

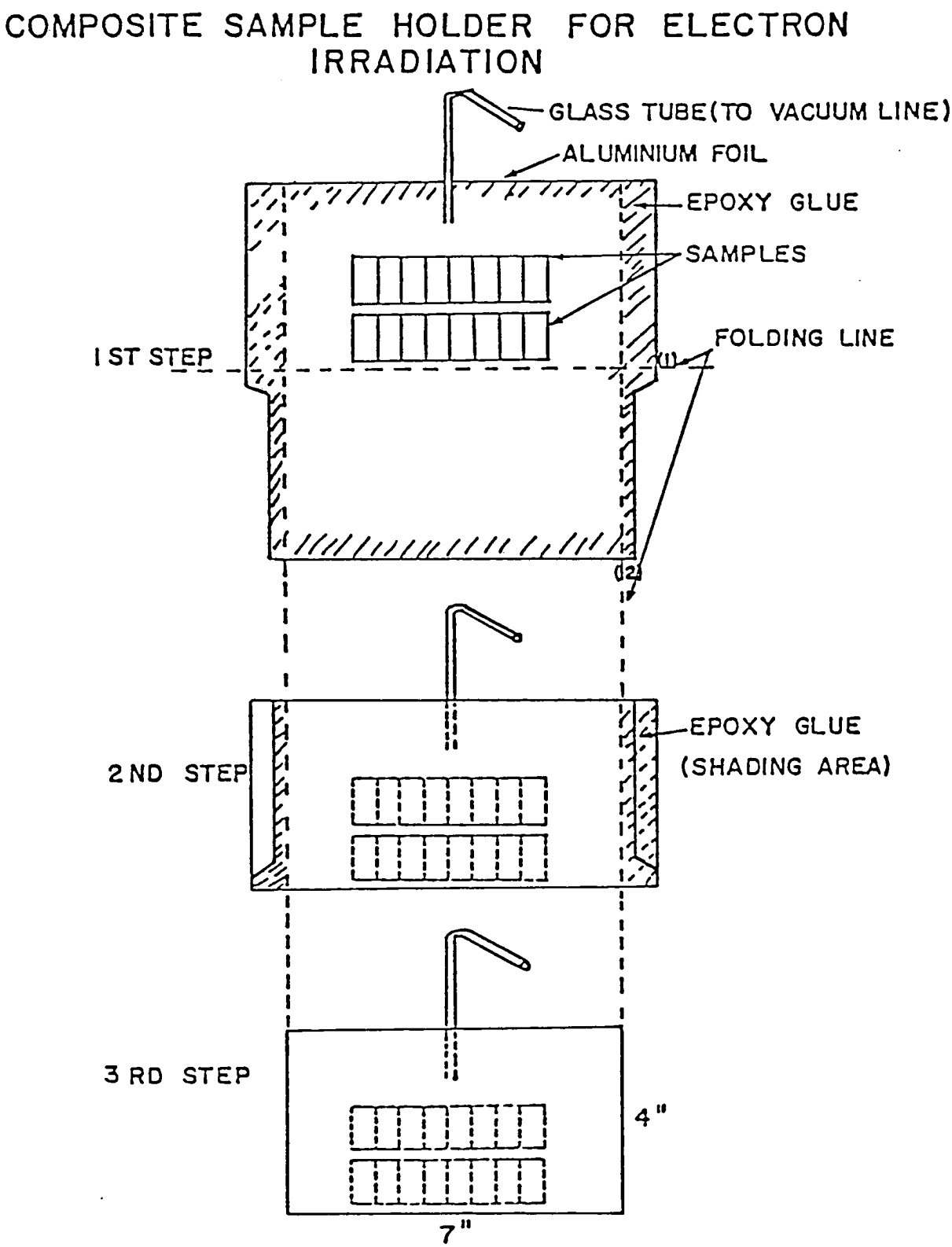

Figure 3.1 Preparation of sample package for electron irradiation [95].

8.3 milliamperes. This instrument utilizes a horizontal beam scanned to 48" by 6" [95]. The samples are hung on a moving conveyor which carries them through the cabinet housing the beam. After passing in front of the beam window, the conveyor track makes a loop and passes the window again; hence, the samples receive half their total exposure from each side. With a conveyor speed of 10 ft/min each revolution through the cabinet results in a 10 Mrad dosage.

Immediately after pre-conditioning, the sealed foil packages were placed in nitrogen-filled Ziploc Baggies® (polyethylene bags by Dow Chemical Corporation) for irradiation. One set of pre-vacuumed samples was attached inside Ziploc Baggies® using masking tape and was irradiated in air. All control samples were kept in the heated vacuum desiccator at 80°C during the course of the irradiation procedure.

In order to determine the actual dose a sample received during one pass through the electron accelerator a standard calibration curve was obtained by irradiating radiachromic films (nylon film containing aminotriphenylmethane dye derivatives made by Far West Technology, Inc.). These initially colorless films undergo radiation-induced coloration by photoionization and this change is a direct function of the radiation exposure received. Thus, the color intensity or optical density (OD) is a means of measuring the amount of incident radiation. By calculating the change in optical density from readings before and after radiation exposure one can construct a response curve of ΔOD vs. dose from a series of known irradiations [98]. This plot of known irradiations can be used to determine unknown doses. The calibration

curve, shown in Figure 3.2, was constructed using the Gamma Cell 220, Cobalt 60 source with known dose rate of 0.197 Mrad per hour. The optical density measurements were made on a Radiachromic Reader - 91R (by Far West Technology, Inc.) using the "hi" range (510 nm wave length).

3.3.2 Proton

The radiation source was a proton accelerator manufactured by High Voltage Engineering Corporation and located in the Department of Physics, North Carolina State University. It was operated with an energy of 1.6 MeV and a beam current of 200 nanoamperes. The sample holder had a capacity of six and a slide mechanism enabled each of the six samples to, in turn, be the target of the beam. Thus the samples received their total dosage in a continuous exposure - 1 hour for the 10,000 Mrad samples and 4 hours for the 40,000 Mrad samples.

3.4 Mechanical Tests

After irradiation, the samples were conditioned in the physical testing laboratory at standard conditions (70°F, 65% RH) for a minimum of two weeks before mechanical tests were performed. A three-point bending test was used to evaluate the ultimate stress and modulus of the composites. Because it is a convenient method for determining environmental effects, the interlaminar shear test was selected to assess the interfacial bond strength.

3.4.1 Three-Point Bending Test

The three-point bending test is a flexural strength test used to determine the ultimate stress and average modulus. In this test the

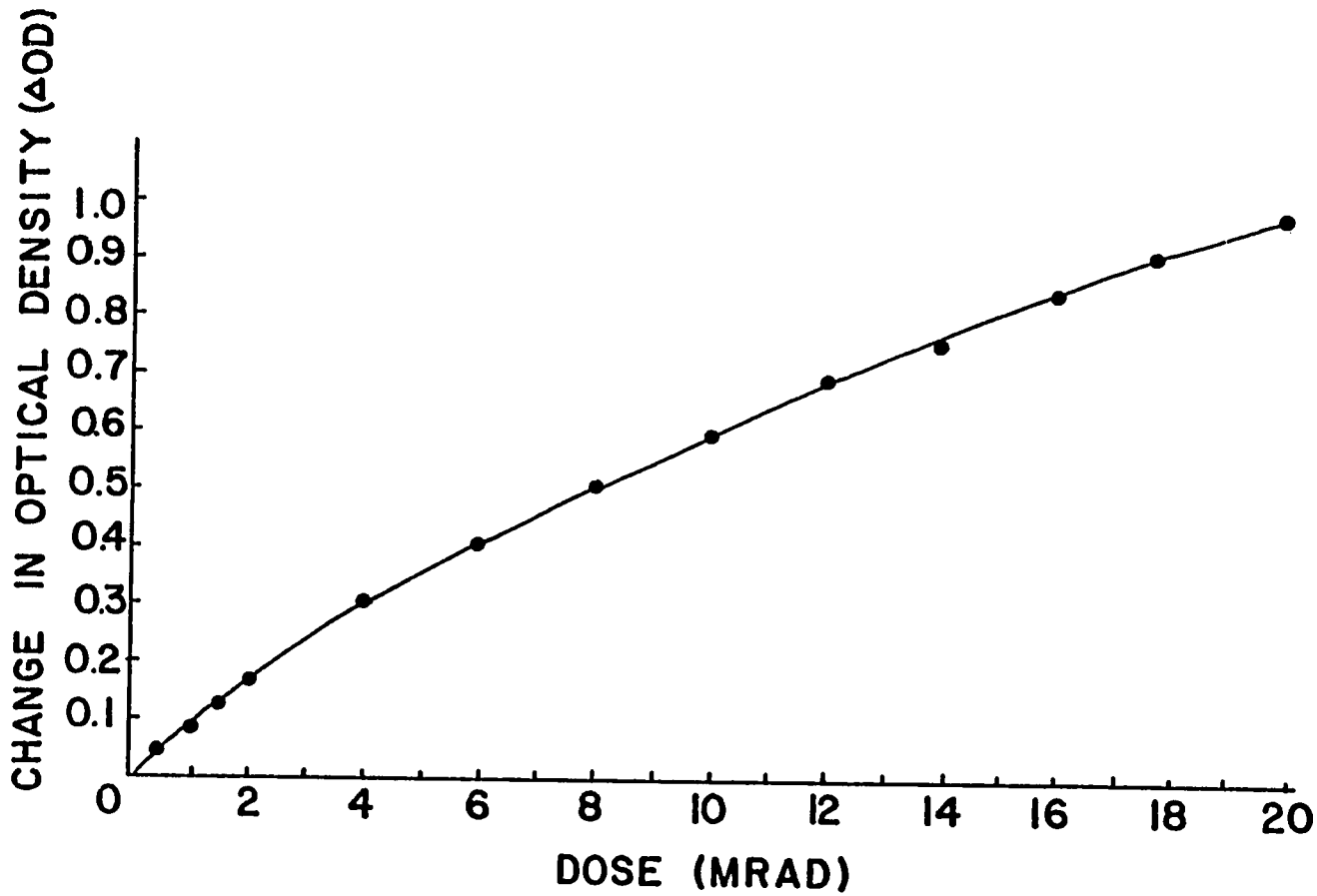

Figure 3.2 Calibration curve of known dose (from Gamma Cell-220) versus change in optical density.

composite sample is supported by two stationary noses which are a fixed distance apart. This distance is referred to as the span length. A third nose, the loading nose, moves at a constant rate and strikes the sample midway between the supports, thus applying a load to it. As seen in Figure 3.3, the load is applied perpendicular to the plane of the composite. The sample is deflected until rupture occurs in the outer fibers. According to ASTM D-790-71 [99], the maximum stress in the outer fibers (composite ultimate stress) can be calculated by the following equation:

$$S = \frac{3PL}{2bd^2} \tag{3.1}$$

where S = stress in the outer fibers at midspan

P = load at break

L = span length

b = width of sample

d = depth or thickness of sample.

The average modulus of the composite is given by the following relation [99]:

$$E = \frac{SL^2}{6d\varepsilon} \tag{3.2}$$

where E = average modulus

ε = deflection.

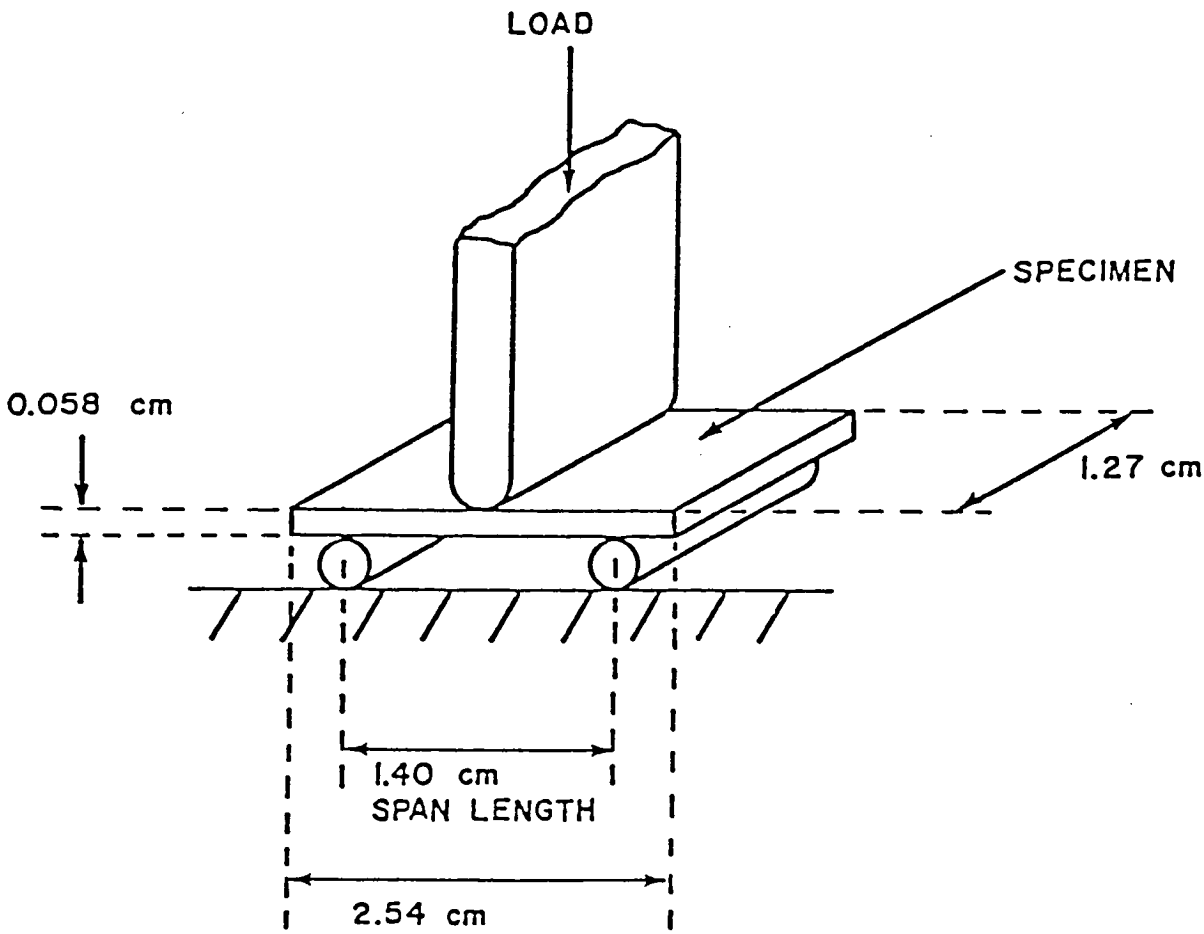

Figure 3.3 Diagram of a three-point bending tester, with a specimen in place [95].

A special device, shown in Figure 3.4, was built so that an Instron tensile testing machine could be used for this test. A compression load cell with maximum load range of 200 lbs and a crosshead speed of 0.1 in/min (0.254 cm/min) were used. The span length was 0.55 in (1.40 cm). The load required to rupture the sample, P, was determined from the Instron load-deflection plot then the composite ultimate stress was determined from Equation 3.1. Using this and the deflection, the average modulus of the composite was determined from Equation 3.2.

3.4.2 Interlaminar Shear Test

The interlaminar shear test is an indirect method for assessing interfacial bond strength. Interlaminar shear strength is defined by ASTM D-2733 [100] as the shear strength at rupture in which the plane of fracture is located between the layers of reinforcement of a plastic reinforced structure.

The test specimen, shown in Figure 3.5, is a flat coupon with a saw cut on each face having a depth which is half the total laminate thickness. These saw cuts are parallel to each other and, according to ASTM D-2733 [100], are spaced 1/2 inch apart. The specimen is gripped in the clamps of an Instron tensile tester and slowly extended at a constant rate. Due to the saw cuts, shearing occurs and the total applied load is registered by the Instron. For this test the Instron was interfaced with a Microcon microprocessor which gave a digital read-out of the applied load. The interlaminar shear strength S can

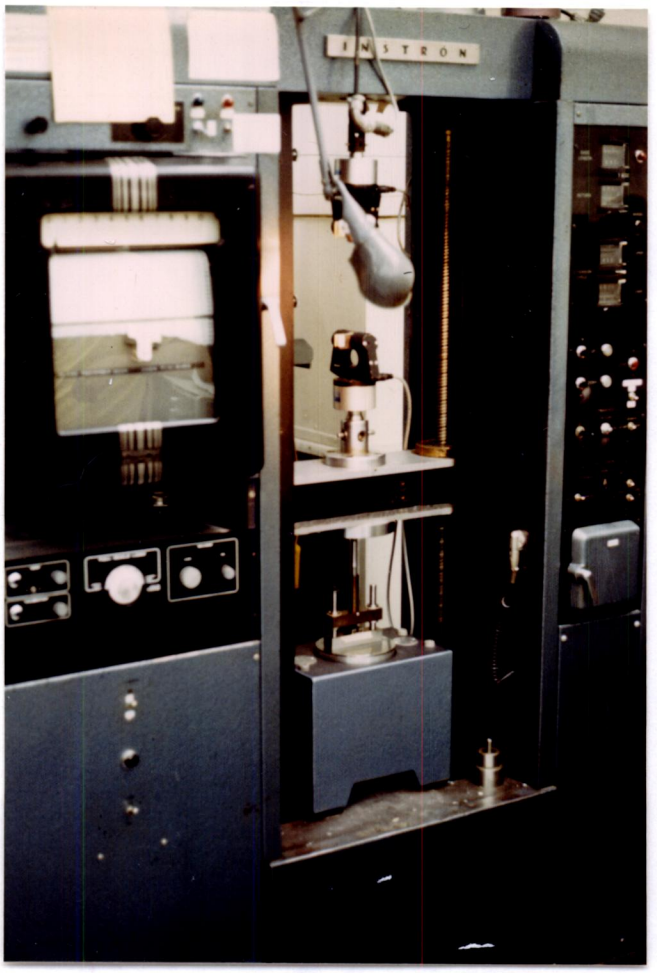

Figure 3.4 Photograph of three-point bending tester attached to Instron machine.

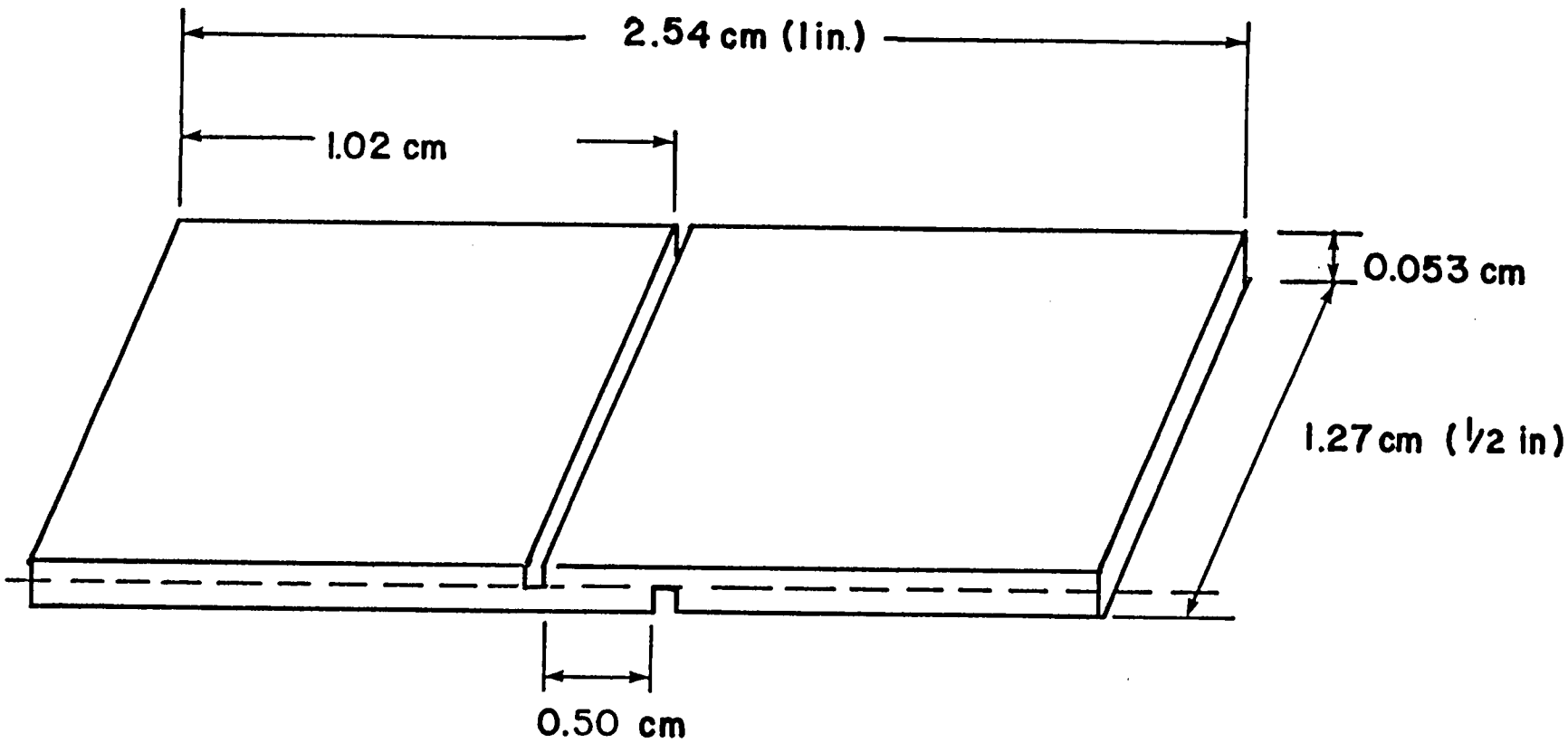

Figure 3.5 Dimensions of specimen for interlaminar shear test for composites.

then be determined by the following relation [100]:

$$S = \frac{P}{Wa} \tag{3.3}$$

where P = total applied load

W = width of specimen

a = distance between sawcuts.

Since the specimens were fabricated and pre-cut at NASA Langley Research Center, the specimen dimensions for this test were modified from those prescribed by ASTM D-2733. The specimen dimensions used were approximately 2.54 cm x 1.27 cm x 0.058 cm. The gauge length was 15.88 mm (5/8 inch) and the crosshead speed was 5 mm/min (0.2 in/min). A preliminary experiment was conducted in order to determine the optimum saw cut separation distance. Based on the values of standard deviation and coefficient of variation, a saw cut separation distance of 0.50 cm was selected.

To ensure precision-depth cutting and smoothness of the grooves, a special cutting device was built and is shown in Figure 3.6. This device incorporates a 6" Raytech diamond-edged circular blade. The blade height is adjustable in order to adapt to differences in specimen thickness.

3.5 Characterization Techniques

3.5.1 Scanning Electron Microscopy

Scanning electron microscopy was used to study the fracture surfaces of the ruptured composite specimens. This technique is useful in surface studies since the image is produced from signals from

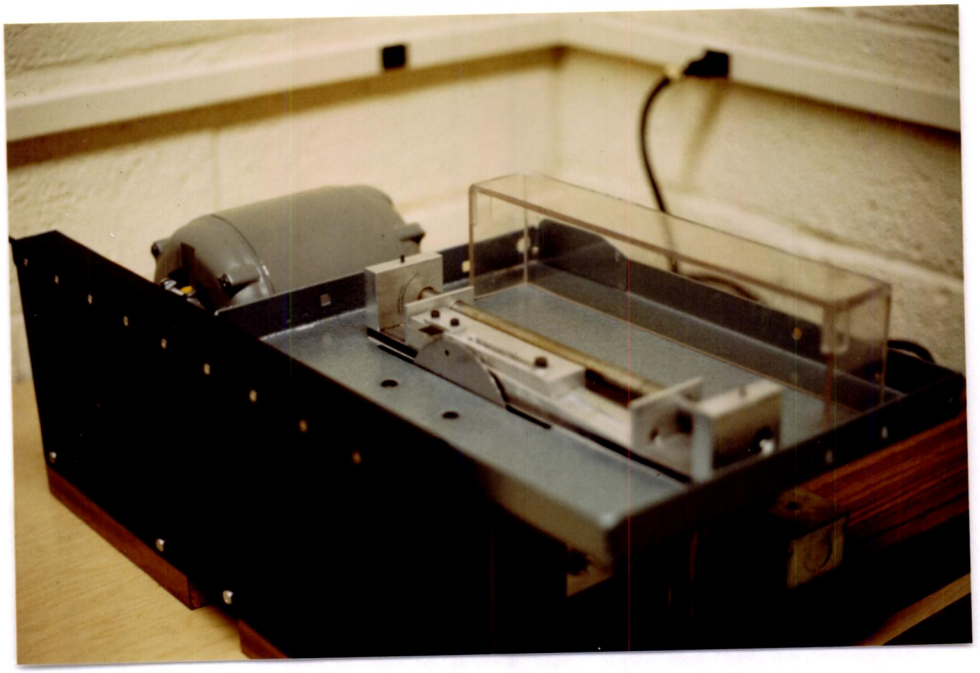

Figure 3.6 Photograph of diamond saw used to cut specimens for interlaminar shear test.

secondary and backscattered electrons rather than transmitted electrons.

In a typical scanning electron microscope (SEM) an electron beam is produced by an electron gun and focused by multiple condenser lenses. Two sets of scan coils deflect the beam back and forth across the specimen. The signals from secondary and backscattered electrons are collected by a detector then amplified and sent to a cathode-ray tube (CRT) where the image is displayed. The scan coils and the CRTs are powered by the same scan generator so the image is formed in synchronization with the mapping of the specimen [101].

The SEM used in this investigation was an ETEC Autoscan located in the Department of Biological Sciences, North Carolina State University. It had a useful magnification range of 20-100,000X. It was operated with an accelerating voltage of 20 kilovolts to give the best resolution.

The specimens were mounted on the microscope stubs using DAG 154 (graphite in isopropyl alcohol). Due to the high volume fraction of graphite fibers present (~67%) and their high degree of conductivity, it was not necessary to coat the specimens to prevent charging during beam exposure.

Photomicrographs were taken using Polaroid® type 55 film. These were taken in the magnification range of 700-7,000X. These micrographs were used to make a visual assessment of the fiber-matrix bonding characteristics.

3.5.2 Electron Spectroscopy for Chemical Analysis (ESCA)

Electron spectroscopy for chemical analysis is the determination of the photoelectron spectra created by irradiation of the sample with monoenergetic x-rays. Monochromatic x-ray photons of quantum $h\nu$ are directed onto the sample. The photons are absorbed by sample atoms with each absorption event resulting in the emission of an electron. The ejected electrons pass into the energy analyzer of the electron spectrometer where the kinetic energy of the photoelectron is sorted and detected [102]. The energies of the photoelectrons are related to the energies of the incident x-rays by the following expression [103,104,105]:

$$E_{h\nu} = E_b + E_k + \phi_{sp}$$

where $E_{h\nu}$ = energy of incident x-rays

E_b = binding energy of ejected electron

E_k = kinetic energy of ejected electron

ϕ_{sp} = work function of the spectrometer material (normally incorporated in the spectrometer calibration procedure).

Since the x-ray energy is known and the kinetic energy is measured with the electron spectrometer, the binding energy of the electron in the atomic orbital can be obtained. The spectrometer then provides a suitable output of signal intensity as a function of electron binding energy.

The effect is confined to the outer layers of the sample surface since the escape depth of the photoelectrons will be limited to a few

Ångstroms. Recent work has shown that typical sampling depths (more explicitly defined as the electron mean free path) are in the range of 5-25 Å for metals and metal oxides, while values ranging from 40 to 100Å are common for organic and polymeric materials. The mean free path is a function both of sample composition and of the kinetic energy of the escaping electons. Thus, the effective sampling depth may not be exactly the same at all points on the sample surface. It should also be remembered that a larger portion of ESCA signal comes from atoms near the surface since electrons emitted from them have a higher probability of escape [102,105].

A characteristic which sets ESCA apart from other well known surface characterization techniques is the chemical shift effect. A decrease in electron density in the valence region around an atom in a molecule produces an increase in the binding energy of core level electrons. Thus, binding energy shifts can be readily interpreted in terms of well understood chemical concepts [105]. Chemical shifts can be correlated with oxidation state, or more precisely with atomic charge. They are also related to functional groups in organic molecules [102]. In general, atoms with highly electronegative substituent groups can be expected to exhibit higher binding energies than the same atoms bound to groups with lower electronegativity. Consequently, substitution of highly electronegative elements, such as fluorine, will induce the largest chemical shifts. Since the atomic structure of each element in the periodic table is distinct from all the others, the accurate measurement of peak positions allows the ready identification of an element present at a sample surface. Each element

of a compound produces at least one electron line in the spectrum, except for hydrogen which is not detected by ESCA. Lines from adjacent elements are widely separated and since it is possible to resolve electron binding energies to ± 0.1eV, there is no ambiguity in identification of adjacent elements [102,105].

Since ESCA uses a photon probe it is much less destructive than techniques such as Auger electron spectroscopy which use an electron probe. This can be a great advantage if the signal intensity is weak since signal averaging can be used without concern that the sample surface is changing as a function of experiment time [105].

The ESCA analysis for this investigation was performed on a Physical Electronics electron spectrometer located in the Department of Chemistry, University of North Carolina at Chapel Hill. Prior to examination, the surface of the composite sample was washed with acetone. The sample was first placed in the pre-vacuum chamber of the spectrometer then in the vacuum chamber which had a pressure of approximately 10^{-9} torr. A general survey scan plotting intensity versus binding energy was made to identify the elements present at the sample surface. A low energy survey scan was made to enlarge the region below 280 eV so that the peaks in this region were more distinguishable. A high resolution window was plotted for the peak of each element present. A computer interfaced with the spectrometer calculated the area under each peak. Atomic ratios were obtained by dividing this area by the number of scans and the atomic sensitivity factor. The number of scans was 6 for most elements but for a few low-

intensity elements either 12 or 20 scans were made. The atomic sensitivity factors were referenced to fluorine; i.e., fluorine was assigned an atomic sensitivity of one and all other elemental sensitivities were relative to this number.

4. RESULTS AND DISCUSSION

In the initial phase of this investigation the long-term effects of radiation on the mechanical properties of graphite fiber composites were examined. A three-point bending test was used to evaluate the ultimate stress and average modulus of the composites. Based on the results of this experiment, the focus of the investigation was directed to interfacial aspects of composites. The techniques used in this phase were transverse tensile test, interlaminar shear test, scanning electron microscopy, and electron spectroscopy for chemical analysis (ESCA). Results obtained from each of these methods of characterization will be discussed separately.

The statistical analysis was performed using the programming package SAS (Statistical Analysis System). The effects of radiation were analyzed using analysis of variance (ANOVA) and Duncan's multiple range analysis. In the Duncan analysis, means that are characterized by the same letter are not significantly different. The 95% confidence interval limits are calculated by the following expressions:

$$UCL = \bar{X} + t_{.05}\, s_{\bar{X}}$$

$$LCL = \bar{X} - t_{.05}\, s_{\bar{X}}$$

where UCL = upper confidence limit

LCL = lower confidence limit

$\bar{X}$ = mean value of trial repetitions

$t_{.05}$ = statistical value from student's t-distribution

$s_{\bar{X}}$ = standard error of mean.

4.1 Three-Point Bending Test

4.1.1 T300/5208

Three different constructions of T300/5208 samples were irradiated by 0.5 MeV electron radiation. The maximum dosage for all types was 10,000 Mrad except for the T300/5208 longitudinal samples which were irradiated to 8000 Mrad. The ultimate stress and average modulus were calculated by computer using Equations 3.1 and 3.2. The average values of stress and modulus for each radiation level are given in Tables 4.1-4.2 along with the standard deviations and coefficients of variation of these parameters. Breaking stress as a function of radiation dose is shown graphically in Figures 4.1-4.3; similarly, average modulus is shown in Figures 4.4-4.6.

All irradiated samples show an increase in stress compared with the control. For the longitudinal samples and the 0/±45/0 crossplies the increase is slight, approximately 5% in each case. The 90/±45/90 crossplies exhibit a more marked increase with the 10,000 Mrad value being 30% higher than the control value. These increases are statistically significant at the 5% level. The modulus values of all constructions remain approximately constant regardless of radiation level.

As mentioned in Section 3.3.1, one set of T300/5208 longitudinal samples was irradiated in air rather than in the simulated vacuum environment. There are no significant differences (at the 5% level) between stress or modulus values of samples irradiated in air and those irradiated in vacuum.

Table 4.1 Ultimate stress of T300/5208 composites as a function of radiation level

Sample Construction	Radiation Dose (Mrad)	No. of Specimen	Ultimate Stress (kg/cm^2)	Standard Deviation	% CV	Duncan Analysis 5%	Duncan Analysis 10%
T300/5208 longitudinal (irradiated in vacuum)	0	8	21,825	613	2.8	C	D
	500	8	22,265	811	3.6	BC	CD
	1000	8	22,465	669	3.0	BC	BCD
	2000	8	22,439	608	2.7	AB	BC
	3000	8	22,818	1075	4.7	AB	AB
	4000	8	22,672	348	1.5	AB	AB
	5000	8	22,848	608	2.7	AB	AB
	6500	8	22,657	802	3.5	AB	AB
	8000	8	22,878	552	2.4	A	A
0/±45/0	0	8	16,888	619	3.7	CD	DE
	1000	8	16,727	991	5.9	D	E
	2000	8	17,326	609	3.5	ABCD	ABCDE
	3000	8	17,012	588	3.5	BCD	CDE
	4000	8	17,636	638	3.6	ABC	ABC
	5000	8	16,822	574	3.4	CD	DE
	6500	8	17,230	523	3.0	ABCD	BCDE
	8000	8	17,480	556	3.2	ABCD	ABCD
	9000	8	17,913	1127	6.3	A	A
	10,000	8	17,761	690	3.9	AB	AB
90/±45/90	0	8	2521	72	2.9	E	D
	1000	8	2831	102	3.6	BCDE	BC
	2000	8	2861	170	5.9	BCD	BC
	3000	8	2665	123	4.6	DE	CD
	4000	8	2504	425	17.0	E	D
	5000	8	2752	295	10.7	CDE	CD
	6500	8	3141	180	5.7	AB	A
	8000	8	3073	410	13.3	ABC	AB
	9000	8	3325	471	14.2	A	A
	10,000	8	3277	373	11.4	A	A

Note: In the Duncan analysis means with the same letter are not significantly different.

Table 4.2 Average modulus of T300/5208 composites as a function of radiation level

Sample Construction	Radiation Dose (Mrad)	No. of Specimen	Average Modulus (kg/cm^2)	Standard Deviation	% CV	Duncan Analysis 5%	Duncan Analysis 10%
T300/5208 longitudinal (Irradiated in vacuum)	0	8	1,408,501	47,295	3.4	A	A
	500	8	1,421,787	48,211	3.4	A	A
	1000	8	1,428,193	58,517	4.1	A	A
	2000	8	1,412,001	46,922	3.3	A	A
	3000	8	1,410,784	95,704	6.8	A	A
	4000	8	1,424,479	48,820	3.4	A	A
	5000	8	1,432,430	64,068	4.5	A	A
	6500	8	1,385,924	61,759	4.5	A	A
	8000	8	1,407,531	36,386	2.6	A	A
0/±45/0	0	8	1,012,216	37,309	3.7	A	A
	1000	8	1,009,697	40,143	4.0	A	A
	2000	8	1,000,179	48,575	4.9	AB	A
	3000	8	999,402	26,504	2.7	AB	A
	4000	8	996,874	29,251	2.9	AB	A
	5000	8	950,767	60,231	6.3	B	B
	6500	8	1,007,020	39,790	4.0	A	A
	8000	8	1,017,835	42,785	4.2	A	A
	9000	8	1,025,759	48,817	4.8	A	A
	10,000	8	1,015,675	72,720	7.2	A	A
90/±45/90	0	8	43,254	2277	5.3	A	B
	1000	8	44,796	2605	5.8	A	AB
	2000	8	45,780	2578	5.6	A	AB
	3000	8	43,651	2294	5.3	A	AB
	4000	8	43,944	5337	12.1	A	AB
	5000	8	44,915	4729	10.5	A	AB
	6500	8	43,893	1798	4.1	A	AB
	8000	8	45,562	5868	12.9	A	AB
	9000	8	46,653	3565	7.6	A	AB
	10,000	8	47,259	3078	6.5	A	A

Note: In the Duncan analysis means with the same letter are not significantly different.

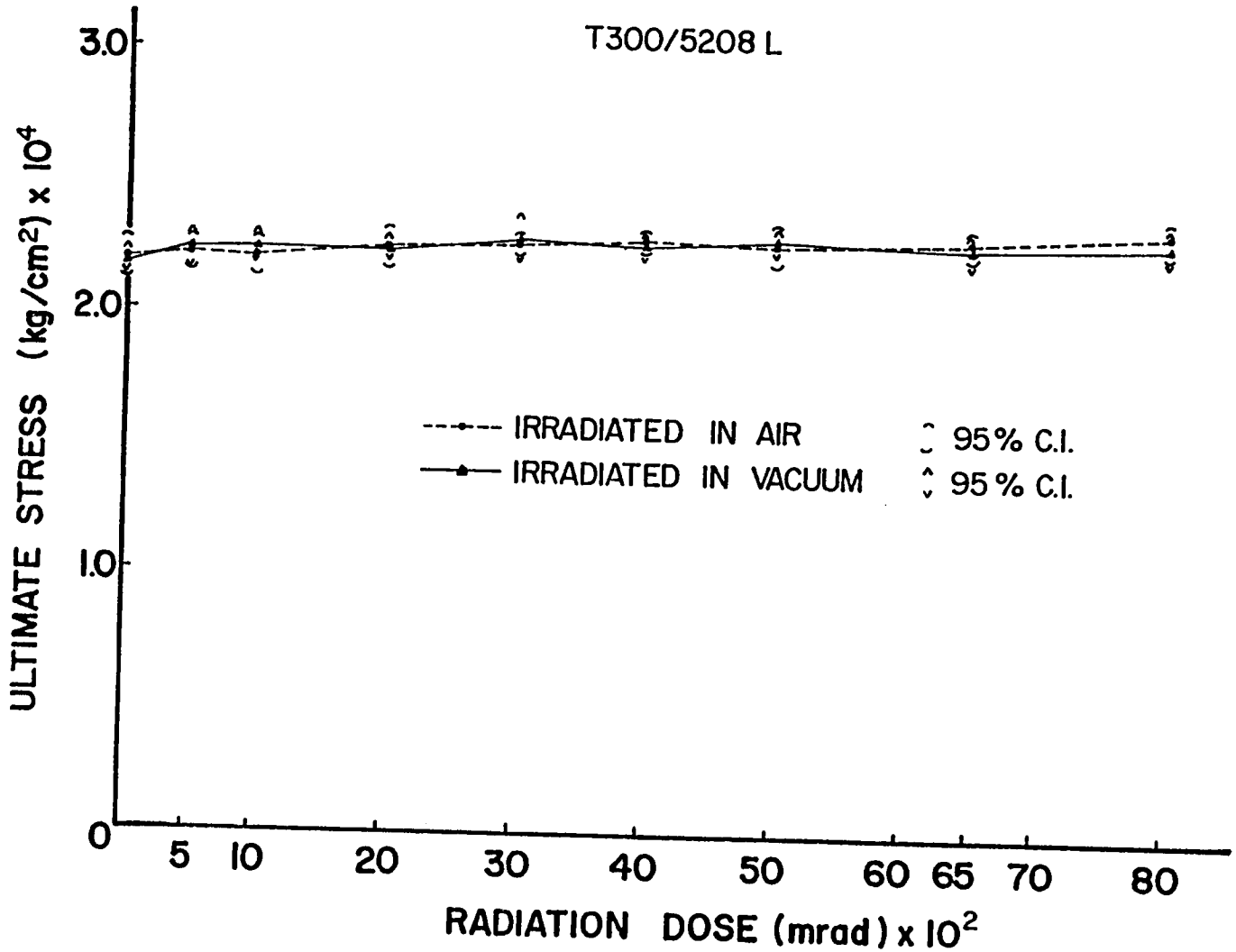

Figure 4.1 Ultimate stress versus radiation dose for T300/5208 longitudinal composites determined from three-point bending.

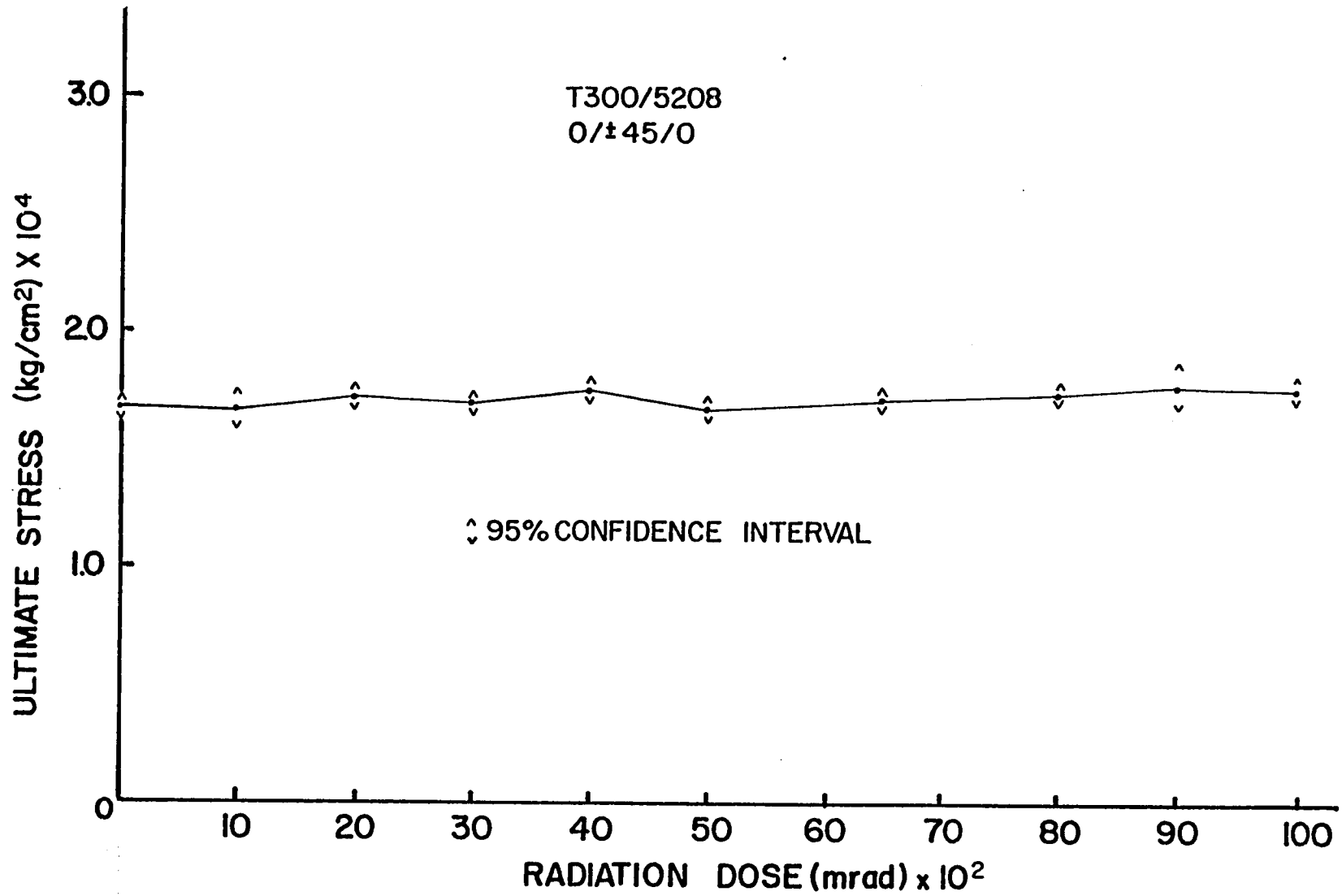

Figure 4.2 Ultimate stress versus radiation dose for T300/5208 0/±45/0 crossplies determined from three-point bending.

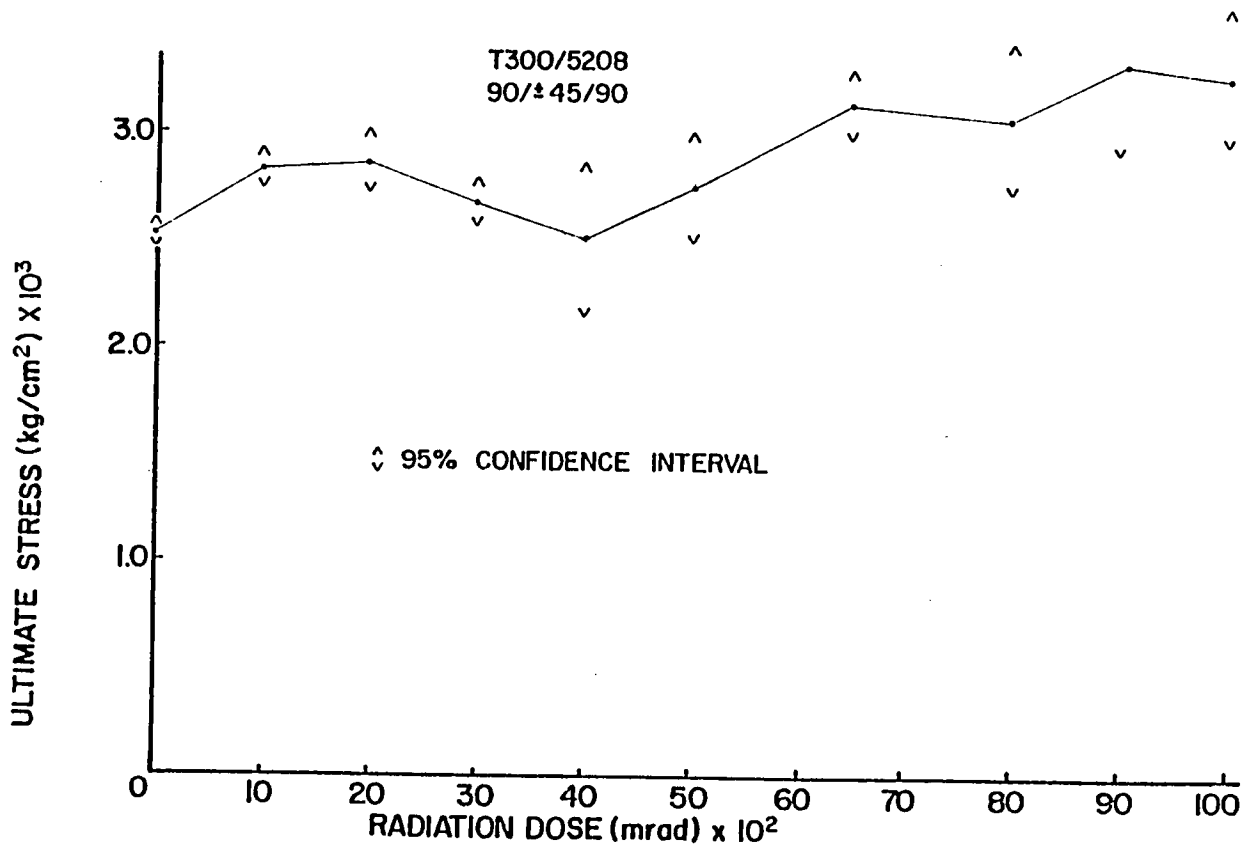

Figure 4.3 Ultimate stress versus radiation dose for T300/5208 90/±45/90 crossplies determined from three-point bending.

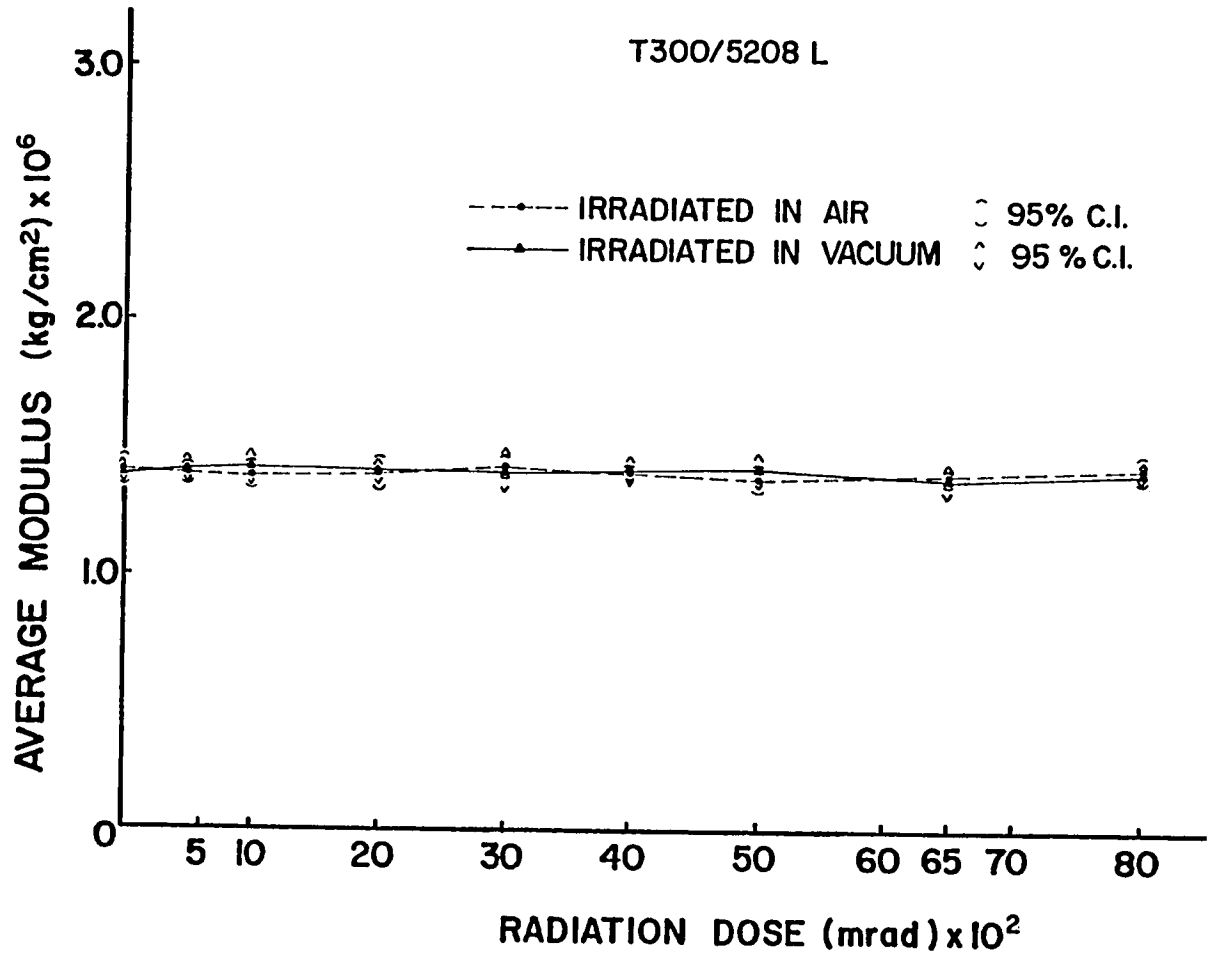

Figure 4.4 Average modulus versus radiation dose for T300/5208 longitudinal composites determined from three-point bending.

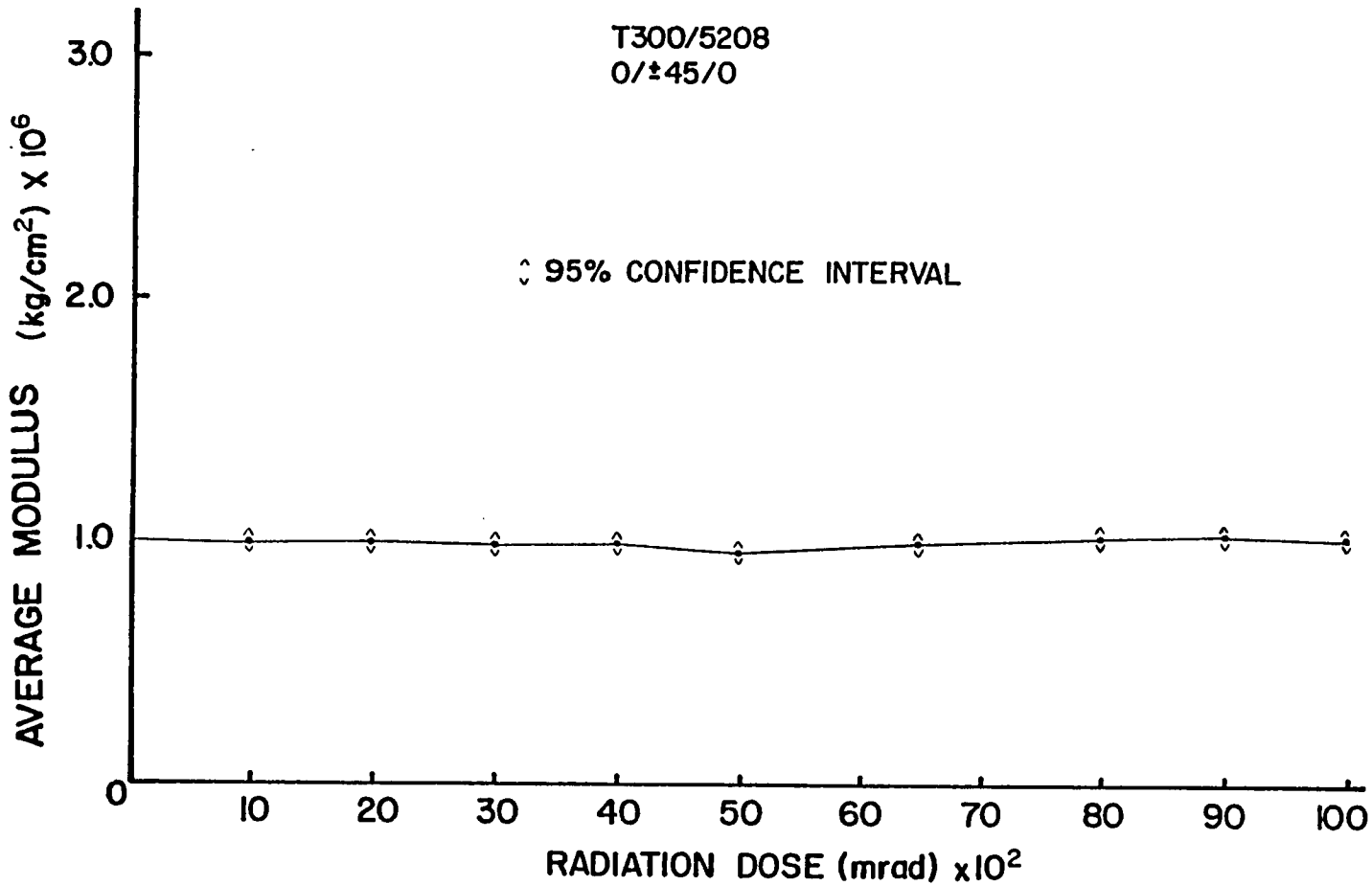

Figure 4.5 Average modulus versus radiation dose for T300/5208 0/±45/0 crossplies determined from three-point bending.

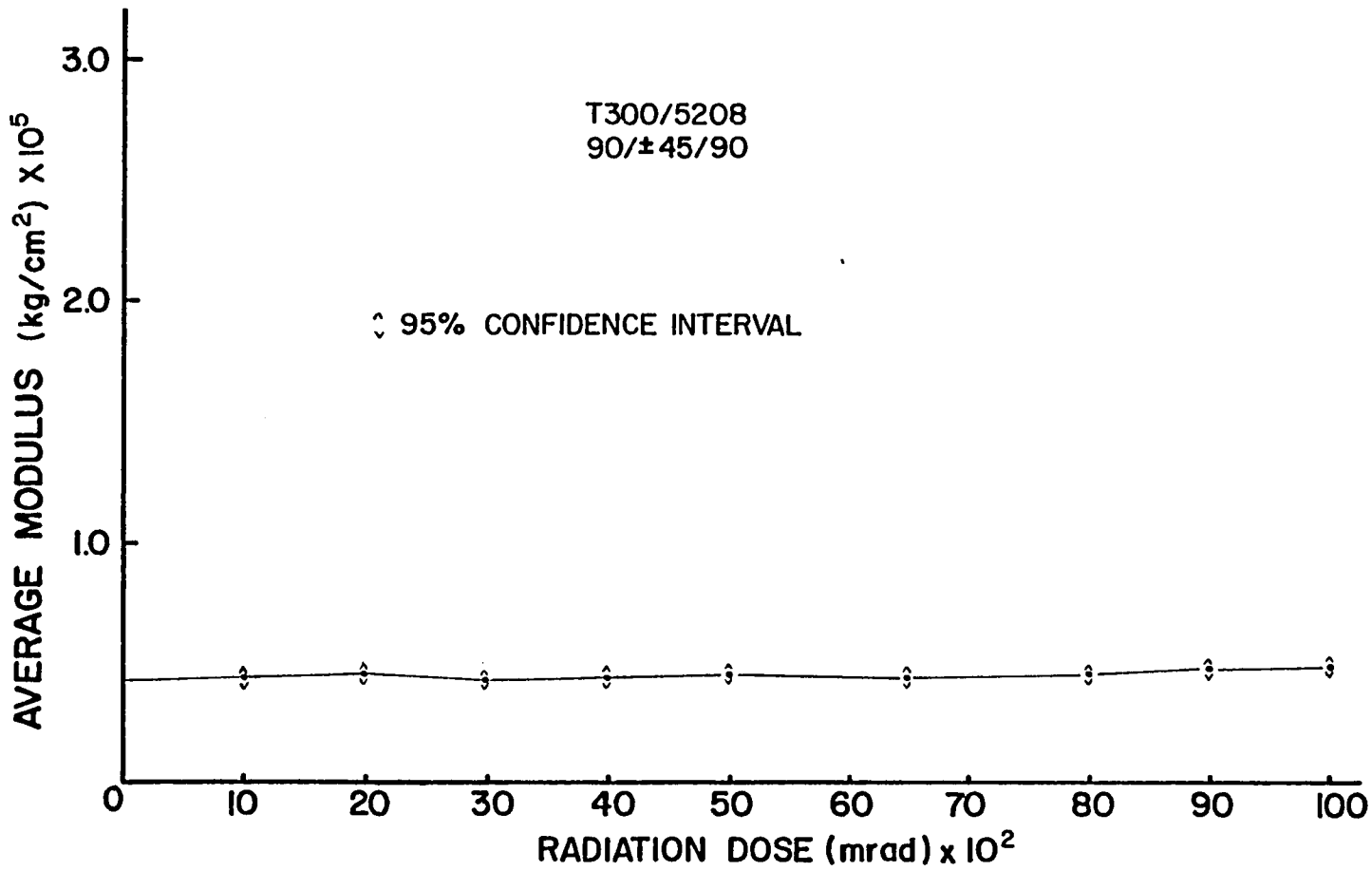

Figure 4.6 Average modulus versus radiation dose for T300/5208 90/±45/90 crossplies determined from three-point bending.

4.1.2 C6000/PMR 15

The C6000/PMR 15 longitudinal samples were irradiated with 0.5 MeV electron radiation to 8000 Mrad. The average values of ultimate stress and average modulus for each radiation level are given in Tables 4.3-4.4 along with the standard deviations and coefficients of variation of these parameters. Stress and modulus are shown as a function of radiation dose in Figures 4.7 and 4.8, respectively.

There is an upward trend in the stress values with increasing radiation dose but it is not statistically significant at the 5% level. The modulus values remain approximately constant with a slight upturn at 8000 Mrad. As with the T300/5208 longitudinal samples there are no significant differences (at the 5% level) in stress or modulus values for samples irradiated in air and in vacuum.

4.1.3 Discussion

The results obtained in this study compare well with those reported by Naranong [95]. The flexural strength and modulus values of T300/5208 and C6000/PMR 15 longitudinal composites irradiated up to 5000 Mrad are within 8% of each other. In most cases, the values obtained by Naranong are slightly higher. In general, as the radiation level increases, the difference between values obtained in the two studies increases.

When polymer resins are exposed to ionizing radiation two phenomena are known to occur: crosslinking and chain scission. These effects are in competition with one another and depending on which one dominates, the strength of the material may increase or decrease. In the composite form, reinforcing fibers have been added to the system

Table 4.3 Ultimate stress of C6000/PMR 15 composites as a function of radiation level

Sample Construction	Radiation Dose (Mrad)	No. of Specimen	Ultimate Stress (kg/cm^2)	Standard Deviation	% CV	Duncan Analysis 5%	Duncan Analysis 10%
C6000/PMR 15 longitudinal (irradiated in vacuum)	0	8	20,963	1062	5.1	AB	AB
	500	8	20,632	541	2.6	B	B
	1000	8	20,838	478	2.3	AB	AB
	2000	8	20,384	356	1.7	B	B
	3000	8	20,771	845	4.1	AB	AB
	4000	8	20,777	952	4.6	AB	B
	5000	8	21,043	1158	5.5	AB	B
	6500	8	20,767	750	3.6	AB	B
	8000	8	21,503	753	3.5	A	A

Note: In the Duncan analysis means with the same letter are not significantly different.

Table 4.4 Average modulus of C6000/PMR 15 composites as a function of radiation level

Sample Construction	Radiation Dose (Mrad)	No. of Specimen	Average Modulus (kg/cm^2)	Standard Deviation	% CV	Duncan Analysis 5%	Duncan Analysis 10%
C6000/PMR 15 longitudinal (irradiated in vacuum)	0	8	1,100,710	155,632	14.1	AB	AB
	500	8	1,106,036	160,024	14.5	AB	AB
	1000	8	1,045,427	52,352	5.0	AB	AB
	2000	8	1,054,091	122,471	11.6	B	B
	3000	8	1,095,516	186,585	17.0	AB	AB
	4000	8	1,059,668	127,986	12.1	AB	B
	5000	8	1,060,621	144,253	13.6	AB	B
	6500	8	1,016,380	26,912	2.6	B	B
	8000	8	1,126,675	163,968	14.6	A	A

Note: In the Duncan analysis means with the same letter are not significantly different.

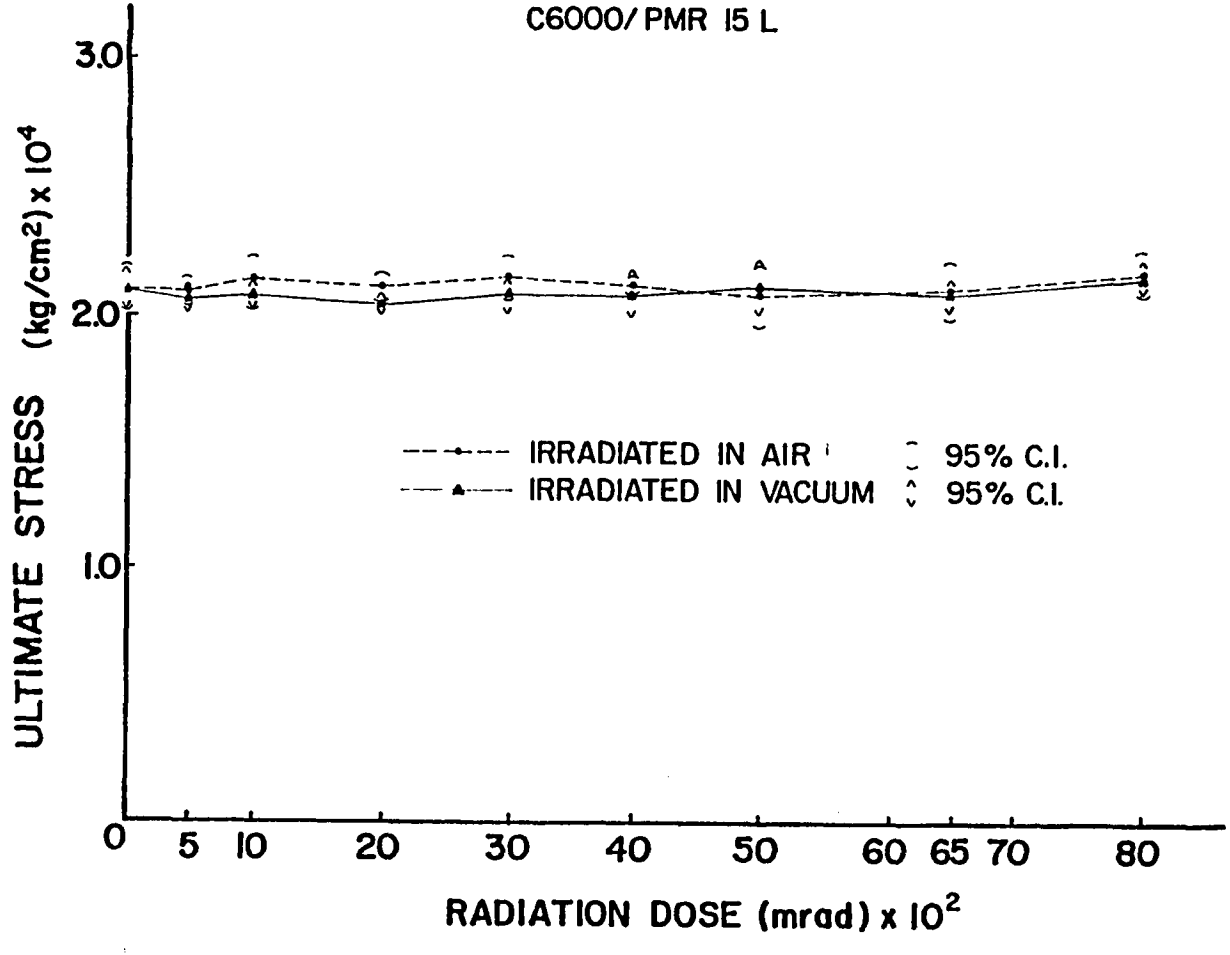

Figure 4.7 Ultimate stress versus radiation dose for C6000/PMR 15 longitudinal composites determined from three-point bending.

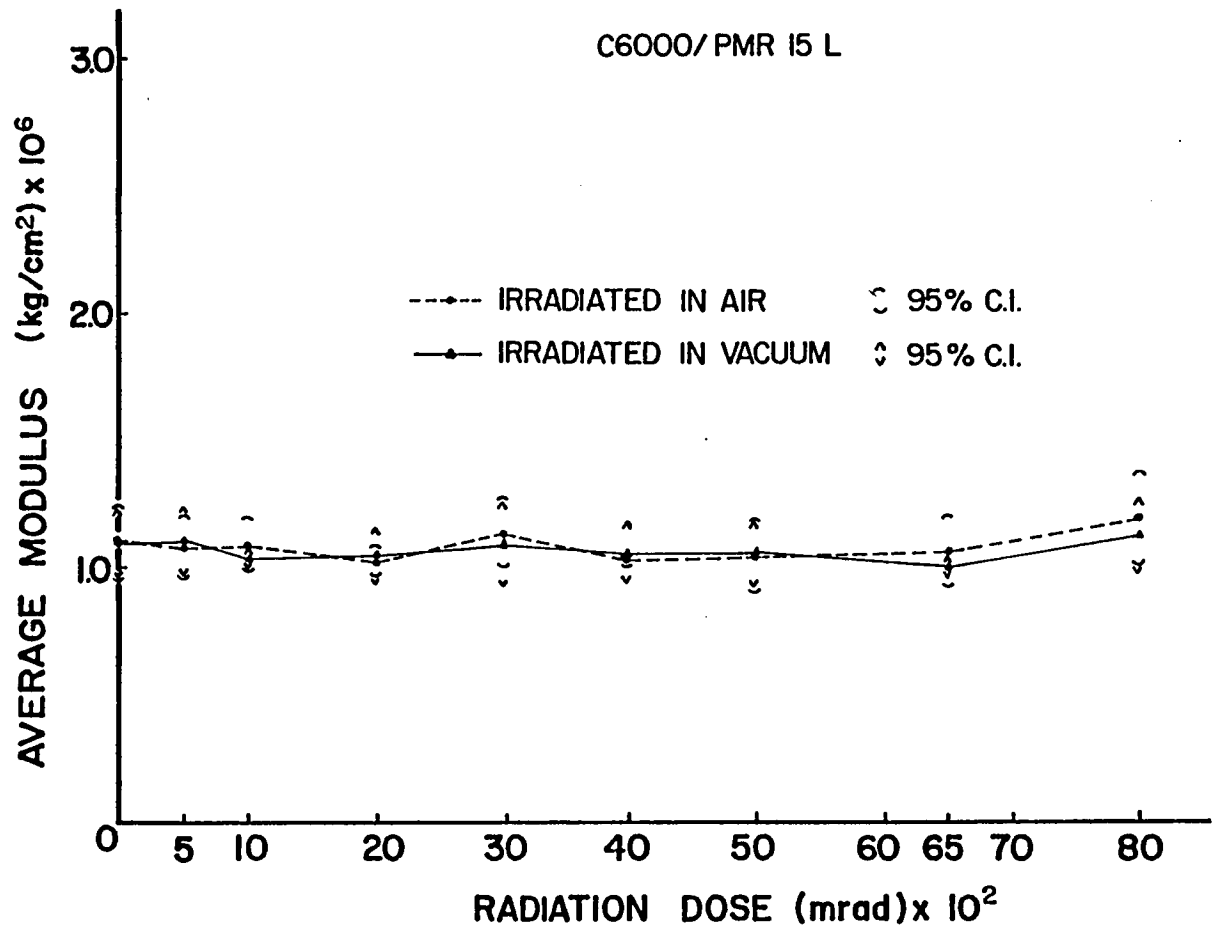

Figure 4.8 Average modulus versus radiation dose for C6000/PMR 15 longitudinal composites determined from three-point bending.

and it was thought that crosslinking would dominate initially, hence producing an increase in strength. At some critical point of radiation exposure it was believed that chain scission would take over and the composites would begin to degrade. However, the data in the preceding sections indicates that degradation due to radiation exposure is not apparent in longitudinal samples or crossplies until extremely high doses, e.g. greater than 10,000 Mrad, have been reached. In an effort to more fully understand these results, the emphasis of the investigation was focused on the interfacial aspects of composites.

4.2 Transverse Tensile Test

The transverse tensile test is an indirect method of assessing interfacial bond strength. Specimens for this test are cut with the fiber axis lying perpendicular to the long axis of the composite. The test is carried out in three-point bending on the Instron machine as described in Section 3.4.1. This test was performed on T300/5208 and C6000/PMR 15 composite samples.

4.2.1 T300/5208

The T300/5208 transverse samples were irradiated with 0.5 MeV electron radiation to 10,000 Mrad. The average values of ultimate stress and average modulus for each radiation level are given in Tables 4.5-4.6 along with the standard deviations and coefficients of variation of these parameters. Stress and modulus are shown as a function of radiation dose in Figures 4.9 and 4.10, respectively.

There is an increase in stress and modulus values of the irradiated samples compared to the control values. This increase is about 29% for stress and about 17% for modulus. Both the analysis of

Table 4.5 Ultimate stress of T300/5208 transverse composites as a function of radiation level

Sample Construction	Radiation Dose (Mrad)	No. of Specimen	Ultimate Stress (kg/cm^2)	Standard Deviation	% CV	Duncan Analysis 5%	Duncan Analysis 10%
T300/5208 transverse	0	8	892	93	10.4	D	D
	1000	8	1025	107	10.4	ABCD	BC
	2000	8	1032	116	11.3	ABC	BC
	3000	8	927	46	5.0	CD	CD
	4000	8	1022	107	10.5	ABCD	BC
	5000	8	1047	101	9.6	ABC	B
	6500	8	983	223	22.7	BCD	BCD
	8000	8	1024	135	13.1	ABCD	BC
	9000	8	1092	80	7.3	AB	AB
	10,000	8	1155	101	8.7	A	A

Note: In the Duncan analysis means with the same letter are not significantly different.

Table 4.6 Average modulus of T300/5208 transverse composites as a function of radiation level

Sample Construction	Radiation Dose (Mrad)	No. of Specimen	Average Modulus (kg/cm^2)	Standard Deviation	% CV	Duncan Analysis 5%	Duncan Analysis 10%
T300/5208 transverse	0	8	86,286	5738	6.7	C	D
	1000	8	91,951	9485	10.3	BC	BC
	2000	8	92,907	6245	6.7	BC	BC
	3000	8	88,301	6405	7.3	C	CD
	4000	8	88,654	4343	4.9	C	CD
	5000	8	88,311	3986	4.5	C	CD
	6500	8	92,120	6653	7.2	BC	BC
	8000	8	96,399	3700	3.8	AB	AB
	9000	8	100,617	6848	6.8	A	A
	10,000	8	95,418	3457	3.6	AB	AB

Note: In the Duncan analysis means with the same letter are not significantly different.

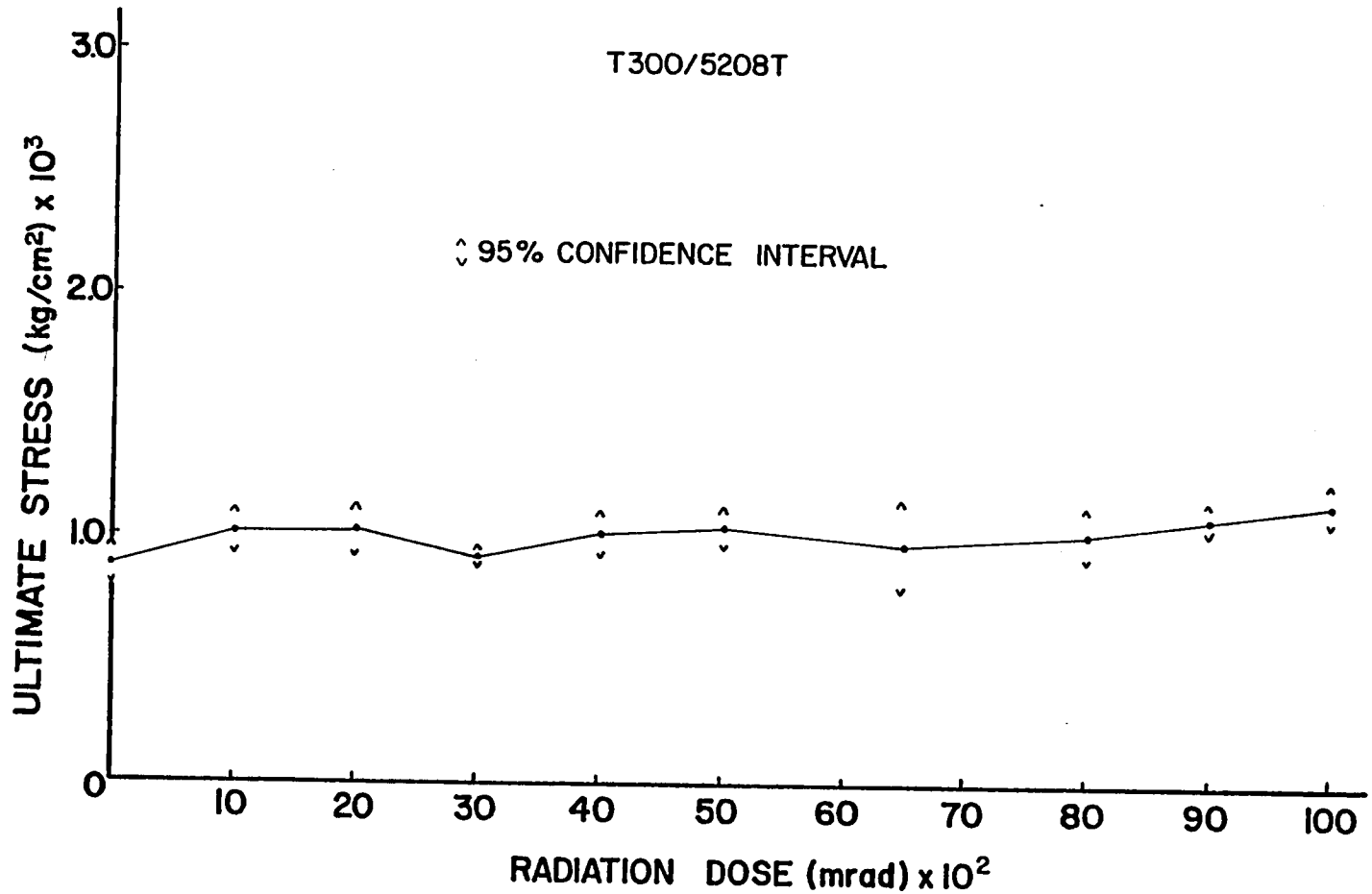

Figure 4.9 Ultimate stress versus radiation dose for T300/5208 transverse composites determined from three-point bending.

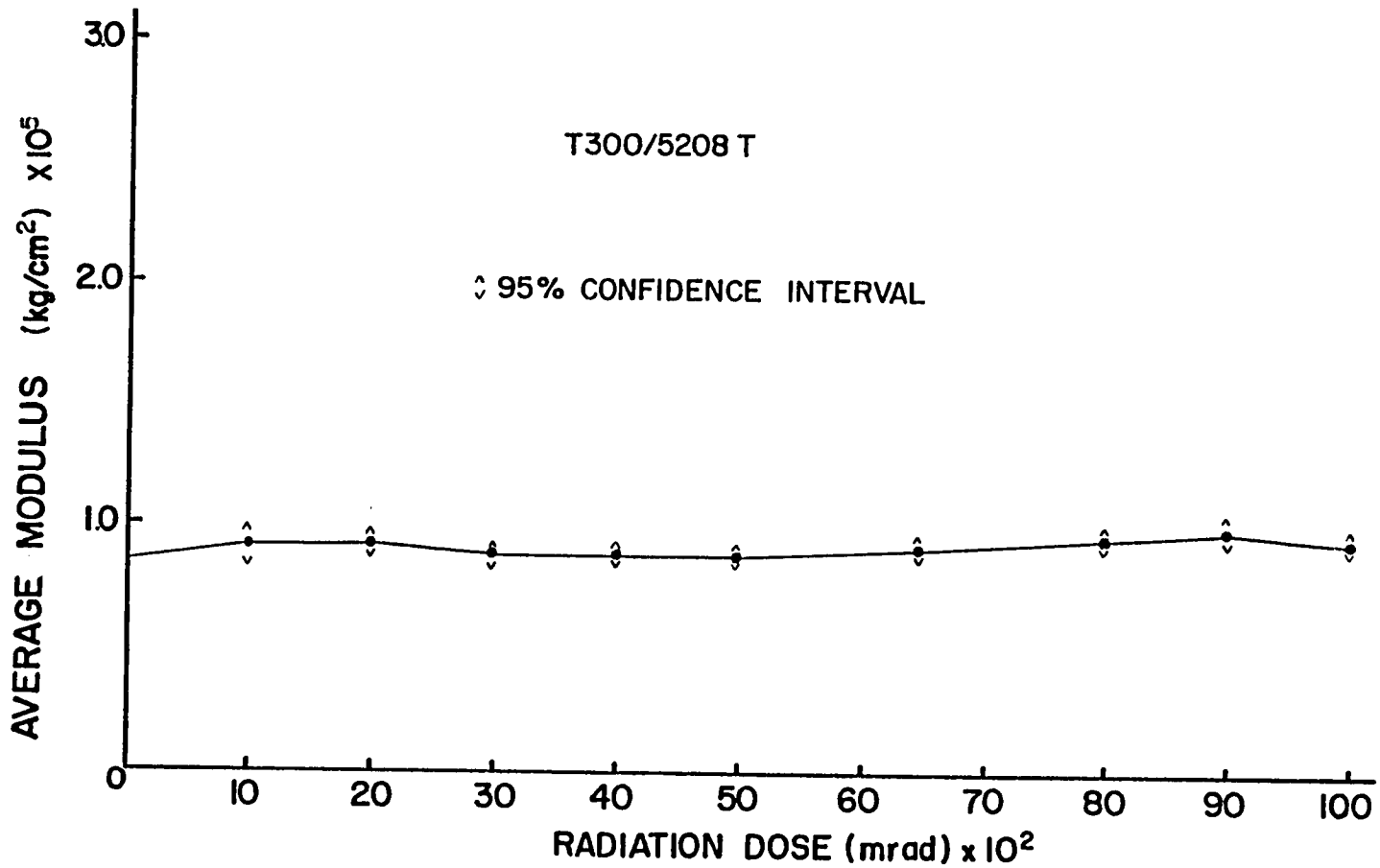

Figure 4.10 Average modulus versus radiation dose for T300/5208 transverse composites determined from three-point bending.

variance and Duncan's multiple range analysis indicate that these increases are statistically significant at the 5% level.

4.2.2 C6000/PMR 15

The C6000/PMR 15 transverse samples were irradiated with 0.5 MeV electron radiation to 8000 Mrad. The average values of ultimate stress and average modulus for each radiation level are given in Tables 4.7-4.8 along with the standard deviations and coefficients of variation of these parameters. Stress and modulus are shown graphically as a function of radiation dose in Figures 4.11 and 4.12, respectively.

The values of stress for the irradiated samples are slightly lower than the control value. For the samples irradiated in vacuum, this decrease is about 12%. It is significant at the 5% level according to the analysis of variance and Duncan's multiple range analysis. The modulus values remained approximately constant with increasing radiation dose. There are no significant differences (at the 5% level) in stress or modulus values for samples irradiated in air and those irradiated in vacuum.

4.2.3 Discussion

Transverse tensile tests are essentially a measure of matrix and/or interface properties. The mode of failure (adhesive or cohesive) dictates whether one is measuring interfacial properties or matrix properties. It can be concluded from Section 4.4 that failure in T300/5208 and C6000/PMR 15 composites is predominantly adhesive although the adhesion to T300 is better than to C6000. It has been noted that the transverse tensile strength of T300/5208 composites increases with radiation exposure while that of C6000/PMR 15 composites

Table 4.7 Ultimate stress of C6000/PMR 15 transverse composites as a function of radiation level

Sample Construction	Radiation Dose (Mrad)	No. of Specimen	Ultimate Stress (kg/cm^2)	Standard Deviation	% CV	Duncan Analysis 5%	Duncan Analysis 10%
C6000/PMR 15 transverse (irradiated in vacuum)	0	7	948	90	9.5	A	A
	500	8	933	99	10.6	ABC	AB
	1000	8	970	124	12.8	AB	A
	2000	8	921	137	14.9	ABC	AB
	3000	8	894	84	9.4	ABC	AB
	4000	8	963	41	4.2	ABC	AB
	5000	8	851	103	12.1	D	C
	6500	8	919	79	8.6	BCD	BC
	8000	8	926	112	12.1	CD	BC

Note: In the Duncan analysis means with the same letter are not significantly different.

Table 4.8 Average modulus of C6000/PMR 15 transverse composites as a function of radiation level

Sample Construction	Radiation Dose (Mrad)	No. of Specimen	Average Modulus (kg/cm^2)	Standard Deviation	% CV	Duncan Analysis 5%	Duncan Analysis 10%
C6000/PMR 15 transverse (irradiated in vacuum)	0	7	79,747	3416	4.3	A	A
	500	8	78,869	9511	12.1	A	A
	1000	8	81,777	6746	8.2	A	A
	2000	8	79,958	7123	8.9	A	A
	3000	8	79,340	4759	6.0	A	A
	4000	8	78,642	2886	3.7	A	A
	5000	8	78,733	5743	7.3	A	A
	6500	8	82,837	8768	10.6	A	A
	8000	8	81,550	5375	6.6	A	A

Note: In the Duncan analysis means with the same letter are not significantly different.

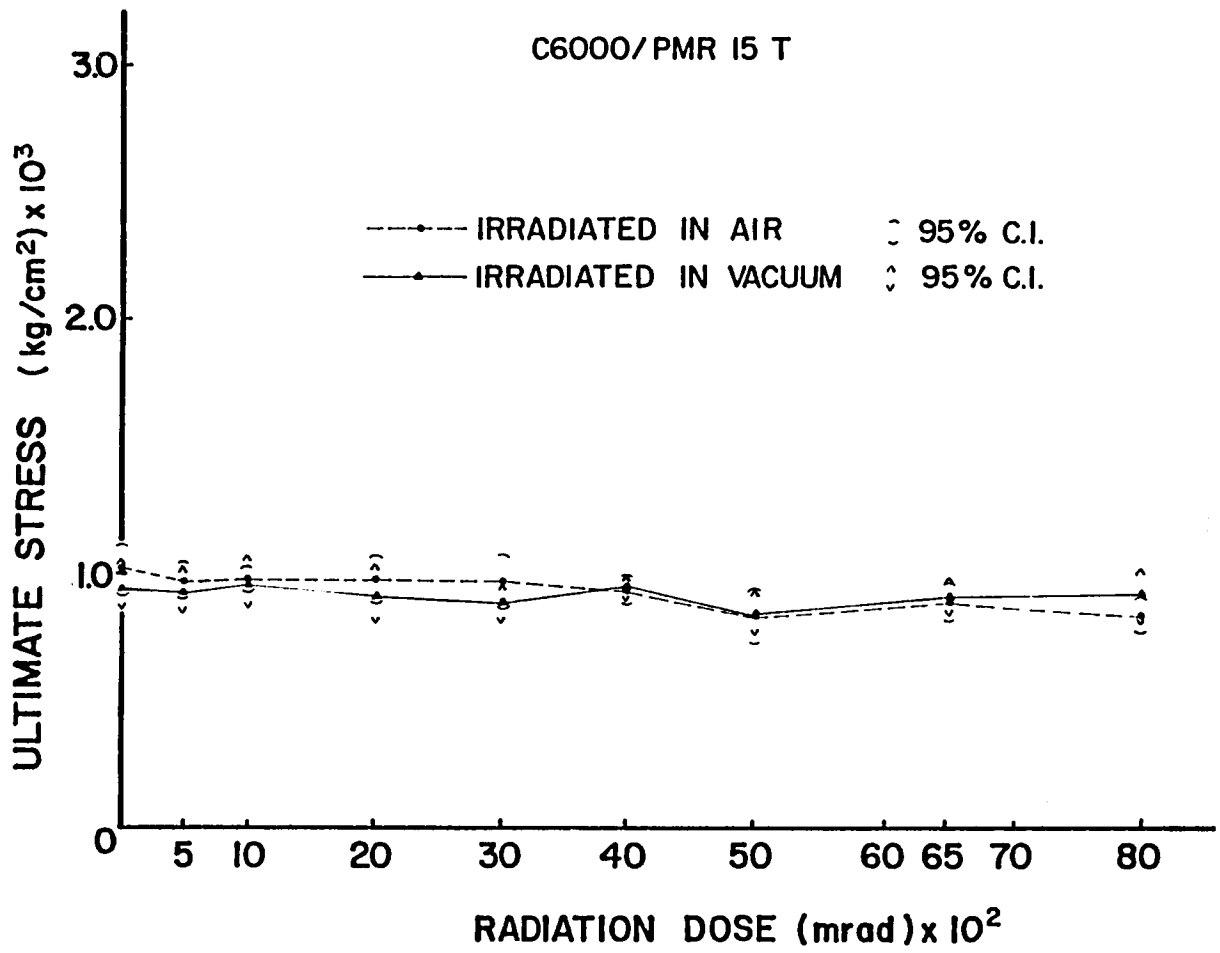

Figure 4.11 Ultimate stress versus radiation dose for C6000/PMR 15 transverse composites determined from three-point bending.

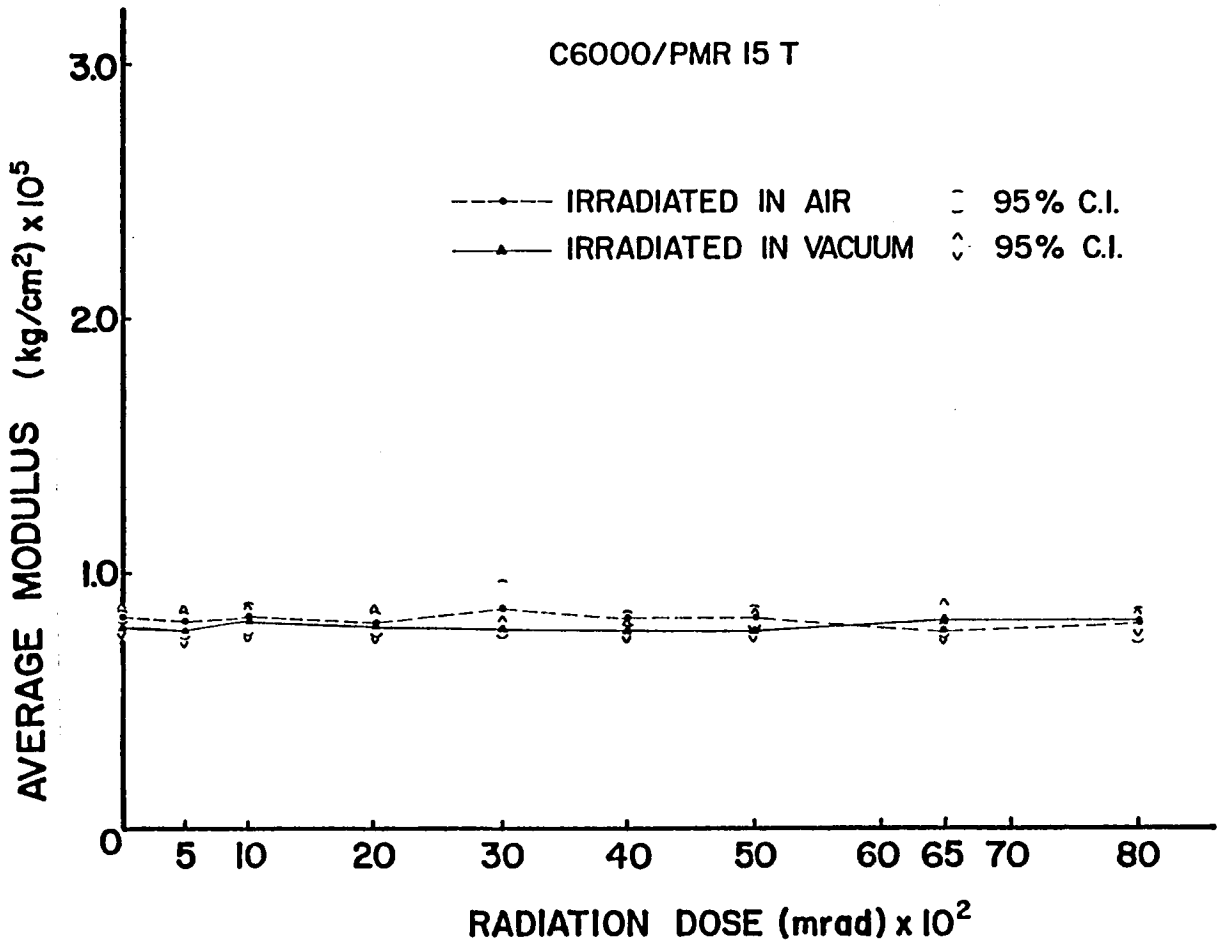

Figure 4.12 Average modulus versus radiation dose for C6000/PMR 15 transverse composites determined from three-point bending.

decreases slightly. In order to rationalize this difference in behavior, consider the equation given in Section 2.4.4.3 for the case of a strong interfacial bond [8]:

$$\sigma_t = \sigma_m \left(1 - \sqrt{\frac{4V_f}{\pi}}\right) + \sigma_i' \left(\sqrt{\frac{4V_f}{\pi}}\right)$$

where σ_t = composite transverse tensile strength
σ_m = matrix tensile strength
σ_i' = average tensile stress necessary to separate the fiber from the matrix under transverse loading.

With radiation exposure the interfacial component σ_i' decreases while the matrix component σ_m increases slightly. The net effect on transverse tensile strength depends on the rates of change of these parameters. Apparently the interface in C6000/PMR 15 composites degrades faster than that in T300/5208, thus lowering the transverse strength in these composites. This hypothesis is supported by the data in Section 4.3 indicating that interlaminar shear strength in C6000/PMR 15 composites decreases 54% after a 10,000 Mrad exposure while that of T300/5208 composites decreases 34%.

4.3 Interlaminar Shear Test

4.3.1 T300/5208

Three different constructions of T300/5208 were irradiated with 0.5 MeV electron radiation to a maximum dosage of 10,000 Mrad. The interlaminar shear strength was calculated by computer using Equation 3.3. The average values of interlaminar shear strength for each radiation level are given in Table 4.9 along with the standard deviation and coefficient of variation. Interlaminar shear strength is plotted as a function of radiation dose in Figures 4.13-4.15.

Table 4.9 Interlaminar shear strength of T300/5208 composites as a function of radiation level

Sample Construction	Radiation Dose (Mrad)	No. of Specimen	Interlaminar Shear Strength (kg/cm^2)	% Change of Result to Control	Standard Deviation	% CV	Duncan Analysis 5%	Duncan Analysis 10%
T300/5208 longitudinal	0	8	180	0	37	20.5	AB	AB
	1000	7	192	+7	33	17.0	A	A
	2000	9	176	-2	25	14.2	AB	AB
	3000	9	180	0	21	11.8	AB	AB
	4000	9	165	-8	8	5.0	BC	B
	5000	9	166	-8	16	9.8	BC	B
	6500	9	146	-19	12	8.2	CD	C
	9000	9	137	-24	13	9.3	D	CD
	10,000	9	127	-29	9	7.2	D	D
0/±45/0	0	10	207	0	27	13.0	BC	B
	1000	10	234	+13	20	8.4	A	A
	2000	10	225	+9	23	10.3	AB	A
	3000	10	204	-1	25	12.1	C	B
	4000	10	198	-4	12	6.0	C	B
	5000	10	199	-4	16	8.0	C	B
	6500	10	199	-4	12	5.8	C	B
	9000	10	208	0	11	5.4	BC	B
	10,000	10	193	-7	24	12.6	C	B
90/±45/90	0	10	95	0	18	19.3	C	C
	1000	10	115	+21	21	18.0	AB	AB
	2000	10	108	+14	32	29.9	BC	B
	3000	10	62	-35	12	18.8	DE	E
	4000	10	76	-20	19	25.0	D	D
	5000	10	77	-19	18	23.1	D	D
	6500	10	56	-41	11	20.2	E	E
	9000	10	39	-59	8	21.6	F	F
	10,000	9	35	-63	6	17.1	F	F

Note: In the Duncan analysis means with the same letter are not significantly different.

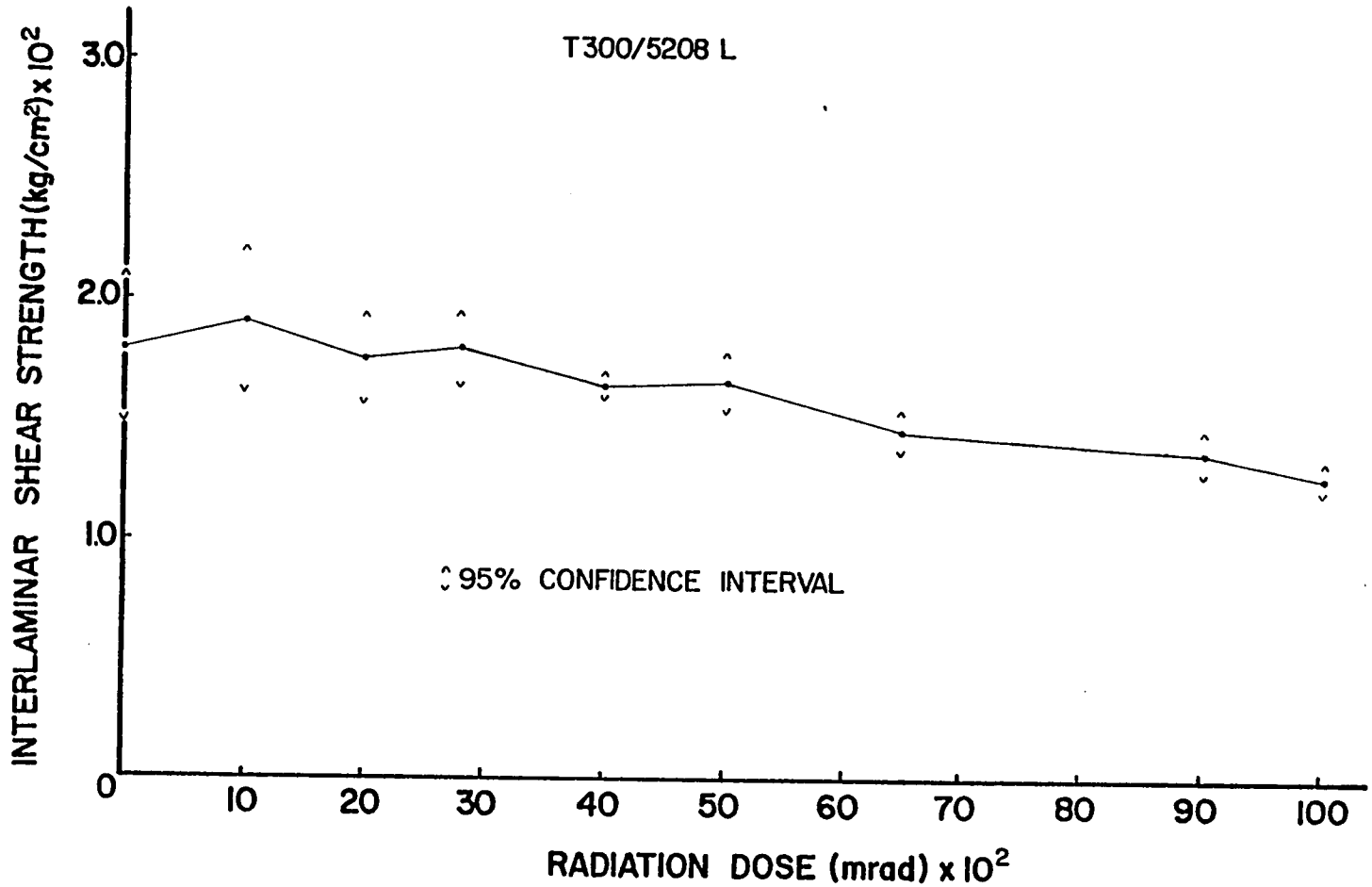

Figure 4.13 Interlaminar shear strength versus radiation dose for T300/5208 longitudinal composites.

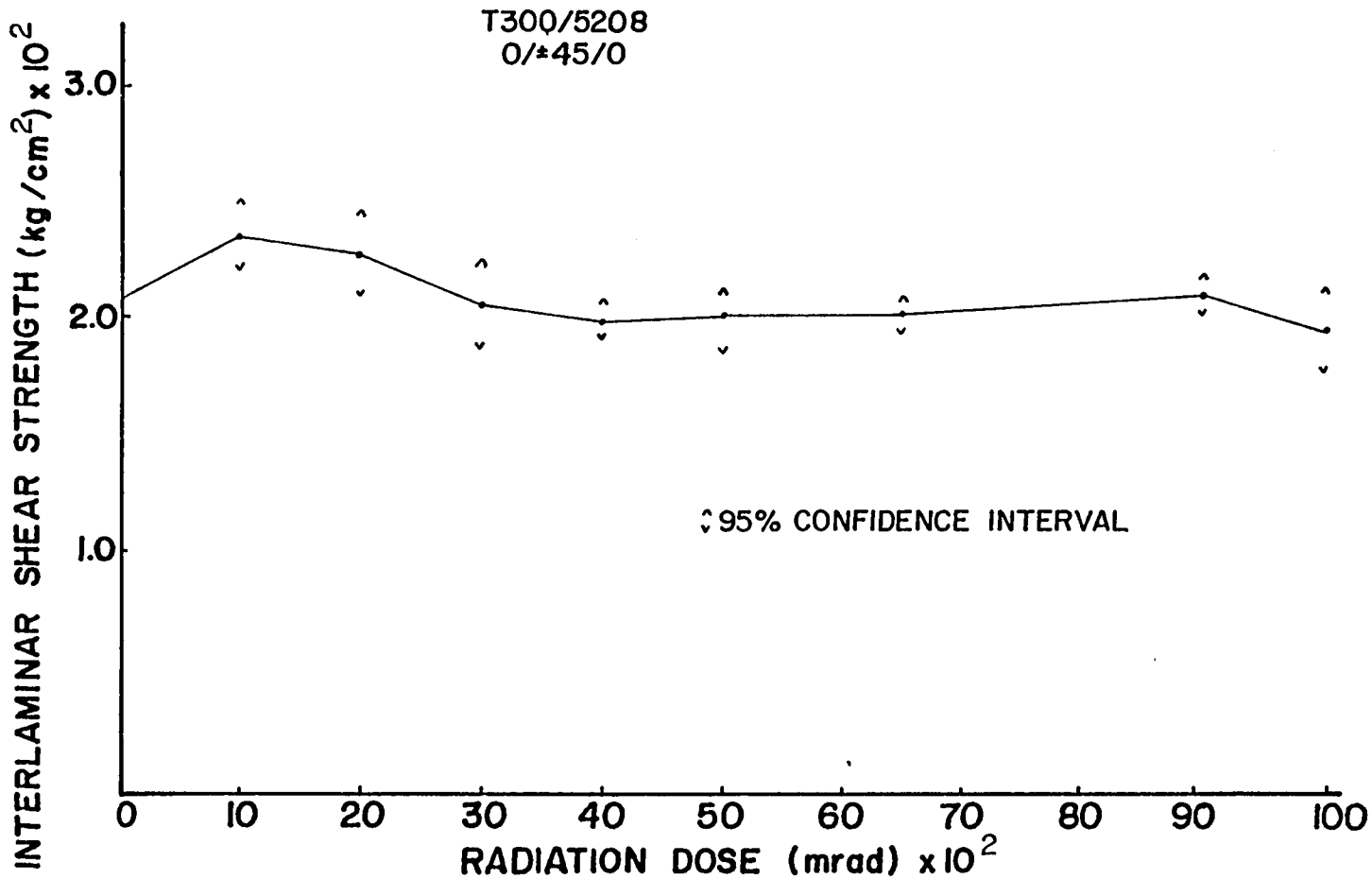

Figure 4.14 Interlaminar shear strength versus radiation dose for T300/5208 0/±45/0 crossplies.

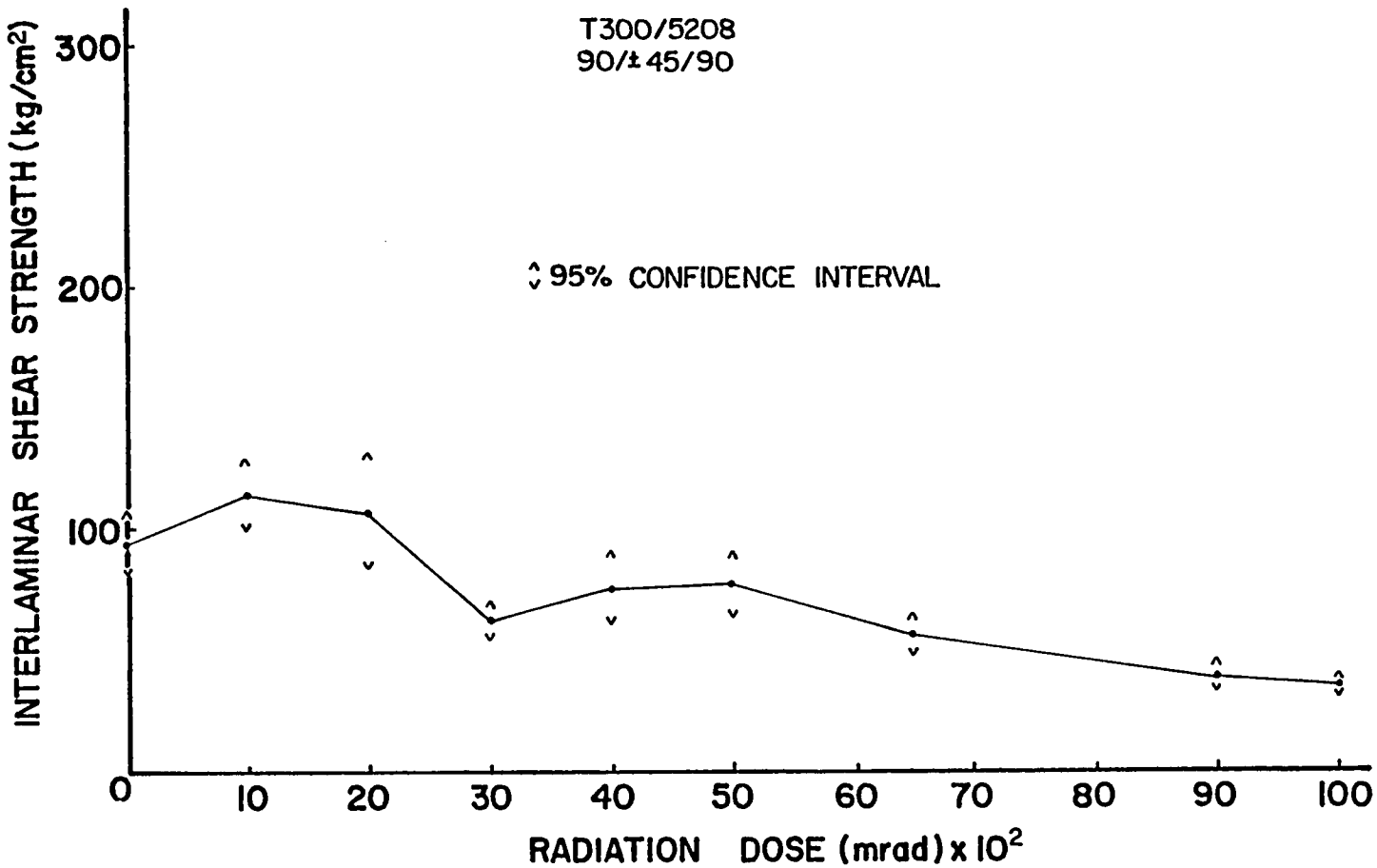

Figure 4.15 Interlaminar shear strength versus radiation dose for T300/5208 90/±45/90 crossplies.

All three composite constructions exhibit an initial increase in interlaminar shear strength with a maximum at 1000 Mrad. This increase is statistically significant at the 5% level for 0/±45/0 and 90/±45/90 crossplies, being 13% and 22%, respectively. Interlaminar shear strength decreases with further radiation exposure. The values at the 10,000 Mrad level are considerably lower than those of the maxima for all three composite constructions--longitudinal (34%), 0/±45/0 (18%), and 90/±45/90 (70%).

4.3.2 C6000/PMR 15

The C6000/PMR 15 longitudinal samples were exposed to 10,000 Mrad of 0.5 MeV electron radiation. The average values of interlaminar shear strength for each radiation level are given in Table 4.10 along with the standard deviation and coefficient of variation. Figure 4.16 diagrams interlaminar shear strength as a function of radiation dose.

The C6000/PMR 15 composites follow the same general trends as the T300/5208 composites with respect to interlaminar shear strength except that the maximum occurs at 2000 Mrad. This maximum is approximately 9% higher than the control value. The value of interlaminar shear strength after the 10,000 Mrad exposure is approximately 54% lower than the value at 2000 Mrad.

4.3.3 Discussion

The initial increase in interlaminar shear strength with radiation exposure is probably due to relaxation of internal stresses created at the interface during composite fabrication. These stresses develop during cooldown when matrix contraction is inhibited by the already-

Table 4.10 Interlaminar shear strength of C6000/PMR 15 composites as a function of radiation level

Sample Construction	Radiation Dose (Mrad)	No. of Specimen	Interlaminar Shear Strength (kg/cm^2)	% Change of Result to Control	Standard Deviation	% CV	Duncan Analysis 5%	Duncan Analysis 10%
C6000/PMR 15 longitudinal	0	6	315	0	43	13.7	A	B
	1000	7	334	+6	25	7.4	A	AB
	2000	7	344	+9	30	8.6	A	A
	3000	7	275	-13	27	9.9	B	C
	4000	7	268	-15	18	6.7	B	C
	5000	7	227	-28	25	11.2	C	D
	6500	7	202	-36	18	8.8	CD	E
	9000	7	183	-42	10	5.6	DE	E
	10,000	7	159	-50	13	8.2	E	F

Note: In the Duncan analysis means with the same letter are not significantly different.

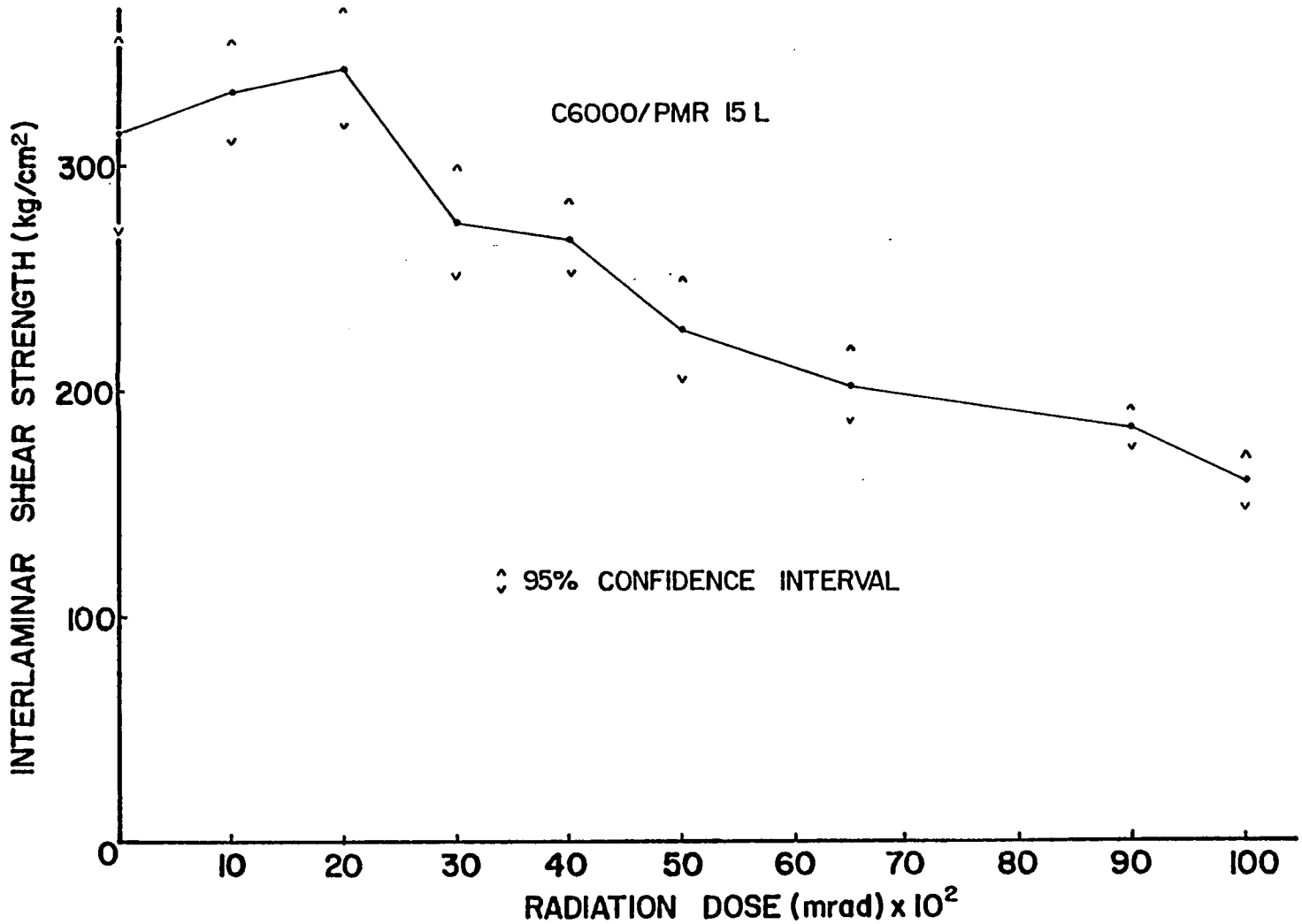

Figure 4.16 Interlaminar shear strength versus radiation dose for C6000/PMR 15 longitudinal composites.

formed interfacial bond. This microresidual stress formation is described in detail in Section 2.4.3.

After the internal stresses are relieved, further radiation exposure leads to bond degradation due to chain scission, and thus the decrease in interlaminar shear strength at levels of radiation greater than 1000 Mrad. Strength values measured by the three-point bending test do not exhibit large negative changes like those seen in interlaminar shear strength. When tested in the fiber direction (longitudinal), composites show no degradation with radiation exposure because of fiber reinforcement and matrix crosslinking. Naranong [95] reported that the tensile strength of graphite fibers was not adversely affected by large doses of radiation. It has been discussed in Section 4.2.3 that the effect of radiation on transverse tensile strength depends on the relative values of matrix and interfacial components. Large decreases are not seen since matrix crosslinking provides a stabilizing effect. Interlaminar shear strength depends only on the interfacial component so without the stabilizing effect of fiber and matrix components, large decreases are seen in this parameter.

4.3.4 Results at 8000 Mrad Level

It should be noted that data from interlaminar shear tests on 8000 Mrad irradiated composite specimens was not included. This data was rejected because of an error in alignment during the cutting procedure. On one edge of the sample the saw cuts did not go halfway through. This resulted in artificially high values of interlaminar shear strength.

A set of T300/5208 transverse samples irradiated to 8000 Mrad but not tested was used to verify the inaccuracy of the original data.

These samples, measuring 1" by 1/2" with the fiber axis parallel to the shorter dimension, were cut in half crosswise giving two 1/2" by 1/2" samples. These samples were rotated so that the fibers were in the longitudinal direction. They were then cut in the manner described in Section 3.4.2 with the same distance (0.50 cm) between the saw cuts. Since these samples were shorter than the samples in the previous tests, this left a smaller grip length at each end. The gauge length of the Instron was reduced to adapt to this difference in specimen dimensions. This change should not affect the experimental results since the shearing area was the same for all tests. The values of interlaminar shear strength obtained for these samples were in agreement with the results of the 6500 and 9000 Mrad levels in the previous tests.

4.4 Scanning Electron Microscopy

Scanning electron microscopy was used to determine whether there were any visual differences between ruptured control samples and ruptured samples which had been exposed to various levels of electron radiation. Changes in the amount of matrix adhering to the fiber or changes in the manner in which the matrix separated from the fiber constitute visual differences. These are related to interfacial bond strength. If the interfacial bond is weak, the fiber-matrix break will be a clean one. If the interfacial bond is strong, fragments of matrix are likely to adhere to the fibers due to matrix-matrix cohesive failure.

Longitudinal samples of T300/5208 and C6000/PMR 15 were examined under the SEM. Figure 4.17 is a low magnification (20 X) micrograph

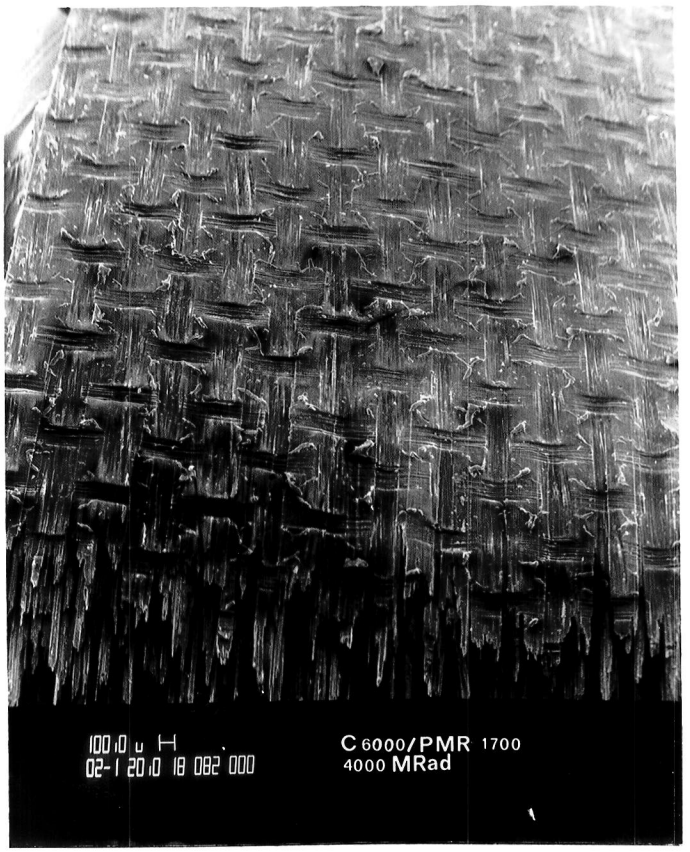

Figure 4.17 Overall view of fracture surface of ruptured composite (20X).

showing an overall view of the fracture surface of a composite ruptured in the three-point bending test. Figures 4.18-4.27 are a representative sample of micrographs taken at higher magnification of the fracture surface of various composites at different levels of radiation. Figure 4.18 shows a T300/5208 control sample at a magnification of 2000X. Figures 4.19 - 4.22 show T300/5208 samples which have been irradiated to 300, 2000, 5000, and 8000 Mrad, respectively. Comparing these micrographs, one detects no visual differences between the control sample and those exposed to the various levels of radiation. In each case, there are a number of matrix fragments adhering to the fibers. These fragments are plate-like and are aligned perpendicular to the fiber axis, creating a "scalloped" effect.

Figure 4.23 shows a C6000/PMR 15 control sample at a magnification of 1000X. Figures 4.24 - 4.27 show C6000/PMR 15 samples which have been irradiated to 300, 2000, 5000 and 8000 Mrad, respectively. As with the T300/5208 samples, there are no visual differences between the unirradiated and irradiated samples. In the C6000/PMR 15 samples the matrix separates from the fibers in large segments and leaves only a few fragments. This is probably due to the fact that C6000 fibers have a relatively smooth surface compared to T300 fibers which have surface striations parallel to the fiber axis.

4.5 Electron Spectroscopy for Chemical Analysis

The objective of this experiment was to determine whether irradiation has an effect on the surface elements present in graphite fiber composites, particularly since crosslinking of the resin is

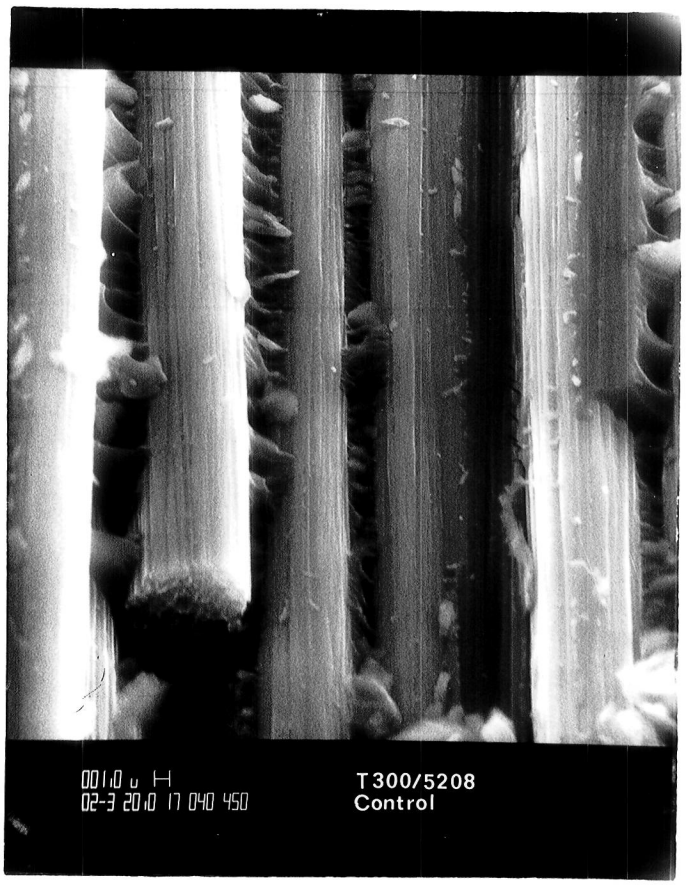

Figure 4.18. Control sample of T300/5208 (2000X).

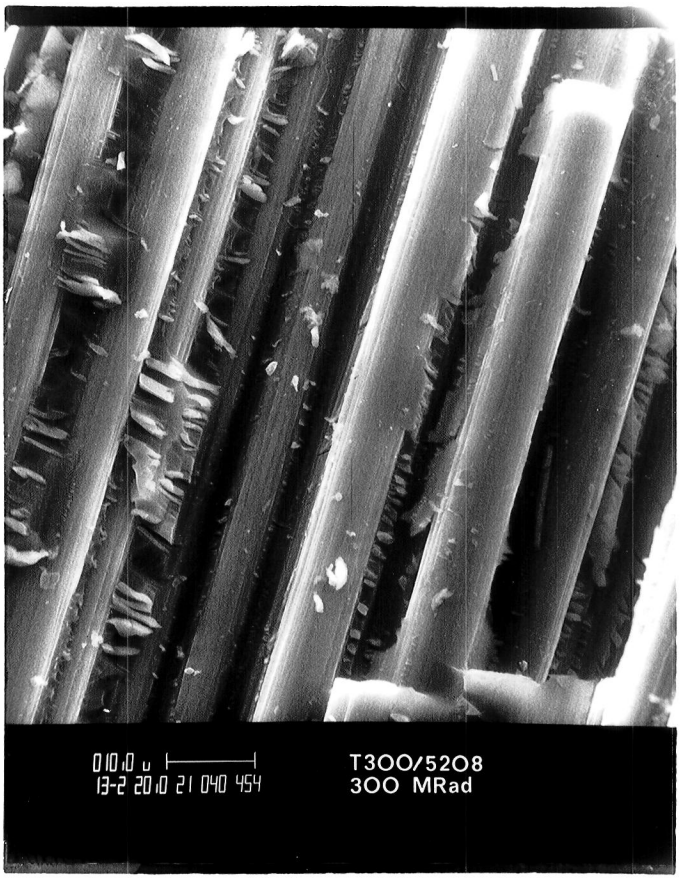

Figure 4.19 T300/5208 sample irradiated to 300 Mrad (1300X).

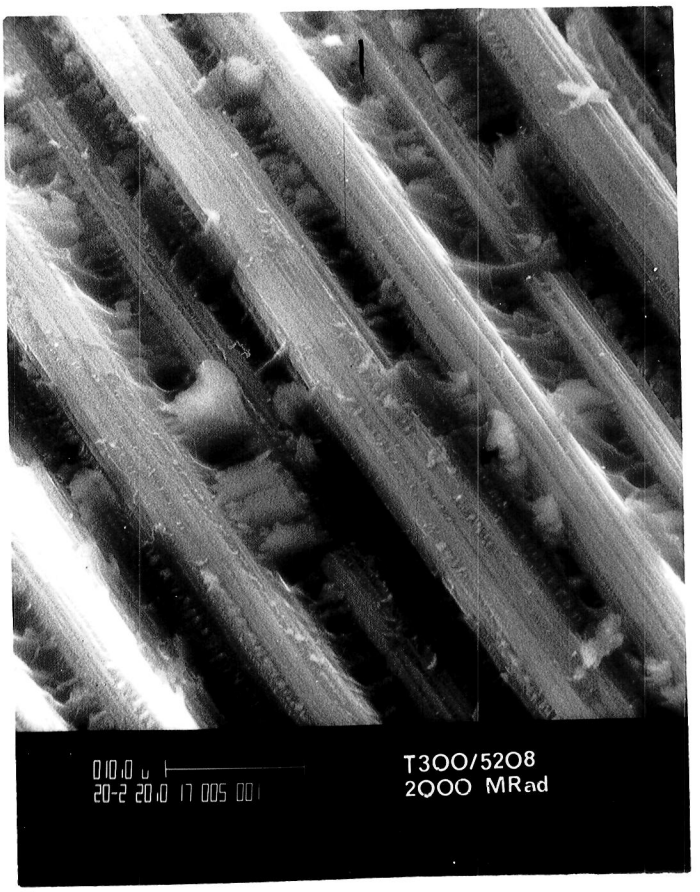

Figure 4.20 T300/5208 sample irradiated to 2000 Mrad (2000X).

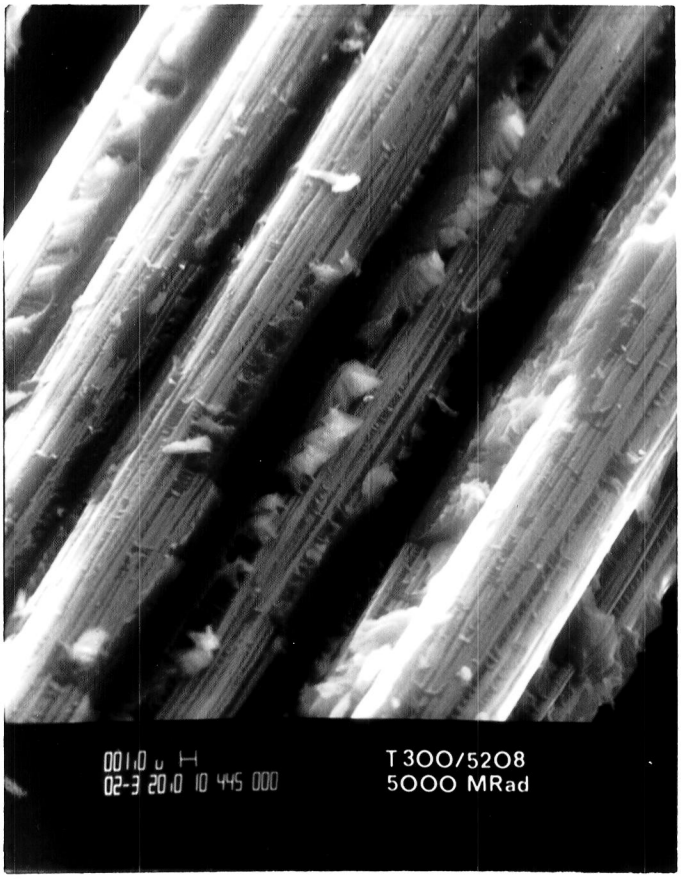

Figure 4.21 T300/5208 sample irradiated to 5000 Mrad (2000X).

Figure 4.22 T300/5208 sample irradiated to 8000 Mrad (1700X).

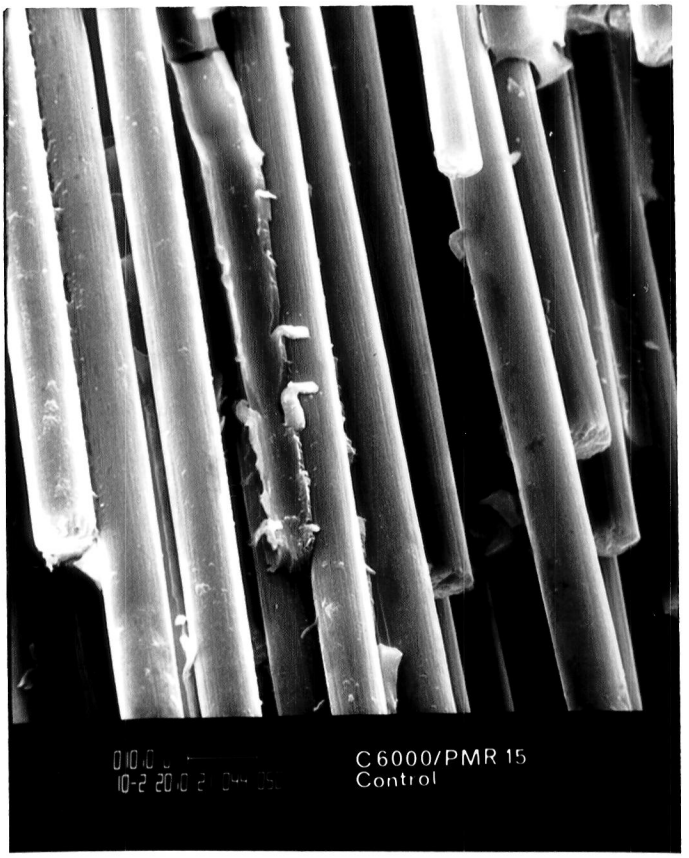

Figure 4.23 Control sample of C6000/PMR 15 (1000X).

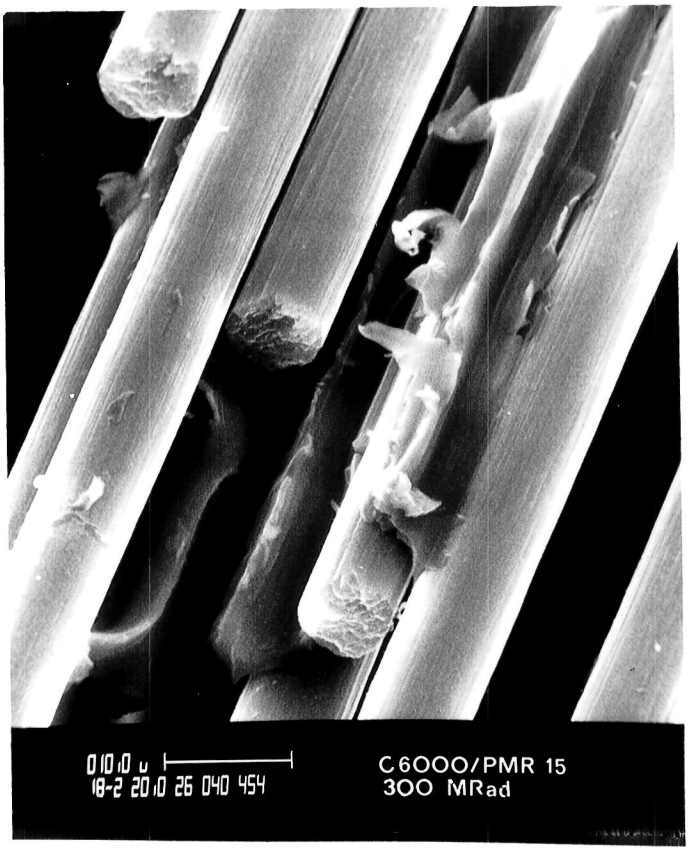

Figure 4.24 C6000/PMR 15 sample irradiated to 300 Mrad (1800X).

Figure 4.25 C6000/PMR 15 sample irradiated to 2000 Mrad (1800X).

Figure 4.26 C6000/PMR 15 sample irradiated to 5000 Mrad (1100X).

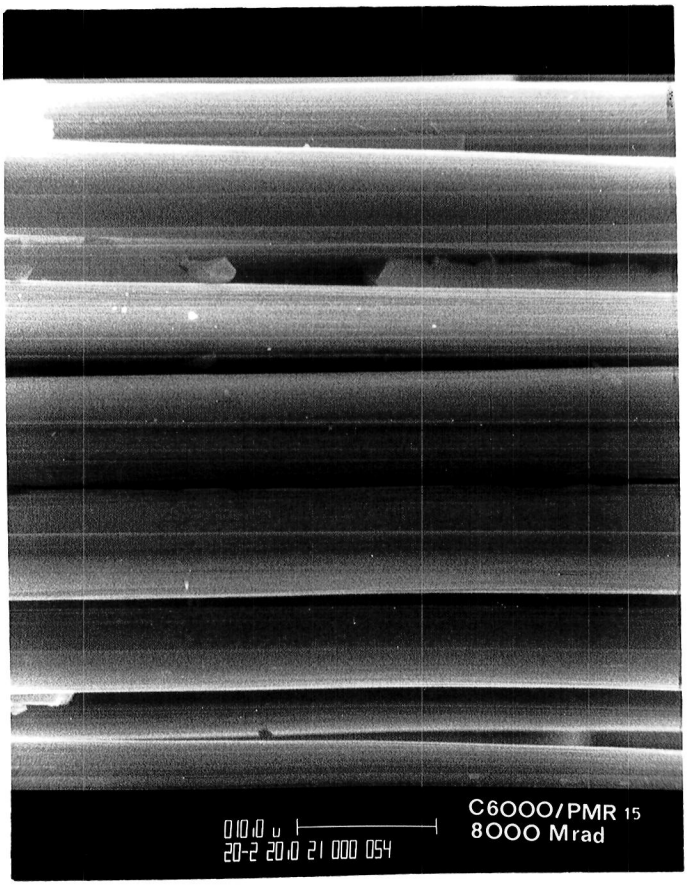

Figure 4.27 C6000/PMR 15 sample irradiated to 8000 Mrad (2000X).

expected. Control samples of T300/5208, samples exposed to 8000 Mrad of electron radiation, and samples exposed to 10,000 and 40,000 Mrad of proton radiation were examined. The results are discussed according to the type of radiation exposure.

4.5.1 Electron Radiation Exposure

Three control samples of T300/5208 were examined. The major elements present are carbon and oxygen. Elements present in lesser amounts are sulfur, fluorine, nitrogen, chlorine, sodium, silicon, and traces of aluminum. For samples irradiated to 8000 Mrad, the major elements are also carbon and oxygen. The minor elements present are sulfur, nitrogen, chlorine, sodium, silicon, and aluminum.

The atomic ratios normalized to carbon are given in Table 4.11. Significant changes in concentration upon irradiation are seen for sulfur, chlorine, sodium, silicon, and fluorine. Sulfur is probably eliminated as SO_2 although some could be trapped at the surface as SO_4^{-2} (e.g. Na_2SO_4). Some sulfur is also present as residual sulfonate. Sodium could have partially migrated to the sample surface due to the negative surface charge caused by electron bombardment. Cl^- ions formed during irradiation could be trapped at the surface by Na^+ ions. Some chlorine may have escaped as Cl_2 or HCl, or been trapped near the surface in these chemical forms. Fluorine disappears completely upon irradiation. It is probably eliminated as F_2 or HF. This phenomenon has been observed when fluorinated polymers were bombarded with electrons.

Possible changes in chemical state are observed for sulfur, carbon, and chlorine. There is a large increase in surface oxidation

Table 4.11 Atomic ratios normalized to carbon of electron-irradiated composites

Element	Sample #	Control	Irradiated	Irradiated/Control
C	1	1	1	--
	2	1	1	--
	3	1	1	--
O	1	.264	.431	1.63
	2	.277	.443	1.60
	3	.295	.419	1.42
S	1	.0096	.020	2.05
	2	.019	.025	1.31
	3	.018	.020	1.13
N	1	.045	.046	1.02
	2	.043	.061	1.43
	3	.052	.046	.89
Cl	1	.019	.047	2.49
	2	.011	.041	3.58
	3	.016	.043	2.79
Na	1	.025	.050	1.97
	2	.037	.034	.91
	3	.032	.026	.82
Si	1	.060	.064	1.07
	2	.035	.085	2.46
	3	.063	.126	2.01
F	1	.058	not detected	< 0.1
	2	.130	not detected	< 0.1
	3	.039	not detected	< 0.1
Al	1	trace	.021	--
	2	trace	.018	--
	3	trace	.021	--

as evident by the growth of the carbon 1s feature at 288 eV. This oxidation is probably manifested as a large increase in ester or ketone type carbons.

4.5.2 Proton Radiation Exposure

Three control samples of T300/5208, two samples exposed to 10,000 Mrad, and two samples exposed to 40,000 Mrad were examined. The elements present in the control and irradiated samples are essentially the same as with electron radiation. The atomic ratios normalized to carbon are listed in Table 4.12. It is interesting to note that fluorine is still present after irradiation with protons. Small amounts of magnesium are present in the samples exposed to proton radiation. Traces of calcium are detected in the samples irradiated to 10,000 Mrad.

4.5.3 Discussion

Given the chemical structure of epoxy resin, it is surprising to find certain elements present at the composite surface. Fluorine, chlorine, and silicon are probably elements in a surface finish applied to make the composite surface more inert. Sodium, magnesium, and calcium are probably surface contamination which was not removed prior to examination. The aluminum detected in the electron-irradiated samples is believed to be fragmentation from the foil packages used during irradiation. However, traces of aluminum are also detected in the proton-irradiated samples which were not packaged in aluminum foil.

It has been mentioned previously that fluorine disappears after electron irradiation but not proton irradiation. Since electrons penetrate deeper into the composite surface than protons, perhaps they

Table 4.12 Atomic ratios normalized to carbon of proton-irradiated composites

Element	Sample #	Control	10,000 Mrad	Irradiated/ Control	40,000 Mrad	Irradiated/ Control
C	1	1	1	--	1	--
	2	1	1	--	1	--
	3	1				
O	1	.271	.230	.85	.170	.63
	2	.290	.208	.72	.210	.72
	3	.270				
Na	1	.040	.047	1.18	.018	.45
	2	.045	.032	.71	.021	.47
	3	.044				
N	1	.033	.026	.79	.046	1.39
	2	.030	.023	.77	.017	.57
	3	.034				
Al	1	.025	.017	.68	.017	.68
	2	.013	.015	1.15	--	--
	3	.016				
Si	1	.029	.071	2.45	.022	.76
	2	.017	.047	2.76	.066	3.88
	3	.020				
S	1	.011	.0070	.64	.0047	.43
	2	.012	.0080	.67	--	--
	3	.0077				
Cl	1	.036	.054	1.50	.0047	.13
	2	.026	.034	1.31	.026	1.00
	3	.040				
F	1	.084	.061	.73	.0059	.07
	2	.038	.033	.87	.010	.26
	3	.051				
Mg	1	trace	.018	--	.0021	--
	2	trace	.015	--	--	--
	3	trace				
Ca	1	--	.0055	--	--	--
	2	--	.0087	--	--	--
	3	--				

break the carbon-fluorine bonds and liberate fluorine (as F_2 or HF) whereas protons may not.

5. CONCLUSIONS

Graphite fiber/epoxy (T300/5208) and graphite fiber/polyimide (C6000/PMR 15) composites with fibers in the longitudinal direction shows increases in flexural strength after exposure to 0.5 MeV electron radiation up to 8000 Mrad. Transverse samples and crossplies of T300/5208 also exhibit increases in stress when irradiated to 10,000 Mrad. Transverse samples of C6000/PMR 15 show a slight decrease in stress with radiation exposure. Modulus values for all types of composites remain approximately constant regardless of the radiation level. Therefore it can be concluded that these graphite fiber composites, with the exception of transverse C6000/PMR 15, can withstand high energy ionizing radiation in the space environment for an extended period of time, e.g. 30 years.

The interlaminar shear strength exhibits an initial increase with radiation exposure (up to 1000 Mrad) probably due to relaxation of internal stresses. After the internal stresses are relieved there is a sharp decline in interlaminar shear strength with further radiation exposure. Since large negative changes are not seen in longitudinal and transverse flexural strength and modulus, one can conclude that interfacial properties are more sensitive than matrix properties to high energy ionizing radiation.

Scanning electron micrographs of the fracture surfaces of ruptured composites indicate that failure in T300/5208 and C6000/PMR 15 is predominantly adhesive although the adhesion to T300 is better than to C6000. No visual differences could be detected between control samples and those exposed to various levels of radiation.

Electron spectroscopy for chemical analysis (ESCA) reveals little change in the surface elements present in control and highly irradiated T300/5208 composite samples. The most notable difference is that fluorine disappears upon irradiation with electrons; however, this is not the case with proton irradiation. Carbon and oxygen are the major elements present and a number of minor elements are present including sulfur, nitrogen, chlorine, sodium, and silicon. Some of the minor elements are probably incorporated in a surface finish applied to produce an inert surface. Others are most likely due to surface contamination.

6. RECOMMENDATIONS

Graphite fiber composites have been designed to maximize strength and modulus. In an effort to accomplish this, impact strength is sacrificed. This aspect of composites should be studied in order to develop a material which has adequate tensile strength, modulus, and impact strength. A possibility to explore would be hybrid composites containing two different types of reinforcing fibers, e.g. graphite and Kevlar. Another phase of this study would be to determine whether Kevlar composites are as resistant to radiation as graphite composites.

In the present investigation all composites reinforced with striated T300 fibers had an epoxy matrix (NARMCO 5208). These composites exhibit good fiber-matrix adhesion. The C6000 fibers used to reinforce the polyimide matrix (PMR 15) composites had a smooth surface. Fiber-matrix adhesion is not as good in these composites and they exhibit lower strength and modulus than T300/5208 composites. In order to determine whether these differences in composite mechanical properties are due to differences in matrix properties or differences in bonding properties, it would be interesting to study radiation effects on T300/PMR 15 and C6000/5208 composites.

7. LIST OF REFERENCES

1. Freeman, W. T. and Campbell, M. D. "Thermal Expansion Characteristics of Graphite Reinforced Composite Materials," Composite Materials: Testing and Design (Second Conference), ASTM STP 497, American Society for Testing and Materials, 1972, 121-142.

2. Freund, N. P. "Measurement of Thermal and Mechanical Properties of Graphite-Epoxy Composites for Precision Applications," Composite Reliability, ASTM STP 580, American Society for Testing and Materials, 1975, 133-145.

3. Goan, J. C. and Prosen, S. P. "Interfacial Bonding in Graphite Fiber-Resin Composites," Interfaces in Composites, ASTM STP 452, American Society for Testing and Materials, 1969, 3-26.

4. Hammer, G. E. and Drzal, L. T. "Graphite Fiber Surface Analysis by X-ray Photoelectron Spectroscopy and Polar/Dispersive Free Energy Analysis," Applications of Surface Science, 4, 1980, 340-355.

5. Kalnin, I. L. "Evaluation of Unidirectional Glass-Graphite Fiber/Epoxy Resin Composites," Composite Materials: Testing and Design (Second Conference), ASTM STP 497, American Society for Testing and Materials, 1972, 551-563.

6. Broutman, L. J. "Measurement of the Fiber-Polymer Matrix Interfacial Strength," Interfaces in Composites, ASTM STP 452, American Society for Testing and Materials, 1969, 27-41.

7. Broutman, L. J. and Krock, R. H. Composite Materials Vol. 6 Interfaces in Polymer Matrix Composites, E. P. Plueddemann, ed., New York: Academic Press, 1974.

8. Cooper, G. A. and Kelly, A. "Role of the Interface in the Fracture of Fiber Composite Materials," Interfaces in Composites, ASTM STP 452, American Society for Testing and Materials, 1969, 90-106.

9. Greszczuk, L. B. "Theoretical Studies of the Mechanics of the Fiber-Matrix Interface in Composites," Interfaces in Composites, ASTM STP 452, American Society for Testing and Materials, 1969, 42-58.

10. Interfaces in Composites, ASTM STP 452, 1969.

11. Davies, J. T. and Rideal, E. K. Interfacial Phenomena, New York: Academic Press, 1963.

12. Holliday, Leslie (ed.) Composite Materials, New York: Elsevier Publishing Co., 1966.

13. Joshi, A. "Role of Interface Chemistry in Failure of Materials," Fractography in Failure Analysis, ASTM STP 645, B. M. Strauss and W. H. Cullen, Jr., eds., American Society for Testing and Materials, 1978, 275-293.

14. Brooks, J. D. and Taylor, G. H. "The Formation of Some Graphitizing Carbons," in Chemistry and Physics of Carbon, Vol. 4, Philip L. Walker, ed., New York: Marcel Dekker, Inc., 1968.

15. Jenkins, G. M. and Kawamura, K. Polymeric Carbons -- Carbon Fibre, Glass and Char, New York: Cambridge Univ. Press, 1976.

16. McKee, D. W. and Mimeault, V. J. "Surface Properties of Carbon Fibers," in Chemistry and Physics of Carbon, Vol. 8, Philip L. Walker and Peter A. Thrower (eds.), New York: Marcel Dekker, Inc., 1973, 152-241.

17. Reynolds, W. N. "Structure and Physical Properties of Carbon Fibers," in Chemistry and Physics of Carbon, Vol. 11, Philip L. Walker and Peter A. Thrower (eds.), New York: Marcel Dekker, Inc., 1973, 1-62.

18. Drzal, Lawrence T. "The Surface Composition and Energetics of Type A Graphite Fibers," Carbon, 15, 1977, 129-138.

19. Drzal, L. T., Mescher, J. A., and Hall, D. L. "The Surface Composition and Energetics of Type HM Graphite Fibers," Carbon, 17, 1979, 375-382.

20. Scola, D. A. and Brooks, C. S. J. Adhesion, 2, 1970, 213.

21. Quackenbush, N. E. and Thomas, R. L. "Investigation of Carbon Filament Reinforced Plastics," Aeronutronic Publication No. U-4065, July 1967.

22. Scola, D. A. and Brooks, C. S. Tech. Rep. TR-67-28, Part II, 1968.

23. Herrick, J. W. "Surface Treatments for Fibrous Carbon Reinforcements," AFML-TR-66-178, Part II, Air Force Material Laboratory, June 1967.

24. Boehm, H. P., Diehl, E., and Heck, W. Colloq. Nat. Cent. Nat. Rech. Sci., No. 24, 1963, 91.

25. Donnet, J. B. Carbon, 6, 1968, 161.

26. Hallum, J. V. and Druchel, H. V. J. Phys. Chem., 62, 1958, 110.

27. Ray, J. D., Steingiser, S., and Cass, R. A. U. S. Patent 3,671,411, 1972.

28. Harris, B. and Beaumont, P. W. R. J. Mater. Sci, 4, 1969, 432.

29. Rivin, D. "Use of Lithium Aluminum Hydride in the Study of Surface Chemistry of Carbon Blacks," Fourth Rubber Technology Conference, London, 1962.

30. Boehm, H. P. "Functional Groups on the Surfaces of Solids," Angewandte Chemie, International Edition, Vol. 5, No. 533, 1966.

31. Lenz, Robert W. Organic Chemistry of Synthetic High Polymers, New York: Interscience Publishers, 1967, 337.

32. Dauksys, R. J. "Graphite Fiber Treatments which Affect Fiber Surface Morphology and Epoxy Bonding Characteristics," J. Adhesion, 1973, Vol. 5, 211-244.

33. Scola, D. A. and Roth, H. A. U. S. Patent 3,660,140, 1972.

34. Drzal, L. T., Rich, M. J., Camping, J. D., and Park, W. J. "Interfacial Shear Strength and Failure Mechanisms in Graphite Fiber Composites," 35th Annual Technical Conference, Reinforced Plastics/Composites Institute, Society of the Plastics Industry, 1980.

35. Zettlemoyer, A. C. "The Physical Chemistry of Surfaces and Surface Heterogeneities," in Interface Conversion for Polymer Coatings, P. Weiss and G. D. Cheever (eds.), New York: American Elsevier Publishing Co., Inc., 1968.

36. Williams, James H., Jr. and Kousiounelos, Petros N. "Thermoplastic Fibre Coatings Enhance Composite Strength and Toughness," Fibre Sci. and Technol., 11, 1978, 83-88.

37. Zisman, W. A. in "Adhesion and Cohesion," P. Weiss, ed., New York: Elsevier, 1962.

38. deBruyne, N. A. Nature (London), 180, 1957, 262.

39. Hull, A. W. and Burger, E. E. Physics, 5, 1934, 384.

40. McBain, J. W. and Hopkins, D. G. J. Phys. Chem., 29, 1925, 88.

41. Sharpe, L. H. and Schonhorn, H. Advan. Chem. Ser., 43, 1964, 189.

42. Bikerman, J. J. in "Adhesion and Cohesion," ed. by P. Weiss, Amsterdam: Elsevier, 1962.

43. Bolger, J. C. and Michaels, A. S. "Molecular Structure and Electrostatic Interactions at Polymer-Solid Interfaces," in Interface Conversion for Polymer Coatings, P. Weiss and G. D. Cheever, eds., New York: American Elsevier Publishing Company, Inc., 1968.

44. Eirich, F. R. "Factors in Interface Conversion for Polymer Coatings," in Interface Conversion for Polymer Coatings, P. Weiss and G. D. Cheever, eds., New York: American Elsevier Publishing Co., Inc., 1968.

45. Girifalco, L. A. and Good, R. J. J. Phys. Chem., 61, 1957, 904.

46. Gardon, J. L. in "Treatise on Adhesion and Adhesives," Vol. 1, ed. by R. L. Patrick, New York: Dekker, 1967, Chapter VIII.

47. Good, R. J. Advan. Chem. Ser., 43, 1964, 74.

48. Huntsberger, J. R. in "Treatise on Adhesion and Adhesives," Vol. 1, ed. by R. L. Patrick, New York: Dekker, 1967, Chapter IV.

49. Bobka, R. J. and Lowell, L. P. AFAPL-TR-66-310, Part I, 1966.

50. Chwiastiak, S. Preprints of Meeting Amer. Chem. Soc. Div. Org. Coatings Plast., 161st 31, No. 1, 1971, 437.

51. Stromberg, R. R. "Polymer Adsorption on Substrates," in Interface Conversion for Polymer Coatings, P. Weiss and G. D. Cheever (eds.), New York: American Elsevier Publishing Co., Inc., 1968.

52. Bikerman, J. J. Adhesives Age, 2, No. 2, 1959, 23.

53. Bikerman, J. J. and Huang, C. R. Trans. Soc. Rheol., 3, 1959, 5.

54. Crow, T. B. J. Soc. Chem. Ind. (London), 65T, 1924, 43.

55. Kaelble, D. H., Dynes, P. J., and Cirlin, E. H. J. Adhesion, Vol. 6, 1974, 23-48.

56. Doner, D. R. and Novak, R. C. Proc SPI, Conf. Reinforced Plast. Div. 24th, 1969.

57. Haener, J., Ashbaugh, N., Chia, C. Y., and Feng, M. Y. "Investigation of Micro-mechanical Behavior of Fiber Reinforced Plastics," USAAVLABS-TR-67-66, AD-667901, 1968.

58. Marloff, R. H. and Daniel, I. M. Exp. Mech., 9, 1969, 156.

59. Mozzo, G. and Chabord, R. "Contribution to the Study of Glass-Resin Adhesion," Proceedings, 23rd Annual Technical Conference, Reinforced Plastics/Composites Division, Society of the Plastics Industry, Feb. 1968.

60. Mullin, J., Berry, J. M., and Gatti, A. J. Compos. Mater., 2, No. 1, 1968, 82.

61. Berg, C. A., Tirosh, J., and Israeli, M. "Analysis of Short Beam Bending of Fiber Reinforced Composites," Composite Materials: Testing and Design (Second Conference) ASTM STP 497, American Society for Testing and Materials, 1972, 206-218.

62. Daniels, B. K., Harakas, N. K., and Jackson, R. C. Fibre Sci. Technol., 3, 1971, 187.

63. Bader, M. G., Bailey, J. E., and Bell, I. "The Effect of Fibre-Matrix Interface Strength on the Impact and Fracture Properties of Carbon-Fibre-Reinforced Epoxy Resin Composites," Journal of Physics D: Applied Phys., Vol. 6, 1973, 572-586.

64. Elkin, R. A., Fust, G., and Hanley, D. P. Composite Materials: Testing and Design, ASTM STP 460, American Society for Testing and Materials, 1969.

65. Chamis, C. C. "Design Oriented Analysis and Structural Synthesis of Multilayered Filamentary Composites." Ph.D. Thesis, Case Western Reserve Univ., 1967 as seen in Broutman, L. J. and Krock, R. H., Composite Materials Vol. 6 Interfaces in Polymer Matrix Composites, E. P. Plueddemann, ed., New York: Academic Press, 1974.

66. Wadsworth, N. J. and Spilling, I. Brit J. Appl. Phys. (J. Phys. D) Ser. 2, 1, 1968, 1049.

67. Agarwal, B. D. and Bansal, R. K. "Effect of an Interfacial Layer on the Properties of Fibrous Composites: A Theoretical Analysis," Fibre Sci. and Technol., 12, 1979, 149-157.

68. Kaelble, D. H., Dynes, P. J., Crane, L. W., and Maus, L. "Kinetics of Environmental Degradation in Graphite-Epoxy Composites," Composite Reliability, ASTM STP 580, American Society for Testing and Materials, 1975, 247-262.

69. Bodnar, M. J. and Wegman, R. F. SAMPE J. Aug/Sept, 1969, 51.

70. Falconer, D. J., MacDonald, N. C., and Walker, P. Chem. Ind., 1964, 1230.

71. Kerr, C., MacDonald, N. C., and Orman, S. Brit. Polym. J., 2, 1970, 67.

72. Orman, S. "Aspects of Adhesion" (D. J. Alner, ed.), Vol. 6, University of London Press Ltd., London, 1971.

73. Patrick, R. L., Gehman, W. G., Dunbar, L., and Brown, J. A. J. Adhesion, 3, 1971, 165.

74. Whitney, J. M. and Ashton, J. E. AIAA J., 9, 1971, 1708.

75. Ashbee, K. H. G. and Farrar, N. "Detection and Identification of Changes in the Physical Properties of Fibre/Matrix Interfaces," Proceedings of the 1975 International Conference on Composite Materials, Vol. 1, edited by E. Scala, E. Anderson, I. Toth, and B. R. Noton, New York: The Metallurgical Society of AIME, 1976, 771-782.

76. Farrer, N. R., Turner, T. W. and Ashbee, K. H. G. "The Physical Mechanisms Responsible for Deterioration in the Properties of Composite Materials," 3rd International Conference on Mechanical Behavior of Materials, Cambridge, England, 20-24 August 1979.

77. Dauksys, R. J. and Browning, C. E. Tech. Rep. AFML-TR-68-333, 1969.

78. Scola, D. A. Internal Rep. K110542-2, United Aircraft Res. Lab., E. Hartford, Connecticut.

79. Scola, D. A. Internal Rep. G213186-5 and P-L84, United Aircraft Res. Lab., E. Hartford, Connecticut.

80. Cuthrell, R. E. J. Appl. Polym. Sci., 12, 1968, 1263.

81. Erath, E. H. and Spurr, R. A. J. Polym. Sci., 35, 1959, 391.

82. Bascom, W. D. and Romans, J. B. Ind. Eng. Chem. Prod. Res. Develop., 7, 1968, 172.

83. Forest, J. D. Progr. Rep. No. 3, GDC-CHB70-001, Air Force Contract F33615-70-C-1442, General Dynamics, Convair Aerospace Div., 1970.

84. Bullock, R. E., Kerlin, E. E., Warwick, J. E. NASA Contract Report, CR-2162, N73-14707 , 1972.

85. Bullock, R. E. "Radiation as a Tool in Studying Relationships Between Various Mechanical Properties of Graphite-Epoxy Composites," Mater. Sci. and Eng., 10, 1972, 178-181.

86. Arrington, M. and Harris, B. "Some Properties of Mixed Fibre CFRP," Composites, 9, No. 3, 1978, 149-152.

87. Lackman, L. M., Losie, D. O., Rohlen, J. A. Advanced Composites Data for Aircraft Structural Design, AD-904 324, September 1972.

88. Naranong, N., Wolf, K., Memory, J. D., Gilbert, R. D., and Fornes, R. E. "Effects of Ionizing Radiation on the Mechanical and Morphological Properties of Graphite Fiber Reinforced Composites," Bulletin of the American Physical Society, Vol. 26, No. 3, March 1981.

89. Fornes, R. E., Memory, J. D., and Naranong, N. "Effect of 1.33 MeV Gamma Radiation and 0.5 MeV Electrons on the Mechanical Properties of Graphite Fiber Composites," J. of Appl. Polym. Sci., 26, 1981, 2061.

90. Parkinson, W. W. and Sisman, O. "The Use of Plastics and Elastomers in Nuclear Radiation," Nuclear Engineering and Design, 17, 1971, 247-280.

91. Bullock, R. E. "The Effects of Fast-Neutron Irradiation on Tensile Strengths of Carbon Fibers," Radiation Effects, 11, 1971, 107.

92. McKague, E. L., Jr., Bullock, R. E., and Head, J. W. "Improved Mechanical Properties of Composites Reinforced with Neutron-Irradiated Carbon Fibers," J. of Compos. Mater., 7, 1973, 288-297.

93. Union Carbide Technical Information Bulletin No. 465-224. "Thornel 300 Material Specification."

94. Bascom, W. D., Bitner, J. L., Cottington, R. L., and Henderson, C. M. "Thermomechanical Properties of High-Performance Polymers," in High Performance Composites and Adhesives for V/STOL Aircraft, May 1979, AD-A069-611, NRL-MR-4005.

95. Naranong, Naraporn. "Effect of High Energy Radiation on Mechanical Properties of Graphite Fiber Reinforced Composites," Master's Thesis, North Carolina State University, Raleigh, North Carolina, 1980.

96. Morgan, R. J. and O'Neal, J. E. "Epoxies as Composite Matrices," American Chemical Society. Division of Organic Coatings and Plastic Chemistry, 38, 1977, 485-490.

97. Carter, H. G., Kibler, K. G. and Reynolds, J. D. "Fundamental and Operational Glass Transition Temperatures of Composite Resins and Adhesives," Advanced Composite Materials-Environmental Effects, ASTM STP 658, J. R. Vinson, ed., American Society for Testing and Materials, 1978, 84-97.

98. FWT Radiachromic Radiation Measurement Material and Reader Manual, Far West Technology, Inc., Goleta, California, 1979.

99. Annual Book of ASTM Standards Part 35, Method D-790-71, American Soceity of Testing and Materials, Philadelphia, Pennsylvania, 1976.

100. Annual Book of ASTM Standards Part 36, Method D-2733, American Society of Testing and Materials, Philadelphia, Pennsylvania, 1976.

101. Rochow, Theodore G. and Rochow, Eugene G. An Introduction to Microscopy by Means of Light, Electrons, X-rays, or Ultrasound, New York: Plenum Press, 1978.

102. Hercules, David M. "Surface Characterization Using Electron Spectroscopy (ESCA)," in Characterization of Metal and Polymer Surfaces, Vol. 1 Metal Surfaces, Lieng-Huang Lee, ed., New York: Academic Press, 1977.

103. Clausen, C. A., III and Good, M. L. "Characterization of Bulk and Surface Properties of Heterogeneous Ruthenium Catalysts by Mössbauer and ESCA Techniques," in Characterization of Metal and Polymer Surfaces Vol. 1 Metal Surfaces, Lieng-Huang Lee, ed., New York: Academic Press, 1977.

104. Oudar, Jacques. Physics and Chemistry of Surfaces, London: Blackie and Son Limited, 1975.

105. Wolsky, S. P. and Czanderna, A. W. Methods and Phenomena: Their Applications in Science and Technology Vol. 1 Methods of Surface Analysis, New York: Elsevier Scientific Publishing Company, 1975.

8. APPENDIX

8.1 Experimentation

Several experiments were conducted to determine the effects of moisture on the mechanical properties of unidirectional graphite fiber composites. In the first experiment, six samples each of T300/5208 longitudinal, C6000/PMR 15 longitudinal, and C6000/PMR 15 transverse were soaked in distilled water at room temperature for one week. The samples were taken from the water, surface dried, and tested with no laboratory conditioning. The ultimate stress and average modulus were evaluated using the three-point bending test described in Section 3.4.1. The results of this experiment are given in Table 8.1. The stress and modulus values of the T300/5208 soaked samples are significantly higher than the control values. The C6000/PMR 15 longitudinal samples follow this same trend but the increase is not statistically significant. There is a decrease in stress and modulus after soaking the C6000/PMR 15 transverse samples but it is not statistically significant.

To examine the effects of prolonged soaking, the above experiment was repeated with samples being soaked for four weeks. In order to accelerate the effects of moisture, samples were soaked in a heated desiccator at 80°C. The results of this experiment are given in Table 8.2. The stress values of the longitudinal samples of both composite types increase after soaking but these increases are not statistically significant. The modulus value for T300/5208 remains approximately constant while that for C6000/PMR 15 increases slightly. For C6000/PMR 15 transverse samples the value of stress after soaking is

Table 8.1 Mechanical properties of composites soaked one week at room temperature

Sample	Condition	Stress (kg/cm^2)	Modulus (kg/cm^2)
T300/5208 longitudinal	Control	21,744	1,379,082
	Soaked	22,373*	1,424,248*
C6000/PMR 15 longitudinal	Control	19,837	971,050
	Soaked	20,212	992,551
C6000/PMR 15 transverse	Control	981	74,826
	Soaked	807	73,484

Note: Each value represents the mean of 6 samples.

* denotes significance at 5% level

Table 8.2 Mechanical properties of composites soaked four weeks at 80°C

Sample	Condition	Stress (kg/cm^2)	Modulus (kg/cm^2)
T300/5208 longitudinal	Control	21,744	1,379,082
	Soaked	22,021	1,349,253
C6000/PMR 15 longitudinal	Control	19,837	971,050
	Soaked	21,049	1,057,611
C6000/PMR 15 transverse	Control	981	74,826
	Soaked	751*	73,914

Note: Each value represents the mean of 6 samples.

* denotes significance at 5% level

This Page Intentionally Left Blank

Table 8.3 Mechanical properties of composites soaked 400 and 800 hours at 80°C

Sample	Condition	Stress (kg/cm^2)	Modulus (kg/cm^2)
T300/5208 longitudinal	Control	20,919	1,335,144
	400 hours	21,086	1,309,549
	800 hours	20,980	1,299,763
C6000/PMR 15 longitudinal	Control	20,457	1,099,567
	400 hours	19,181	914,068
	800 hours	20,371	1,062,997
C6000/PMR 15 transverse	Control	1,016	79,704
	400 hours	842*	73,257
	800 hours	805*	75,097

Note: Each value represents the mean of 3 samples.

* denotes significance at 5% level